Technical University of Denmark

ESO2 Optimization of Supermarket Refrigeration Systems

Mixed Integer MPC and System Performance

Lars Norbert Petersen
Henrik Madsen
Christian Heerup

IMM-Technical Report-2012-01

DTU Informatics
Department of Informatics and Mathematical Modelling

Contents

1 Introduction

Supermarket refrigeration systems consists of a number of display cases, cooling cabinets and cold rooms connected to a central compressor pack. This configuration saves energy compared to placing a compressor at each cooling site.

The classical control setup of a supermarket refrigeration system is highly distributed. The cooling sites are equipped with an individual hysteresis controller that keeps the air temperature in the cooling site within a defined band by manipulating the opening degree of an inlet valve. The compressor bank maintains a desired suction pressure by adjusting the capacity to the given load from the cooling sites. An illustration of the principle is shown in figure 1. This design is flexible and simple, but its major drawback is however that it introduces self-inflicted disturbances and the dynamic coupling of the display cases makes them synchronize. Synchronization results in low efficiency and high wear of the compressor, because the compressor has to work much harder for short periods of time. The problem increases when the load is small compared to the available compressor capacity, which it is in the winter time, at night and when only a few cooling sites are present in the supermarket.

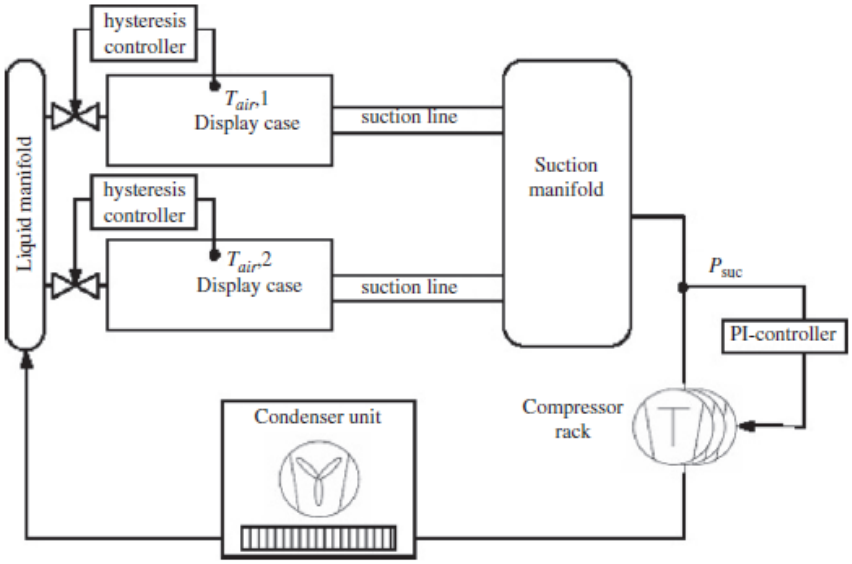

Figure 1: *Classical control setup of a small refrigeration system.*

The first approach to solve this problem is to design an overall control system which coordinates the compressor capacity and the current refrigeration load. The drawback of this approach is the complexity of the single controller. The solution is investigated in the first part of the report. A second solution is investigated where only the compressor control is considered. This controller try to feed-forward the measured disturbances,

i.e. opening and closing of the cooling site AKV's. Last a performance analysis of the refrigeration system is performed.

Part I

Compressor and Cooling Site Control

The idea that motivates this part of the project is to design an overall control system that coordinates the compressor capacity with the refrigeration load. This will be done by coordinating when the display cases, cooling rooms etc. are requesting refrigeration from the compressor pack. The time constants of each cooling site then become important, since the cooling can only be pulled for a curtain amount of time. Otherwise food safety will get compromised.
The supervision system will be based on a Model Predictive Controller (MPC), which has been used with success in many industrial applications. The advantage of this controller is that it handles the dynamic couplings in the system, the constraints of the system explicitly and allows a systematic control design. The normal MPC framework (Maciejowski, 2002) is used, but has to be extended to scope with the discrete-valued integer inputs. The trivial quadratic program therefore turns into a Mixed Integer Quadratic Program (MIQP), which is considerable more difficult/complex to solve.

2 Modeling

In a supermarket a lot of goods have to be refrigerated to ensure a proper food quality. The required storage temperature of the goods varies, as some has to be deep frozen, some kept just above the freezing point and others should only be chilled. No matter the temperature these goods are always placed in display cases, cold rooms or cooling cabinets (in one referred to as cooling sites). A simplified refrigeration system is shown in figure 2. Normally the cooling sites are supplied with refrigerant in parallel from a common central compressor rack. The compressors supply refrigerant by compressing refrigerant from the low pressure side (i.e. suction manifold) to the high pressure side (i.e. gas cooler). On the high pressure side the refrigerant is cooled by a gas cooler. In this process energy is released in the form of heat. The evaporators inside the different cooling sites are fed with refrigerant from the high pressure side. Refrigerant is lead through an expansion valve and hereafter it turns into gas while absorbing heat/energy. Air from the ”hot site” of the cooling sites is then blown through the cold evaporator, which cools the air, and guided back into the cooling site. As the air is colder or at the same temperature as the goods, these are kept cooled at the same temperature as the air. The refrigerant gas is lead to the suction manifold and compressed again. The transport cycle of heat is thus completed and thus the cooling cycle is completed.

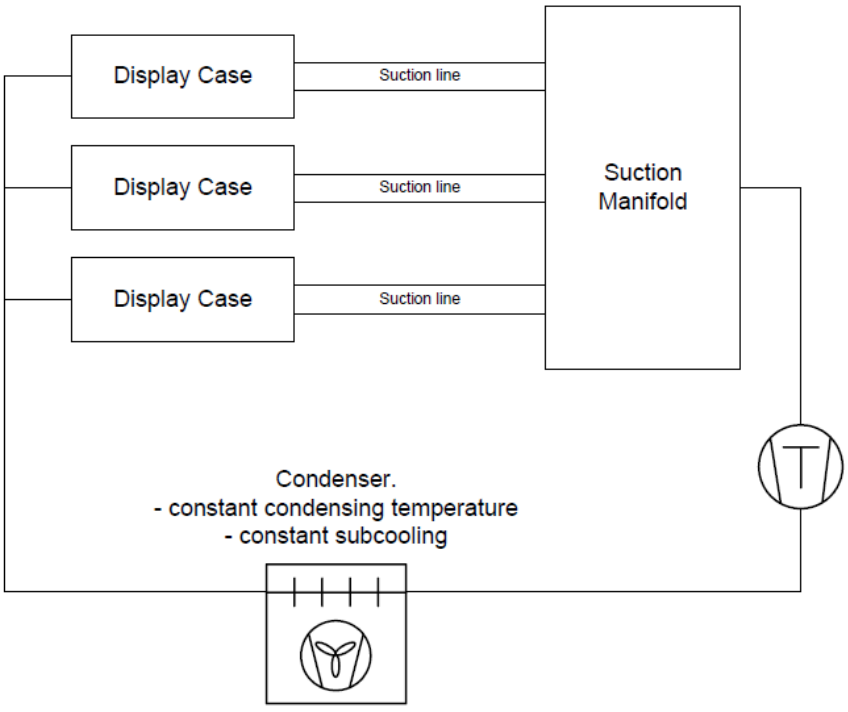

Figure 2: *Illustration of the modeled (simple) refrigeration system*

In reality the system is more advanced, since a bypass-valve is installed to remove flash gas from the refrigerant and the freezers are separated from the fridges. The model used in this project will not describe these parts directly.
A mathematical model is needed in order to design and validate the later control system. For this purpose a nonlinear model was developed. The model is highly inspired by the work of (Larsen, 2005), which model the refrigeration system with emphasis on modeling the cooling sites (display cases) and compressors. The gas cooler is modeled by a fixed pressure, since it has minor effect on the control systems. The model is based on the refrigerant, R744, CO_2.

2.1 The Cooling Sites

The cooling sites are all modeled as display cases, since in reality all cooling sites are very similar in construction. Thus they are modeled by the same set of differential equations. The model is derived by setting up energy balances for the goods, the evaporator wall and the air curtain. A mass-balance is set up for the mass of liquid refrigerant in the evaporator. This gives 4 states; T_{air}, T_{wall}, T_{goods} and M_{ref}. The heat transfer between the first three states are given by

$$\frac{dT_{goods}}{dt} = -\frac{\dot{Q}_{goodsair}}{M_{goods}Cp_{goods}} \tag{2.1}$$

$$\frac{dT_{wall}}{dt} = \frac{\dot{Q}_{airwall} - \dot{Q}_e + \dot{Q}_{fan}}{M_{wall}Cp_{wall}} \tag{2.2}$$

$$\frac{dT_{air}}{dt} = \frac{\dot{Q}_{goodsair} + \dot{Q}_{load} - \dot{Q}_{airwall}}{M_{air}Cp_{air}} \tag{2.3}$$

where the energy flows are

$$\dot{Q}_{goodsair} = UA_{goodsair}(T_{goods} - T_{air}) \tag{2.4}$$

$$\dot{Q}_{airwall} = UA_{airwall}(T_{air} - T_{wall}) \tag{2.5}$$

$$\dot{Q}_e = UA_{wallref}(T_{wall} - T_e) \tag{2.6}$$

$$\dot{Q}_{load} = UA_{airload}(T_{indoor} - T_{air}) \tag{2.7}$$

UA is the heat transfer coefficient with the subscript denoting the media which it insulate. M is the mass and Cp is the heat capacity of the media. T_{indoor} is the indoor temperature of the supermarket and T_e is the evaporation temperature of the refrigerant. $UA_{wallref}$ is a function of $\dot{m}_{ref}$, which means that the more refrigerant there is in the evaporator the better the evaporator cools the air entering the evaporator. It is assumed that the relation is linear and described by

$$UA_{wallref} = UA_{wallref,max}\frac{M_{ref}}{M_{ref,max}} \tag{2.8}$$

The holdup of liquid refrigerant is described by the mass balance below

$$\frac{dM_{ref}}{dt} = \dot{m}_{ref,in} - \dot{m}_{ref,out} \tag{2.9}$$

The mass flow of refrigerant into the evaporator is determined by the opening degree of the expansion valve. The orifice equation determines this flow given the pressures, P_{suc} and P_{gc}, the density of the liquid, ρ_{suc}, and a constant characterizing the valve, KvA. The equation is

$$\dot{m}_{ref,OD} = OD \cdot KvA \cdot \sqrt{2\rho_{suc}(P_{rec} - P_{suc})10^5} \tag{2.10}$$

The opening degree, OD, is a value between 0 and 100% where 0 is completely closed and 100% is completely open. The pressure difference across the valve is given by the receiver pressure minus the suction pressure, since no pressure drop is assumed in the suction and high pressure lines and evaporator. The evaporator has a maximum holdup and when it is filled a local (superheat) controller will automatically reduce the inlet of refrigerant. The inlet mass flow is therefore bounded by the relation

$$\dot{m}_{ref,in} = \min(\dot{m}_{ref,out}, \dot{m}_{ref,OD}) \qquad \text{if } M_{ref} \geq M_{ref,max} \tag{2.11}$$

The refrigerant has to leave the evaporator and flows to the suction manifold. The leaving mass flow is given by

$$\dot{m}_{ref,out} = \begin{cases} 0 & \text{if } M_{ref} \leq 0 \\ \frac{\dot{Q}_e}{\Delta h_{lg}} & \text{if } M_{ref} > 0 \end{cases} \tag{2.12}$$

Naturally there can only be an out-flow of mass when the holdup of mass in the evaporator is greater than zero. When the holdup is positive the refrigerant boils off with a constant rate $\frac{\dot{Q}_e}{\Delta h_{lg}}$, where $\dot{Q}_e$ is the flow of energy supplied to the refrigerant and Δh_{lg} is the specific latent heat of the refrigerant in the evaporator, which is a function of the suction pressure only.

The display cases are fitted with a number of temperature sensors, but only one air and one evaporator temperature will be considered here. At Danfoss these sensors are refereed to as S3 and S4. The temperature of the goods cannot be measured directly. Therefore the air temperature is used as an indirect measure of the food temperature and thus the air temperature is restricted to lie within narrow bands.

The complexity of the model should be reduced, because the heat capacity of the air is close to zero. Setting the heat capacity equal to zero in (2.3) reduce the air temperature to

$$T_{air} = \frac{UA_{goodsair}T_{goods} + UA_{airload}T_{indoor} + UA_{airwall}T_{wall}}{UA_{goodsair} + UA_{airload} + UA_{airwall}} \tag{2.13}$$

Further the holdup of mass must be reduced because of the difficulties in detecting the mass holdup and very fast dynamics. The energy transfer is therefore described by

$$\dot{Q}_e = \Delta h_{lg} \dot{m}_{ref,in} \tag{2.14}$$

Using these expressions makes the system "less stiff" and provide better simulation accuracy and makes the problem less computational expensive. Note that the expression is a simple approximation to the true energy transfer. The transfer is therefore likely to be overestimated by up to 30%.

2.2 The Suction Manifold

The dynamics of the suction manifold are modeled by only one state, describing the dynamics of the suction pressure, P_{suc}. Setting up the mass balance for the manifold gives

$$\frac{dM_{suc}}{dt} = \dot{m}_{in,suc} + \dot{m}_{dist} - \dot{V}_{comp}\rho_{suc} \tag{2.15}$$

where $\dot{m}_{in,suc} = \sum_i^N \dot{m}_{ref,out,i}$ with N equal to the number of display cases. The compressor that drives the freezers does also contribute to an increase of mass directly. This contribution is modeled together with the disturbance mass flow.
Rewriting the derivative term as follows

$$\frac{dM_{suc}}{dt} = V_{suc}\frac{d\rho_{suc}}{dt} = V_{suc}\frac{d\rho_{suc}}{dP_{suc}}\frac{dP_{suc}}{dt} \tag{2.16}$$

the expression in 2.15 can be reformulated as

$$\frac{dP_{suc}}{dt} = \frac{\dot{m}_{in,suc} + \dot{m}_{dist} - \dot{V}_{comp}\rho_{suc}}{V_{suc}\frac{d\rho_{suc}}{dP_{suc}}} \tag{2.17}$$

V_{suc} is the volume of the suction manifold and $\dot{m}_{dist}$ is a disturbance mass flow which can originate from the bypass valve, un-modeled display cases and freezers. ρ_{suc} is the density of the of the refrigerant in the suction manifold.

2.3 The Fridge Compressors

The fridge refrigeration systems in small supermarkets are often fitted with a compressor rack where the capacity is discrete valued. This is due to the simple and cheap

structure where a small number of compressors can only be turned on or off. In slightly larger supermarkets the smallest compressor in the rack is fitted with a frequency converter, making it possible to continuously adjust some of the capacity. The present Fakta Otterup is fitted with a frequency converter and it has therefore been assumed, with great precision, that the requested equals the delivered capacity.
The volume flow is given by

$$\dot{V}_{comp} = \frac{cap}{100} \cdot \eta_{vol} \cdot V_{sl} \tag{2.18}$$

where cap is the running capacity from 0 to 100%, η_{vol} is the constant volumetric efficiency and V_{sl} is the maximal displacement volume. Most of the power consumption originates from the compressor pack. It is therefore of great interest to reduce the power consumption in exactly this part of the refrigeration system. For simplicity we will focus only on the power consumption from the fridge compressors, which is also the largest contributor. The compressor power consumption is given by

$$\dot{W}_{comp} = \frac{1}{\eta_{is}} \dot{V}_{comp} \rho_{suc} (h_{c,out} - h_{c,in}) \tag{2.19}$$

where η_{is} is the isentropic efficiency and ρ_{suc} is the density of the refrigerant. $\dot{V}_{comp}$ is the volume flow through the compressor. $h_{c,in}$ and $h_{c,out}$ are the enthalpy of the refrigerant in and out of the compressor. The enthalpies are found by the software package "RefEqns".

2.4 Refrigerant

Different refrigerants can be used in supermarkets, depending on the temperatures of the outdoor cooling air and legal restrictions. The refrigerant used in this particular case is R744, i.e. CO_2. The refrigerant properties are nonlinear and computed by a free software package "RefEqns" (Skovrup, 2003). The software is available to many languages (including Matlab).
The properties used for this model is given by the function calls below

```
1 Te = TBubP(Psuc);
2 rho_suc = 1/VTP(Te+Tsh,Psuc);
3 dRhodP = (1/VTP(Te+Tsh,Psuc+0.05)-1/VTP(Te+Tsh,Psuc-0.05))/(2*0.05);
4 hcin = HTP(Te+Tsh,Psuc);
5 hcout = HTP(Tgc,Pgc);
6 dhlg = RT(Te+273.15);
```

The package, *RefEqns*, has to be initialized by the commands below

```
SetRNumber('R744');
SetPressureUnit(2);      %Pressure in [bar] [Pa','kPa','Bar','psia']
SetTemperatureUnit(1);   %Temperature in [°C] ['K','°C','°F','R']
```

2.5 Model in- and Outputs

From outside the model can be interpreted as a box consisting of manipulated inputs, measured outputs, controlled outputs and disturbances. To summarize they are listed below

$$\mathbf{u} = \begin{bmatrix} cap \\ OD_1 \\ OD_{..} \\ OD_N \end{bmatrix} \qquad \mathbf{d} = \begin{bmatrix} \dot{m}_{dist} \\ UA_{airload,1} \\ UA_{airload,..} \\ UA_{airload,N} \end{bmatrix} \qquad \mathbf{y} = \begin{bmatrix} P_{suc} \\ \dot{m}_{in,suc} \\ T_{air,1} \\ T_{wall,1} \\ T_{air,..} \\ T_{wall,..} \\ T_{air,N} \\ T_{wall,N} \end{bmatrix} \qquad \mathbf{z} = \begin{bmatrix} P_{suc} \\ T_{air,1} \\ T_{air,..} \\ T_{air,N} \end{bmatrix} \tag{2.20}$$

Where N is the number of cooling sites. The measurement, $\dot{m}_{in,suc}$, could be omitted while still keeping the system observable. The measurement serves to ease the later parameter identification problem.

3 Parameter Estimation

The non-linear model stated in section 2 is a so-called gray-box model where theoretical knowledge about the system has to be combined with information from measurements performed on the true system . This insure a good model quality. Two important advantages of using this approach, compared to using stochastic black-box models, are the flexibility and physicality.

The initial model has been formulated from mass and energy balances and the list of unknown parameters are

Suction Manifold	**Cooling Site(s)**
V_{suc}, T_{sh}, η_{vol}, η_{is}, T_{indoor}	$UA_{airwall}$, Cp_{wall}, M_{wall}, $\dot{Q}_{fan}$, P_{rec}
V_{sl}, P_{rec}, P_{gc}, T_{gc} and $\dot{m}_{dist}$	$UA_{goodsair}$, Cp_{goods}, M_{goods}, $UA_{airload}$ and KvA

The parameters associated with the cooling sites are individual for each cooling site.

It has not been possible to estimate all the unknown parameters in the model, due to the fact that the parameters are linearly dependent seen from the model outputs. The parameters below are therefore manually defined.

Manually defined parameters
Suction Manifold $T_{sh} = 11$, $V_{sl} = 6.5 \cdot 70/50 + 12.0$, $P_{rec} = 38$, $P_{gc} = 50$, $T_{gc} = 70$, $T_{indoor} = 26$, $\eta_{is} = 0.6$ and $V_{suc} = 2$
Cooling Site(s) $Cp_{wall} = 385$ and $Cp_{goods} = 1000$

This leaves the set of parameters below which has to be estimated

Estimated parameters
Suction Manifold η_{vol} and $\dot{m}_{dist}$
Cooling Site(s) M_{wall}, $UA_{airwall}$, M_{goods}, $UA_{goodsair}$, $UA_{airload}$, $\dot{Q}_{fan}$ and KvA

The estimation of these parameters has been performed by an off-line method. The advantage of the off-line method (against an on-line method) is its robustness and ability to estimate more parameters. The down side is that it can naturally only be performed off-line and time dependence in the parameters will not be described. It is known that the cooling sites are isolated better at night than at day time and only the day time is estimated here. Beside the isolation parameters, $UA_{airload}$, the parameters estimated here should be time independent and an on-line adaptation is deemed unnecessary.

The parameter estimation has been formulated as an optimization problem. The standard cost function is used where the sum of squared errors between the experimental data and simulated response are penalized. This type of optimization is not guaranteed to be convex and many local minimizers are likely. One has to be careful not to find one of these.
The method is called prediction-error minimization method (Ljung, 1999) (PEM) and the dynamic system is described by the set of ordinary differential equations (or ODEs) from section 2. In short the grey-box model can be written

$$\dot{\boldsymbol{x}}(t) = \boldsymbol{f}(\boldsymbol{x}(t), \boldsymbol{u}(t), \boldsymbol{\theta}) \tag{3.1}$$
$$\widehat{\boldsymbol{y}}(t_k) = \boldsymbol{g}(\boldsymbol{x}(t_k), \boldsymbol{u}(t_k), \boldsymbol{\theta}) + \boldsymbol{v}(t) \tag{3.2}$$

The optimization problem is

$$\boldsymbol{\epsilon}(t_k, \boldsymbol{\theta}) = \boldsymbol{y}(t_k) - \widehat{\boldsymbol{y}}(t_k, \boldsymbol{\theta}) \tag{3.3}$$
$$V_N(\boldsymbol{\theta}) = \frac{1}{N} \sum_{t_k=1}^{N} \frac{1}{2} \boldsymbol{\epsilon}(t_k, \boldsymbol{\theta}) \boldsymbol{\epsilon}^T(t_k, \boldsymbol{\theta}) \tag{3.4}$$
$$\widehat{\boldsymbol{\theta}}_N = \arg\min_{\boldsymbol{\theta} \in D_m} V_N(\boldsymbol{\theta}) \tag{3.5}$$

where $\boldsymbol{y}(t_k)$ and $\widehat{\boldsymbol{y}}(t_k, \boldsymbol{\theta})$ is the measured and estimated output at time t_k. $\boldsymbol{\epsilon}$ is the estimation error (residual) and V_N is the value of the cost function. There exists lots of implementations of this algorithm and `Matlab` of cause also has a build in PEM algorithm. A wrapper for the nonlinear estimation problem is made and the algorithm returns both the estimated parameters and the standard deviation of the estimate.

The estimated parameters are

Suc. Manifold	$\eta_{vol} = 0.916$
POS 40A	$UA_{airload} = 11.5$, $M_{wall} = 172.1$, $M_{goods} = 574.1$, $UA_{goodsair} = 222.9$, $UA_{airwall} = 128.2$, $\dot{Q}_{fan} = 481.7$ and $KvA = 0.76 \cdot 10^{-6}$
POS 40B	$UA_{airload} = 14.4$, $M_{wall} = 296.8$, $M_{goods} = 349.4$, $UA_{goodsair} = 477.9$, $UA_{airwall} = 193.9$, $\dot{Q}_{fan} = 639.6$ and $KvA = 1.19 \cdot 10^{-6}$
POS 40C	$UA_{airload} = 46.1$, $M_{wall} = 387.4$, $M_{goods} = 3794.2$, $UA_{goodsair} = 288.2$, $UA_{airwall} = 272.5$, $\dot{Q}_{fan} = 881.7$ and $KvA = 1.47 \cdot 10^{-6}$
POS 30	$UA_{airload} = 37.3$, $M_{wall} = 178.9$, $M_{goods} = 1416.5$, $UA_{goodsair} = 440.1$, $UA_{airwall} = 169.1$, $\dot{Q}_{fan} = 0.0$ and $KvA = 0.97 \cdot 10^{-6}$
POS 30B	$UA_{airload} = 20.1$, $M_{wall} = 87.4$, $M_{goods} = 439.7$, $UA_{goodsair} = 983.3$, $UA_{airwall} = 197.1$, $\dot{Q}_{fan} = 8.03$ and $KvA = 1.44 \cdot 10^{-6}$
POS 45	$UA_{airload} = 11.1$, $M_{wall} = 234.2$, $M_{goods} = 368.5$, $UA_{goodsair} = 210.7$, $UA_{airwall} = 188.4$, $\dot{Q}_{fan} = 779.7$ and $KvA = 0.82 \cdot 10^{-6}$
POS 50	$UA_{airload} = 12.6$, $M_{wall} = 244.9$, $M_{goods} = 449.9$, $UA_{goodsair} = 127.6$, $UA_{airwall} = 145.3$, $\dot{Q}_{fan} = 20.4$ and $KvA = 0.89 \cdot 10^{-6}$

The set of parameters for the cooling sites are individual and the total number of estimated parameters are therefore, $7n + 1 = 50$, where n is the total number of display cases.

The estimated output is validated against the observed outputs in figure 3 and 4. The first comparison, figure 3, is based on training data. Next the comparison is made for the test data. The comparison is made using simulation, without feedback from the data. This means that the 1-step predictor used in the Kalman filter will be even better than achieved here. The two figures show that the model fits very accurately. The open display cases have a tendency to have a slightly worse fit than the others, but in general the fit is of very high quality. The fit can get improved by modeling the delay from the air temperature sensors originating from the physical delay of moving the air around the display case. An improvement can also be found by describing the opening and closing of the door in the cold room. The bad fit of the suction pressure is due to fast un-described transients and the bad excitation.
The model is deemed satisfactory for our control purpose.

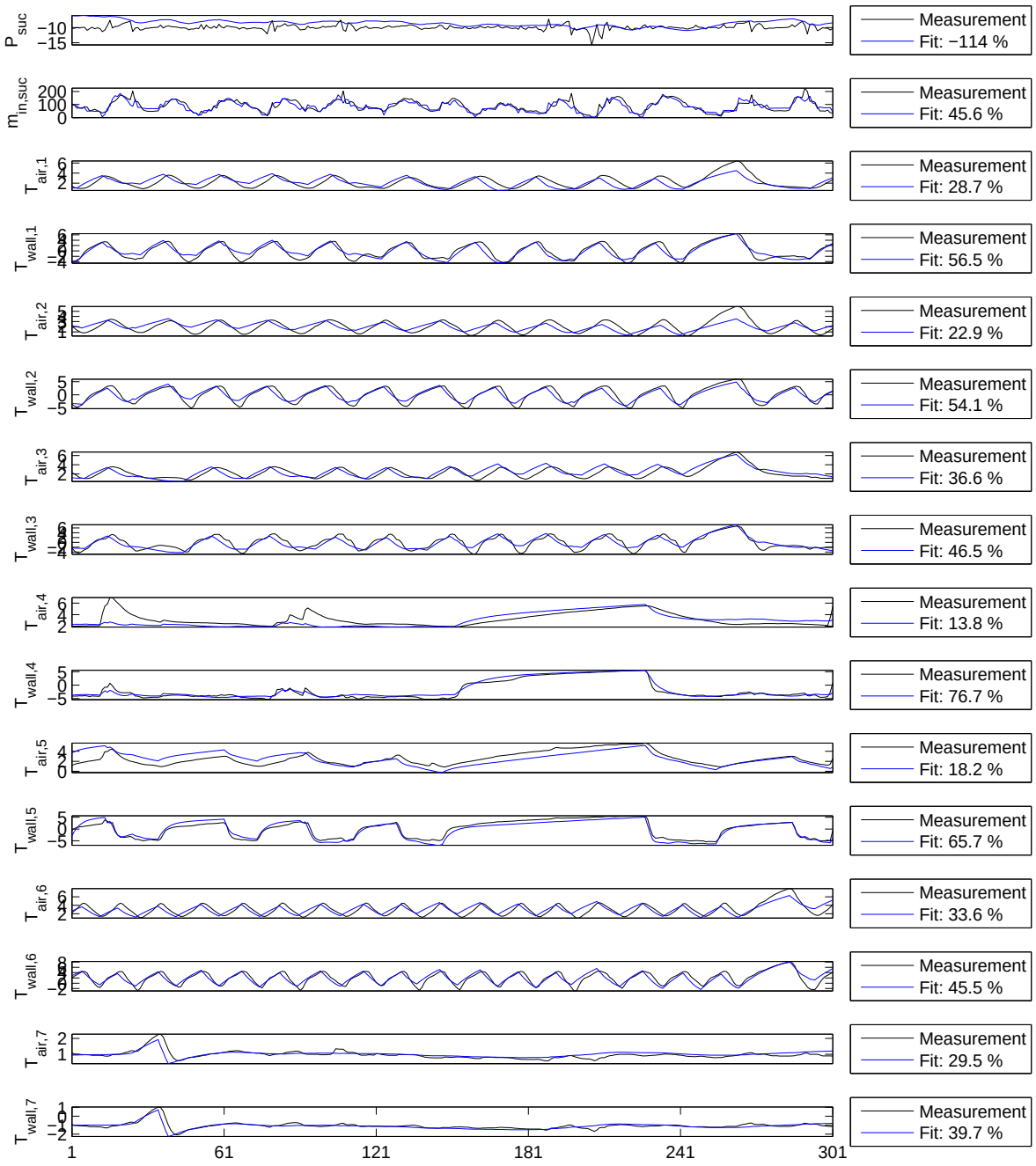

Figure 3: *Validation of the gray-box fit quality using training data. A somewhat good estimate is expected and achieved. The fast transients of the suction pressure are not captured.*

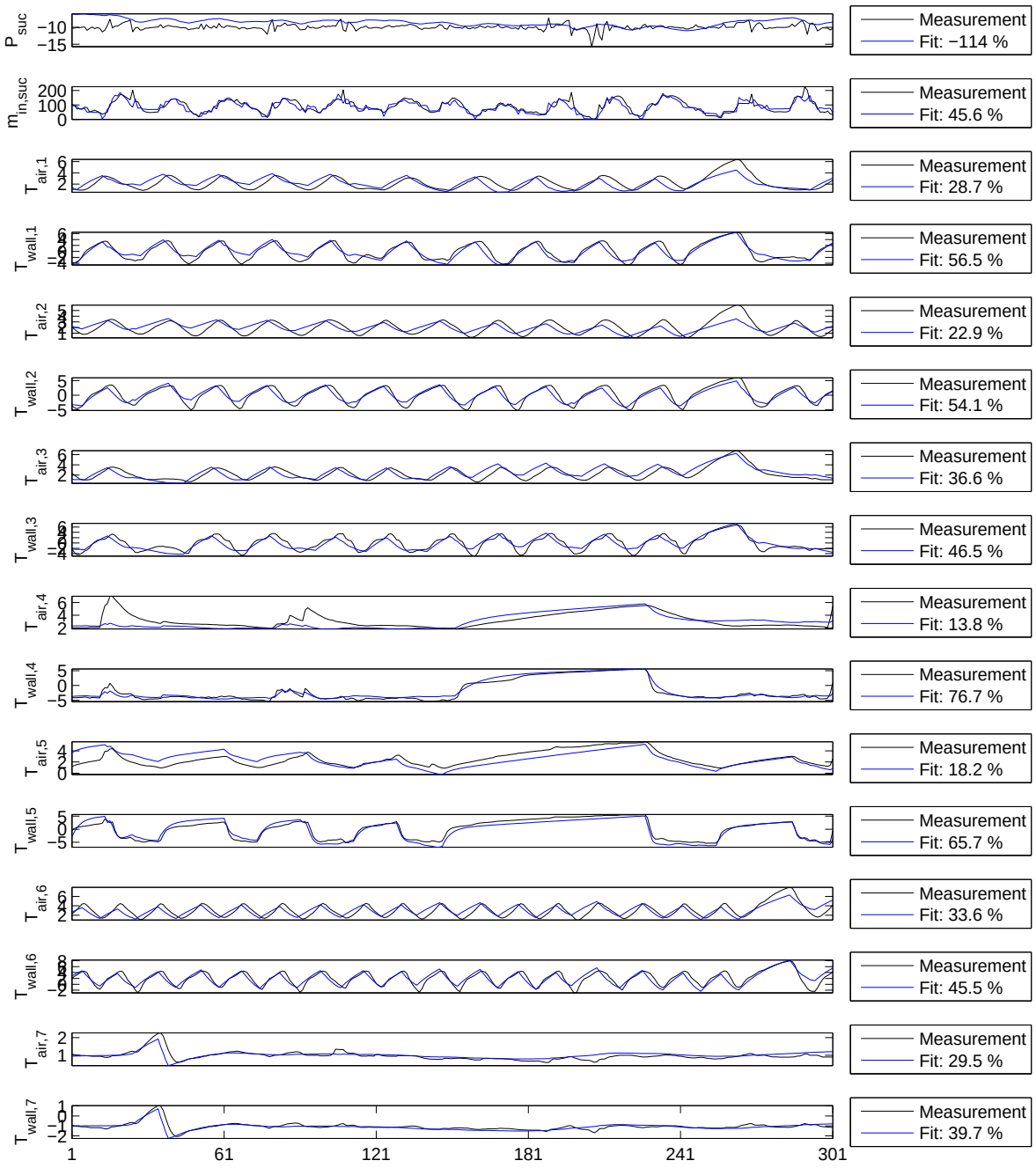

Figure 4: *Validation of the gray-box fit quality using test data. The quality of the fit is high and the model is deemed use-able for control.*

4 Linear Model

When designing a linear controller, whether it might be an MPC or PI-controller, a linear model of the controlled system is advantageous to base the design upon. There are several ways to identify a linear model. In this section a numerical and stochastic black-box method will be considered.

4.1 Numerical Linearization

First the linear model is formed by the first order terms in the Taylor expansion of the system equations. If the point of linearization is at a steady-state of operation the linear model can in short be written

$$\dot{\mathbf{x}} = \mathbf{A}\mathbf{x} + \mathbf{B}\mathbf{u} + \mathbf{E}\mathbf{d} + \sigma_x \tag{4.1a}$$

$$\mathbf{y} = \mathbf{C}_y\mathbf{x} + \mathbf{D}\mathbf{u} + \mathbf{F}_y\mathbf{d} + \sigma_y \tag{4.1b}$$

$$\mathbf{z} = \mathbf{C}_z\mathbf{x} + \mathbf{F}_z\mathbf{d} + \sigma_z \tag{4.1c}$$

The linear system is in continuous time and time invariant. The matrices $\mathbf{A}$, $\mathbf{B}$, $\mathbf{D}$, $\mathbf{E}$, $\mathbf{F}_y$, $\mathbf{F}_z$, $\mathbf{C}_y$ and $\mathbf{C}_z$ are most easily found by a numerical finite difference approximation. The constants, $\sigma_{x,y,z}$, are given by

$$\sigma_x = -\mathbf{A}\underline{\mathbf{x}} - \mathbf{B}\underline{\mathbf{u}} - \mathbf{E}\underline{\mathbf{d}} \quad , \quad \sigma_y = \underline{\mathbf{y}} - \mathbf{C}_y\underline{\mathbf{x}} - \mathbf{D}\underline{\mathbf{u}} - \mathbf{F}_y\underline{\mathbf{d}} \quad , \quad \sigma_z = \underline{\mathbf{z}} - \mathbf{C}_z\underline{\mathbf{x}} - \mathbf{F}_z\underline{\mathbf{d}} \tag{4.2}$$

where the underline indicate a value at steady-state and point of linearization.

The linear model provides the possibility to study how the system behaves by looking at the eigenmodes. These tell about speed of convergence, damping and simply whether the system is stable. The system considered here consists of 15 states, which gives the same number of eigenvalues. From these it was simply found that the system consists of only real stable poles. Their time constants range from 190 to 98,190 seconds, which is a large span and indicate that the system can be difficult to handle by one controller.

4.2 Discrete model

The system is described in continuous-time, but the state estimation and controller are implemented in digital electronics using zero-order-hold. This requires a transformation from continuous to discrete time dynamics. For a system with piecewise constant input and with sampling time T_s, the state at time $k + T_s$ is given by

$$\Delta\mathbf{x}_{k+1} = e^{\mathbf{A}T_s}\Delta\mathbf{x}_k + \int_0^{T_s} e^{\mathbf{A}\tau}\mathbf{B}d\tau\Delta\mathbf{u}_k + \int_0^{T_s} e^{\mathbf{A}\tau}\mathbf{E}d\tau\Delta\mathbf{d}_k$$

which is converted into a linear *difference* equation

$$\begin{aligned}\mathbf{x}_{k+1} &= \overline{\mathbf{A}}\mathbf{x}_k + \overline{\mathbf{B}}\mathbf{u}_k + \overline{\mathbf{E}}\mathbf{d}_k + \sigma_{k,x} \\ \sigma_{k,x} &= -\overline{\mathbf{A}}\underline{\mathbf{x}}_k - \overline{\mathbf{B}}\underline{\mathbf{u}}_k - \overline{\mathbf{E}}\underline{\mathbf{d}}_k\end{aligned}$$

where $\overline{\mathbf{A}}$, $\overline{\mathbf{B}}$ and $\overline{\mathbf{E}}$ are computed by the matrix exponential shown in the expression below (Jørgensen, 2004).

$$\begin{bmatrix}\overline{\mathbf{A}} & \overline{\mathbf{BE}} \\ \mathbf{0} & \mathbf{I}\end{bmatrix} = \exp\left(\begin{bmatrix}\mathbf{A} & \mathbf{BE} \\ \mathbf{0} & \mathbf{0}\end{bmatrix} T_s\right)$$

with $\mathbf{BE}$ equal to $[\mathbf{B}\ \mathbf{E}]$. The future notation will not distinguish between continuous and discrete time system matrices, so the reader has to figure it out from the context i.e. subscript of $\mathbf{x}$.

The system output matrices are not changed and are

$$\begin{aligned}\mathbf{y}_k &= \mathbf{C}_y\mathbf{x}_k + \mathbf{D}\mathbf{u}_k + \mathbf{F}_y\mathbf{d}_k + \sigma_{k,y} \\ \mathbf{z}_k &= \mathbf{C}_z\mathbf{x}_k + \mathbf{F}_z\mathbf{d}_k + \sigma_{k,z}\end{aligned}$$

$$\sigma_{k,y} = \underline{\mathbf{y}}_k - \mathbf{C}_y\underline{\mathbf{x}}_k - \mathbf{D}\underline{\mathbf{u}}_k - \mathbf{F}_y\underline{\mathbf{d}}_k \qquad \sigma_{k,z} = \underline{\mathbf{z}}_k - \mathbf{C}_z\underline{\mathbf{x}}_k - \mathbf{F}_z\underline{\mathbf{d}}_k$$

The choice of sampling period, T_s, is found by trial and error. As a first step to determine the sample period a set of empirical rules have been used given by (Hendricks et al., 2008, p. 545):

$$T_s < \frac{\tau_d}{10} = \frac{400\text{ sec}}{10} = 40\text{ sec} \qquad T_s < \frac{\tau_s}{10} = \frac{100\text{ sec}}{10} = 10\text{ sec}$$

where τ_d and τ_s is the dominant time constant of the process and the closed loop settling time respectively. The trial and error method revealed that the fast dynamics and short settling time made it necessary to use a sample period of $T_s = 20$ sec.

4.3 Black-Box model by PEM

PEM is a method for estimating model parameters using an iterative prediction-error minimization method. This method can also be used to estimate a black-box model from measurements. The state-space will have the form

$$\begin{aligned}\mathbf{x}_{k+1} &= \mathbf{A}\mathbf{x}_k + \mathbf{B}\mathbf{u}_k + \mathbf{K}\mathbf{e}_k \\ \mathbf{y}_k &= \mathbf{C}\mathbf{x}_k + \mathbf{D}\mathbf{u}_k + \mathbf{e}_k\end{aligned}$$

This model is slightly different from the earlier state-space model, since the input and output noise are correlated. Correlated noise has to be handled by both the Kalman filter and the optimal controller (Jørgensen et al., 2011). Through this project only non-correlated noise has been considered and the term **K** is forced to zero in the estimation procedure. Further the system has a different sample time of 1 min.

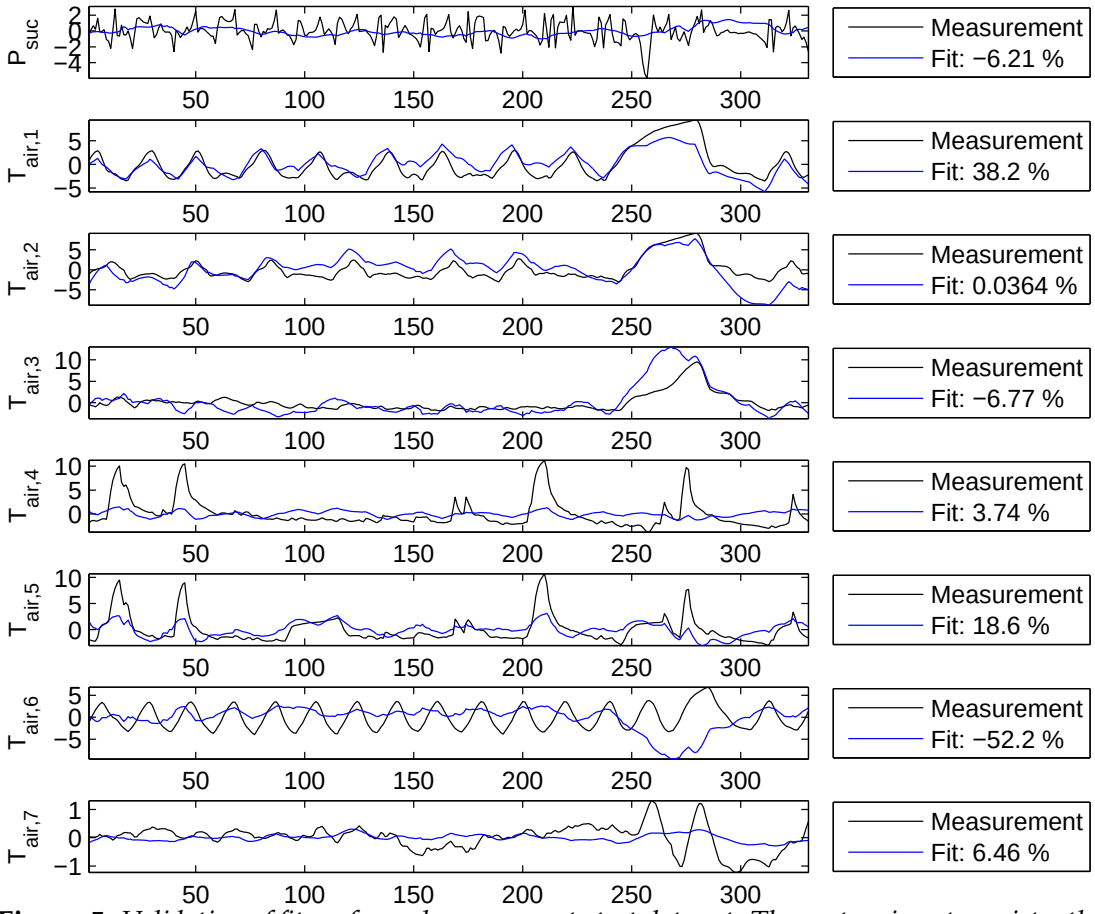

Figure 5: *Validation of fit performed on a separate test data set. The system is not persistently excited and the estimate can therefore not be used.*

As seen, in figure 5, the fit is not good compared to the gray-box estimate. The problem is, that for instance the first three cooling sites are strongly correlated in their response due to a not persistently excited system. Generally this is a problem in the data and the model cannot be estimated correctly. The model can therefore not be used.

5 On-line (load) estimation

The display cases, cold rooms and cooling cabinets in the supermarket are subject to a load disturbance. The sum of all the loads determines the total load which the compressor rack has to remove from the cooling sites in the supermarket. It is therefore obviously of large interest to reduce the load on each cooling site to reduce the total load and thereby the total power consumption. The load on each cooling site originates from a number of individual factors. A number of these are listed below

- Loss of energy through the insulation of the cooling sites
- The new goods are put into the cooling site without the proper temperature
- Customer and employee activity
- Temperature and humidity of the supermarket
- Temperature set-point in the cooling site
- Heat from evaporator fan
- Heat from the lights in the shop
- Defrost action
- Air infiltration from the shop

Some of the disturbances are time depended and will therefore vary over the day. This means that the total load is also time depended which could be utilized by a predictive controller. If the capacity of the compressor rack is limited, as it is on very hot summer days, or if time varying power prices are introduced, the MPC could cool more at night and/or cool when power is cheap without compromising food quality.
The task is to estimate the cooling load as a disturbance (and state of the system). The idea is then, that the owner of the supermarket will be supplied with information about the power consumption of each cooling site, and with that be able to take action in order to reduce the power consumption. In some situations it could be to replace the worst performing cooling site(s) with new more energy efficient ones.

The just estimated model will be used to determine the current refrigeration load of each cooling site. The estimation can be carried out by for instance a linear or nonlinear Kalman filter. The advantage of the linear filter is its simplicity and robustness while the nonlinear filter gives a better estimate sacrificing simplicity and introduces a larger computational burden. Both filters will be investigated.

5.1 Linear Kalman filter

In order to determine the load (and use full state feedback in a controller) an estimator has to be designed. The estimator is essential since it is not possible and/or desirable to measure the load (nor all the states of the system). The task is therefore to estimate the states and disturbances from the available measurements and system inputs. As both measurements and system in general are influenced by noise, the estimation task is to find an estimate which is optimal in some sense. A Kalman filter is optimal in the sense that it minimizes the expected mean-square estimation/prediction error and finds the mean value of the state.

The linear Kalman filter assumes that the observed system is linear and the noise process which corrupts the measurements and system is zero-mean Gaussian random sequences. For non-Gaussian noise and nonlinear systems, the Kalman filter is no longer optimal.

5.1.1 Offset-free estimation

The disturbance estimation is handled by introducing a number of integrators in the model description. In the same way as offset-free control is achieved by introducing integrators in the control loop. Using the same integrators for both purposes make it possible to use the estimator as both a state and disturbance estimator. The system can be controlled offset-free since the number of controlled variables is smaller than the number of inputs and measurements. Further the controlled variables are independent.

The disturbances (and load disturbances) are modeled as either constant input or output-disturbances. The system model from section (4.1) is therefore augmented with the disturbances. The augmented system is then

$$\mathbf{x}_{k+1} = \mathbf{A}\mathbf{x}_k + \mathbf{B}\mathbf{u}_k + \mathbf{G}_d\mathbf{d}_k + \mathbf{v}_k \tag{5.1a}$$
$$\mathbf{d}_{k+1} = \mathbf{d}_k + \mathbf{v}_{d,k} \tag{5.1b}$$
$$\mathbf{p}_{k+1} = \mathbf{p}_k + \mathbf{e}_{d,k} \tag{5.1c}$$
$$\mathbf{y}_k = \mathbf{C}_y\mathbf{x}_k + \mathbf{D}\mathbf{u}_k + \mathbf{G}_p\mathbf{p}_k + \mathbf{G}_{dp}\mathbf{d}_k + \mathbf{e}_k \tag{5.1d}$$

where $\mathbf{d}$ is the input disturbances and $\mathbf{p}$ is the output disturbances. The matrices $\mathbf{G}_d$, $\mathbf{G}_{dp}$ and $\mathbf{G}_p$ describes how the disturbances influence the states. The noise sources of the disturbance states are $\mathbf{v}_{d,k} \in N_{iid}(0, \mathbf{R}_d)$ and $\mathbf{e}_{d,k} \in N_{iid}(0, \mathbf{R}_p)$.

How to choose the structure of the disturbances and noise variances is a challenging task. First of all (Pannocchia and Rawlings, 2003, Lemma 3) states that there has to be as many disturbance states as there are measurements. Further in order to obtain offset-free control the augmented system has to be observable, because the augmented

states are not stable. (Muske and Badgwell, 2002, Theorem 1) states that iff the following condition is satisfied

$$\text{rank}\begin{bmatrix}\mathbf{A}-\mathbf{I} & \mathbf{G}_d & \mathbf{0}\\ \mathbf{C}_y & \mathbf{0} & \mathbf{G}_p\end{bmatrix} = n_x + n_d + n_p \tag{5.2}$$

then the augmented system is observable.
In order to be able to estimate the physical disturbances, such as the load, the input disturbances are chosen equal to the true input disturbance matrix. Further the total number of disturbances has to be equal to the number of measurements. Therefore output disturbances are placed on the temperature measurement of the evaporator. The input and output disturbance matrices are shown below

$$\mathbf{G}_{dp} = \mathbf{F}_y \qquad \mathbf{G}_d = \mathbf{E}_d \qquad \mathbf{G}_p = \begin{bmatrix}0&0&1&0&0&0&...&0&0&0\\0&0&0&0&1&0&...&0&0&0\\0&0&0&0&0&0&...&0&0&0\\0&0&0&0&0&0&...&0&0&0\\0&0&0&0&0&0&...&0&0&0\\0&0&0&0&0&0&...&1&0&0\\0&0&0&0&0&0&...&0&0&1\end{bmatrix}^T \tag{5.3}$$

The size of the elements in $\mathbf{G}_d$, $\mathbf{G}_{dp}$ and $\mathbf{G}_p$ alone are not important, because the size of the elements and the associated noise sources $\mathbf{e}_{d,k}$ and $\mathbf{v}_{d,k}$, determines the speed of which the steady-state error is removed. The noise sources are selected by trial and error where the sensitivity to noise is weighted against the speed of which step disturbances are rejected.
Through numerous simulations it has been found that good performance is achieved with

$$\mathbf{e}_{d,k} \in N_{iid}(0, \mathbf{R}_p); \quad \mathbf{R}_p = \text{diag}\left(\begin{bmatrix}10^{-4} & 10^{-2} & 10^{-4} & 10^{-4} & 10^{-4} & 10^{-4} & 10^{-4}\end{bmatrix}\right) \tag{5.4}$$

$$\mathbf{v}_{d,k} \in N_{iid}(0, \mathbf{R}_d); \quad \mathbf{R}_d = \text{diag}\left(\begin{bmatrix}44.4 & 0.64 & 0.64 & 0.64 & 0.64 & 0.64 & 0.64 & 0.64\end{bmatrix}\right) \tag{5.5}$$

These has been selected so that the disturbances which are likely to change have ”large” variance and those which are not likely to be changed are set to a ”small” value with respect to the absolute size of the disturbance or measurement.
The input and output noise sources are given by

$$\mathbf{e}_k \in N_{iid}(0, \mathbf{R}_2); \quad \mathbf{R}_2 = \text{diag}\left(\begin{bmatrix}15 & 95 & 15 & 15 & 15 & 15 & 15 & 15 & 15\end{bmatrix}\right) \cdot 10^{-4} \tag{5.6}$$

The state noise variance, $\mathbf{R}_{1c}$, has to be transformed to discrete time from continuous time. This is simply done by the transformation in (Poulsen, 2007, p. 231) and the result

is

$$\mathbf{v}_k \in N_{iid}(0, \mathbf{R}_1); \quad \mathbf{R}_1 = \int_0^{T_s} e^{A\tau} \mathbf{R}_{1c} e^{A^T s \tau} d\tau$$

where

$$\mathbf{R}_{1c} = \mathbf{B} \cdot 10^{-5} \cdot \text{diag}\left(\begin{bmatrix} 8.2 \cdot 10^5 & 30 & 30 & 30 & 30 & 30 & 30 & 30 \end{bmatrix} \right) \mathbf{B}^T$$

The noise sources and linear model is now stated and the filter recursions can be made.

5.1.2 The filter

The problem of estimating the system states is handled as a filter problem where the system is given by (5.1). Combining the integral states and the system states into one combined state, $\widetilde{\mathbf{x}}_k$, gives the formulation

$$\widetilde{\mathbf{x}}_{k+1} = \widetilde{\mathbf{A}}\widetilde{\mathbf{x}}_k + \widetilde{\mathbf{B}}\mathbf{u}_k + \widetilde{\sigma}_x + \widetilde{\mathbf{v}}_k \tag{5.7a}$$

$$\mathbf{y}_k = \widetilde{\mathbf{C}}_y\widetilde{\mathbf{x}}_k + \widetilde{\mathbf{D}}\mathbf{u}_k + \widetilde{\sigma}_y + \widetilde{\mathbf{e}}_k \tag{5.7b}$$

which makes the notation of the filter simpler.

The Kalman filter is often grouped into an ordinary and predictive type. The predictive type will be used, where the filter is predicting the state at the next sample, without including the present measurement in the estimate. This gives the computer one sample to compute the control signal, so that it is ready to be applied at the next sample.

The optimal estimate is given by (Poulsen, 2007, paragraph 7.6) and the recursions for the filter are

$$\widehat{\mathbf{x}}_{k+1} = \widetilde{\mathbf{A}}\widehat{\mathbf{x}}_k + \widetilde{\mathbf{B}}\mathbf{u}_k + \widetilde{\sigma}_x + \mathbf{K}_k[\mathbf{y}_k - \widetilde{\mathbf{C}}_y\widehat{\mathbf{x}}_k - \widetilde{\mathbf{D}}\mathbf{u}_k - \widetilde{\sigma}_y] \tag{5.8a}$$

$$\mathbf{K}_k = \widetilde{\mathbf{A}}\mathbf{P}_k\widetilde{\mathbf{C}}_y^T \left[\widetilde{\mathbf{C}}_y\mathbf{P}_k\widetilde{\mathbf{C}}_y^T + \widetilde{\mathbf{R}}_2\right]^{-1} \tag{5.8b}$$

$$\mathbf{P}_{k+1} = \left[\widetilde{\mathbf{A}} - \mathbf{K}_k\widetilde{\mathbf{C}}_y\right] \mathbf{P}_k\widetilde{\mathbf{A}}^T + \widetilde{\mathbf{R}}_1 \tag{5.8c}$$

The filter is derived in details from a combination of a priori and posteriori filter equations in (Simon, 2006, p. 131). The Kalman filter is initialized with $\mathbf{K}_k$ and $\mathbf{P}_k$ equal to the steady-state values $\mathbf{K}_\infty$ and $\mathbf{P}_\infty$. This eliminates the transients where the filter should otherwise converge to these by itself. The steady-state values are found by solving the discrete algebraic Riccati equation (DARE) and calculate the associated Kalman gain.

5.2 Nonlinear Kalman filter

The idea of an Extended Kalman Filter (EKF) is to extend the linear Kalman filter to directly estimate the states of the nonlinear system. The EKF is undoubtedly the most widely used nonlinear state estimation technique that has been applied in the past few decades (Simon, 2006). Unlike its linear counterpart, the extended Kalman filter is in general not an optimal estimator. In addition, if the initial estimate of the state is wrong, or if the process is modeled incorrectly, the filter may quickly diverge. Despite these limitations, the filter often gives superior results.

The nonlinear system model, which the filter is supposed to track, is given by the nonlinear model in section 2. The model is restated below with noise sources and offset-disturbances added

$$\mathbf{x}_{k+1} = \mathbf{f}_{t,k}(\mathbf{x}_k, \mathbf{u}_k, \mathbf{d}_k + \mathbf{d}_0) + \mathbf{v}_k \tag{5.9a}$$
$$\mathbf{d}_{k+1} = \mathbf{d}_k + \mathbf{v}_{d,k} \tag{5.9b}$$
$$\mathbf{p}_{k+1} = \mathbf{p}_k + \mathbf{e}_{d,k} \tag{5.9c}$$
$$\mathbf{y}_k = \mathbf{g}_t(\mathbf{x}_k, \mathbf{u}_k, \mathbf{d}_k + \mathbf{d}_0) + \mathbf{G}_p\mathbf{p}_k + \mathbf{G}_{dp}\mathbf{d}_k + \mathbf{e}_k \tag{5.9d}$$

where the subscript k in $\mathbf{f}_{t,k}$ indicate that the continuous function $\mathbf{f}_t$ is integrated by an ODE solver to get the discrete state evolution. The extended Kalman filter has been derived in many forms and some are presented in (Simon, 2006, p. 400) and (Poulsen, 2007, p. 275). It has been chosen to use the same form of the predictive Kalman filter as the earlier linear filter from Poulsen (2007), but with the nonlinear modifications from Simon (2006).
The state estimate is given by the recursions below

$$\widehat{\mathbf{x}}_{k+1} = \mathbf{f}_{t,k}(\widehat{\mathbf{x}}_k, \mathbf{u}_k, \mathbf{d}_k + \mathbf{d}_0) + \mathbf{K}_k[\mathbf{y}_k - \widehat{\mathbf{y}}_k] \tag{5.10a}$$
$$\mathbf{K}_k = \widetilde{\mathbf{A}}\mathbf{P}_k\widetilde{\mathbf{C}}_y^T\left[\widetilde{\mathbf{C}}_y\mathbf{P}_k\widetilde{\mathbf{C}}_y^T + \widetilde{\mathbf{R}}_2\right]^{-1} \tag{5.10b}$$
$$\mathbf{P}_{k+1} = \left[\widetilde{\mathbf{A}} - \mathbf{K}_k\widetilde{\mathbf{C}}_y\right]\mathbf{P}_k\widetilde{\mathbf{A}}^T + \widetilde{\mathbf{R}}_1 \tag{5.10c}$$

where

$$\widetilde{\mathbf{A}} = \begin{bmatrix} \left.\frac{\partial \mathbf{f}_{t,k}}{\partial \mathbf{x}}\right|_{\widehat{\mathbf{x}}_k,\mathbf{u}_k} & \mathbf{G}_d & \mathbf{0} \\ \mathbf{0} & \mathbf{I} & \mathbf{0} \\ \mathbf{0} & \mathbf{0} & \mathbf{I} \end{bmatrix} \qquad \widetilde{\mathbf{C}}_y = \begin{bmatrix} \left.\frac{\partial \mathbf{g}_{t,k}}{\partial \mathbf{x}}\right|_{\widehat{\mathbf{x}}_k,\mathbf{u}_k} & \mathbf{G}_{dp} & \mathbf{G}_p \end{bmatrix} \tag{5.11}$$

$$\widehat{\mathbf{y}}_k = \mathbf{g}_t(\widehat{\mathbf{x}}_k, \mathbf{u}_k, \mathbf{d}_k + \mathbf{d}_0) + \mathbf{G}_p\mathbf{p}_k \tag{5.12}$$

It can be shown that the system matrices $\mathbf{C}_y$, $\mathbf{D}$ and $\mathbf{F}$ are not depending on the point of linearization and as a consequence do not need to be recomputed at every sample.

5.3 Validation

The two filters are first validated against the nonlinear system model to check their ability to predict the output generated by the system model. Secondly the filters are validated against measured data from Fakta Otterup. Finally the filters are validated against the system model in their ability to estimate the load disturbances.

5.3.1 Model validation

The linear Kalman filter in figure 6 follow the temperatures very close, but with a small error even though it can be difficult to see at the figure. The air and wall temperature estimation error never exceeds 0.2 degrees. The small error is due to the nonlinearities. The nonlinearities are handled by the extended Kalman filter. The estimation error for this filter is always less than 1.1 degrees through the whole period for both the suction pressure and the air temperatures. One should keep in mind that the good results for both filters are due to the fact that the model used in the filters are almost the same as used to generate the data.

The larger error when using the nonlinear filter might be due to the very abrupt excitation of the system, since the more steady suction pressure is better estimated by the extended filter.

5.3.2 True data validation

The filters are also tested using data from the real system. As the data are sampled only every minute and the Kalman filters are sampled every 20 seconds, the data is linearly interpolated between samples. The result is shown in figure 8 and 9. The extended Kalman filter is not performing as good as the linear counter part of the filter. This is seen from the mean square error of the suction pressure and air temperature, not shown here. It is difficult to spot the difference by just inspecting the plots, since the air temperature is spread over such a large span. The maximum estimated error of the air temperature is approx. 0.2 degrees for the linear filter and 1.0 for the nonlinear one.

The same plots as, 8 and 9, but containing the night operation, show that the cooling sites are synchronized. As stated before, the synchronized behavior originates from the coupling of the individual cooling sites through the suction pressure (Larsen, 2005) but also from the defrost planning which are planned to be performed at the same

time. The behavior decreases the lifespan of the compressors and makes the system run uneconomically, when the variable speed compressor cannot meet the cooling request. The novel way of reducing synchronism is to use different upper and lower limits to the hysteresis of the temperature-controllers. This will force them to desynchronize over time.

5.3.3 Disturbance estimation

The ability to estimate the load on the cooling sites are tested against the nonlinear model. This is because it has not been possible to do a real experiment where the load was altered and known. The estimates given by the linear and nonlinear Kalman filter is given in figure 10 and 11 respectively.

The load on the cooling sites are changed 60 minutes after the simulation starts. Both before and after the load is changed, it is noticed that the linear filter do not estimate the load as precise as the extended Kalman filter. Because of the large uncertainty when using the linear filter, it is deemed impossible to use this filter for load estimation. But since the filter show advantageous for state estimation purposes, it will be used for that purpose.

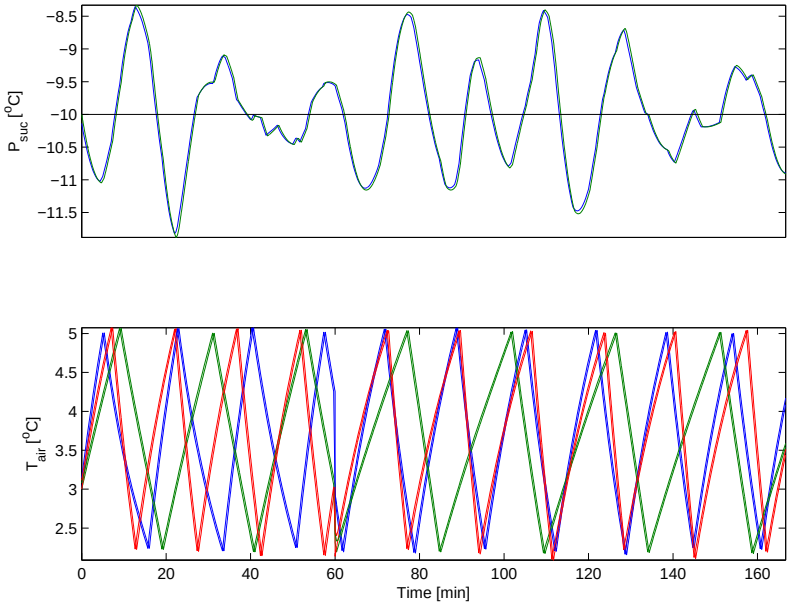

Figure 6: *Validation plot of the 1-step predictor of the simulated output performed by a linear Kalman filter. Only POS 40 A,B and C are shown.*

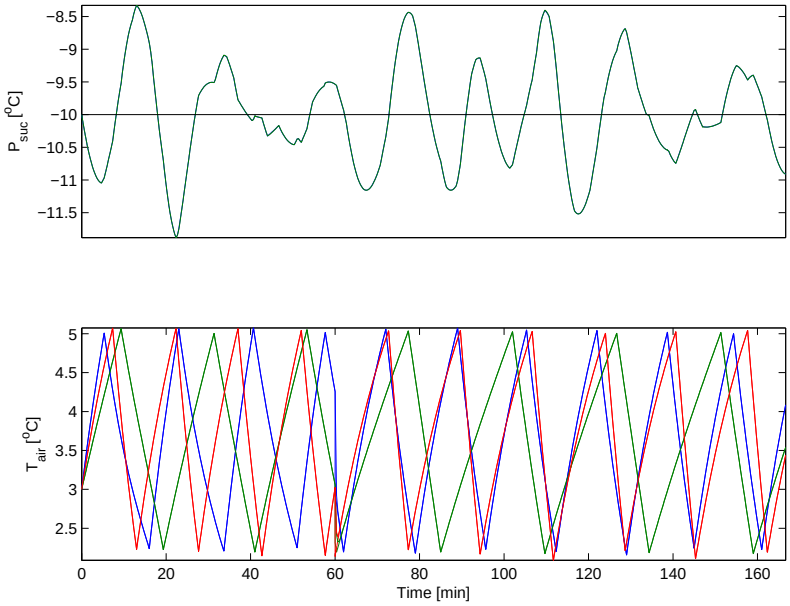

Figure 7: *Validation plot of the 1-step predictor of the simulated output performed by an extended Kalman filter. Only POS 40 A,B and C are shown.*

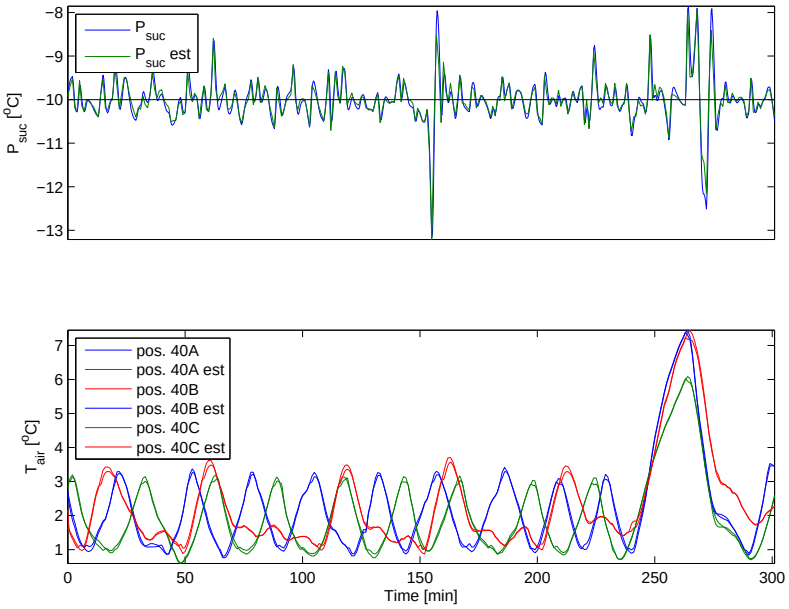

Figure 8: *Validation plot of the 1-step predictor of the measured output performed by a linear Kalman filter. Only POS 40 A,B and C are shown.*

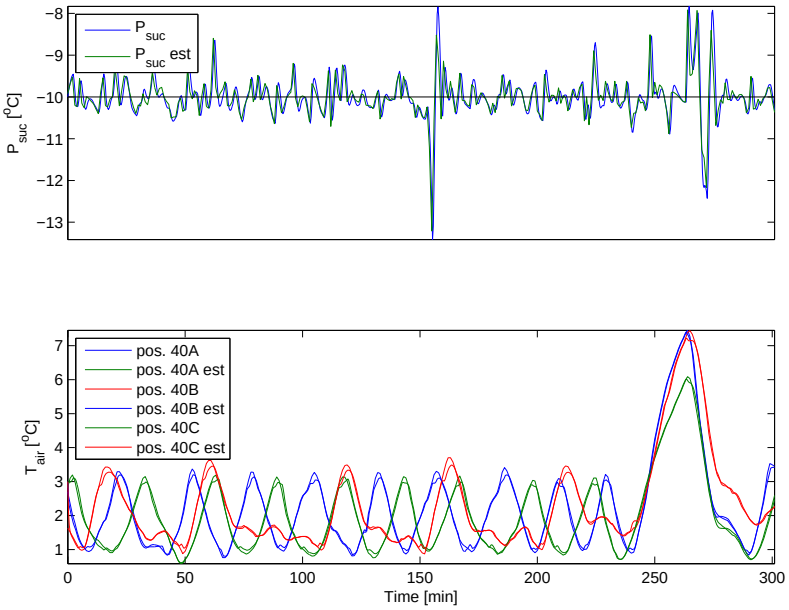

Figure 9: *Validation plot of the 1-step predictor of the measured output performed by an extended Kalman filter. Only POS 40 A,B and C are shown.*

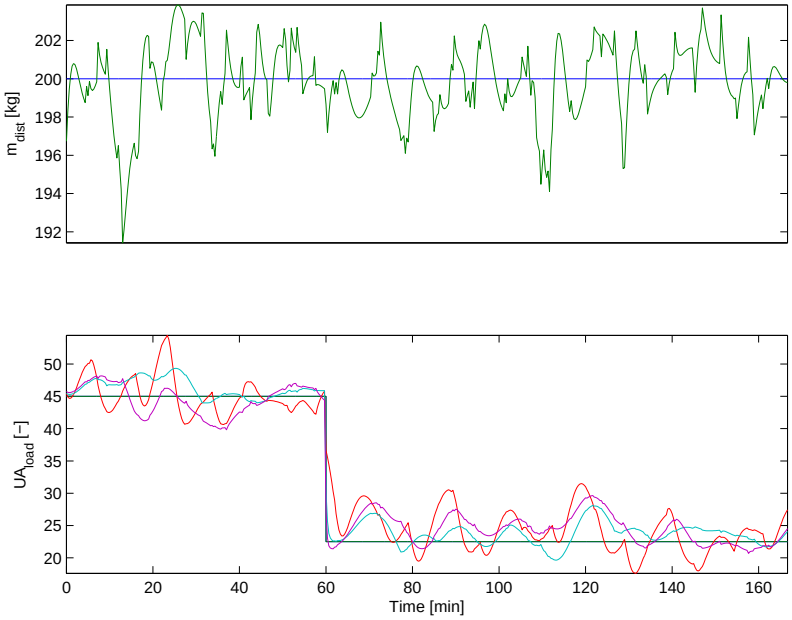

Figure 10: *Validation plot of the 1-step predictor of the simulated disturbance using a linear Kalman filter. Only POS 40 A,B and C are shown.*

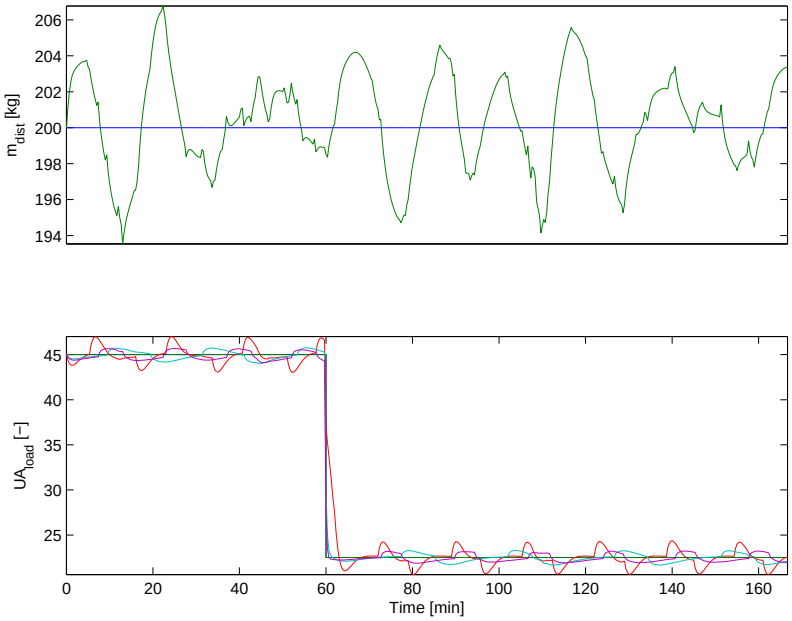

Figure 11: *Validation plot of the 1-step predictor of the simulated disturbance using an extended Kalman filter. Only POS 40 A,B and C are shown.*

6 Model Predictive Control

This chapter describes the development of an MPC. The theory is based on the work of Maciejowski (2002).
The discrete-time system description in (5.1) will be used in the later derivation of the model predictive controller. The ability to reject disturbances and obtain offset-free control, is fulfilled by including the disturbance models in the controller. The controller uses the un-augmented system model, in (4.1), in the predictions while the disturbance states are added to the states and outputs before the control signals are calculated. This reduces the computational load due to the un-controllable integrators.

6.1 Control Problem

In the following the control problem of the MPC will be investigated, and the problem will be transformed to a MI-QP. The MPC uses the objective function in (6.1), which penalizes the future errors between the controlled output and reference plus a term that penalizes control moves.

$$\phi = \frac{1}{2}\sum_{j=1}^{N_z} \|\widetilde{\mathbf{z}}_{k+j|k} - \mathbf{r}_{k+j|k}\|^2_{\mathbf{Q}_z} + \frac{1}{2}\sum_{j=0}^{N_u-1} \|\Delta\mathbf{u}_{k+j|k}\|^2_{\mathbf{S}} \tag{6.1}$$

where $\Delta\mathbf{u}_{k+j|k} = \mathbf{u}_{k+j|k} - \mathbf{u}_{k+j-1|k}$. The control and prediction horizon can be chosen independently, but is chosen identical i.e. $N_z = N_u = N$ in this project. Here the horizon is chosen short, $N = 5\ \text{min}/T_s$, such that the computational load is kept relatively small. The optimal control problem is to minimize the objective function subject to predictions of the controlled outputs, inputs and output constraints.

The objective function is only dependent on the control signal $\mathbf{u}$, the manipulated variables, and the optimization problem is thus to find the control sequence that minimizes the objective function. The constrained control problem is written as

$$\begin{aligned}
\underset{\{u_{k+j|k}\}_{j=0}^{N-1}}{min} \quad & \frac{1}{2}\sum_{j=1}^{N} \|\mathbf{z}_{k+j|k} - \mathbf{r}_{k+j|k}\|^2_{\mathbf{Q}_z} + \frac{1}{2}\sum_{j=0}^{N-1} \|\Delta\mathbf{u}_{k+j|k}\|^2_{\mathbf{S}} & \\
s.t. \quad & \mathbf{x}_{k+1+j|k} = \mathbf{A}\mathbf{x}_{k+j|k} + \mathbf{B}\mathbf{u}_{k+j|k} + \sigma_x & j = 1, 2 \ldots, N-1 \\
& \mathbf{z}_{k+j|k} = \mathbf{C}_z\mathbf{x}_{k+j|k} + \sigma_y & j = 1, 2 \ldots, N \\
& \mathbf{u}_{min} \leq \mathbf{u}_{k+j|k} \leq \mathbf{u}_{max} & j = 0, 1 \ldots, N-1 \\
& \mathbf{u}_{k+j|k} \in [0, 1] & j = 0, 1 \ldots, N-1 \\
& \mathbf{z}_{min} \leq \mathbf{z}_{k+j|k} \leq \mathbf{z}_{max} & j = 1, 2 \ldots, N
\end{aligned}$$

For simplicity the output constraints are written as hard-constraints, but will later be transformed to soft-constraints. The stated constrained control problem is a constrained convex optimization problem, but not in a standard form. To do that it is desirable to rewrite the problem into a vector-matrix form. The objective function depends on future outputs, references and inputs and the following vectors will therefore be defined.

$$\mathbf{Z}_k = \begin{bmatrix} \mathbf{z}_{k+1|k} \\ \mathbf{z}_{k+2|k} \\ \vdots \\ \mathbf{z}_{k+N|k} \end{bmatrix} \quad \mathbf{R}_k = \begin{bmatrix} \mathbf{r}_{k+1|k} \\ \mathbf{r}_{k+2|k} \\ \vdots \\ \mathbf{r}_{k+N|k} \end{bmatrix} \quad \mathbf{U}_k = \begin{bmatrix} \mathbf{u}_{k|k} \\ \mathbf{u}_{k+1|k} \\ \vdots \\ \mathbf{u}_{k+N-1|k} \end{bmatrix} \quad \Delta\mathbf{U}_k = \begin{bmatrix} \Delta\mathbf{u}_{k|k} \\ \Delta\mathbf{u}_{k+1|k} \\ \vdots \\ \Delta\mathbf{u}_{k+N-1|k} \end{bmatrix}$$

$$\boldsymbol{\Sigma}_x = \begin{bmatrix} \sigma_x & \sigma_x & \dots & \sigma_x \end{bmatrix}^T \quad \boldsymbol{\Sigma}_y = \begin{bmatrix} \sigma_y & \sigma_y & \dots & \sigma_y \end{bmatrix}^T$$

The future outputs can be written as

$$\mathbf{z}_{k+j|k} = \mathbf{C}_z\mathbf{A}^j\mathbf{x}_{k|k-1} + \sum_{i=0}^{j-1}\mathbf{C}_z\mathbf{A}^{j-1-i}\mathbf{B}\mathbf{u}_{k+i|k} + \sum_{i=0}^{j-1}\mathbf{C}_z\mathbf{A}^{j-1-i}\sigma_x + \sigma_y \Leftrightarrow$$

$$\mathbf{z}_{k+j|k} = \mathbf{C}_z\mathbf{A}^j\mathbf{x}_{k|k-1} + \sum_{i=0}^{j-1}\mathbf{H}_{j-i}\mathbf{u}_{k+i|k} + \sum_{i=0}^{j-1}\mathbf{L}_{j-i}\sigma_x + \sigma_y$$

where $\mathbf{H}_i = \mathbf{C}_z\mathbf{A}^{i-1}\mathbf{B}$ and $\mathbf{L}_i = \mathbf{C}_z\mathbf{A}^{i-1}$ for $i \geq 1$. The terms originating from $i = 0$ are neglected because it will not change the control actions (Maciejowski, 2002). The above notation makes it possible to rewrite the predictions into the simple vector-matrix notation below

$$\overbrace{\begin{bmatrix} \mathbf{z}_{k+1|k} \\ \mathbf{z}_{k+2|k} \\ \vdots \\ \mathbf{z}_{k+N|k} \end{bmatrix}}^{=\mathbf{Z}_k} = \overbrace{\begin{bmatrix} \mathbf{C}_z\mathbf{A} \\ \mathbf{C}_z\mathbf{A}^2 \\ \vdots \\ \mathbf{C}_z\mathbf{A}^N \end{bmatrix}}^{=\boldsymbol{\Phi}} \widetilde{\mathbf{x}}_{k|k-1} + \underbrace{\overbrace{\begin{bmatrix} \mathbf{H}_1 & 0 & 0 & 0 \\ \mathbf{H}_2 & \mathbf{H}_1 & 0 & 0 \\ \vdots & \ddots & \ddots & 0 \\ \mathbf{H}_N & \cdots & \mathbf{H}_2 & \mathbf{H}_1 \end{bmatrix}}^{=\boldsymbol{\Gamma}} \overbrace{\begin{bmatrix} \mathbf{u}_{k|k} \\ \mathbf{u}_{k+1|k} \\ \vdots \\ \mathbf{u}_{k+N-1|k} \end{bmatrix}}^{\mathbf{U}_k}}_{\mathbf{H}_i=\mathbf{C}\mathbf{A}^{i-1}\mathbf{B} \quad i=1,2,\dots,N} + \dots$$

$$\underbrace{\overbrace{\begin{bmatrix} \mathbf{L}_1 & 0 & 0 & 0 \\ \mathbf{L}_2 & \mathbf{L}_1 & 0 & 0 \\ \vdots & \ddots & \ddots & 0 \\ \mathbf{L}_N & \cdots & \mathbf{L}_2 & \mathbf{L}_1 \end{bmatrix}}^{=\boldsymbol{\Omega}} \overbrace{\begin{bmatrix} \sigma_x \\ \sigma_x \\ \vdots \\ \sigma_x \end{bmatrix}}^{\boldsymbol{\Sigma}_x}}_{\mathbf{L}_i=\mathbf{C}\mathbf{A}^{i-1} \quad i=1,2,\dots,N} + \overbrace{\begin{bmatrix} \sigma_y \\ \sigma_y \\ \vdots \\ \sigma_y \end{bmatrix}}^{\boldsymbol{\Sigma}_y}$$

Simplifying the notation gives

$$\mathbf{Z}_k = \mathbf{\Phi}\mathbf{x}_{k|k-1} + \mathbf{\Gamma}\mathbf{U}_k + \mathbf{\Omega}\mathbf{\Sigma}_x + \mathbf{\Sigma}_y \tag{6.2}$$

It is now possible to rewrite the first term in (6.1) into the vector-matrix notation

$$\phi = \frac{1}{2}\sum_{j=1}^{N} \|\mathbf{z}_{k+j|k} - \mathbf{r}_{k+j|k}\|^2_{\mathbf{Q}_z} = \frac{1}{2}\|\mathbf{Z}_k - \mathbf{R}_k\|^2_{\mathbf{Q}_z} = \tag{6.3}$$

$$\frac{1}{2}\|\mathbf{\Gamma}\mathbf{U}_k - \left(\mathbf{R}_k - \mathbf{\Phi}\mathbf{x}_{k|k-1} - \mathbf{\Omega}\mathbf{\Sigma}_x - \mathbf{\Sigma}_y\right)\|^2_{\mathbf{Q}_z} \tag{6.4}$$

To reduce the length of the equations the constant $\widetilde{\mathbf{b}}$ is defined as

$$\mathbf{b}_k = \mathbf{\Phi}\mathbf{x}_{k|k-1} + \mathbf{\Omega}\mathbf{\Sigma}_x + \mathbf{\Sigma}_y \tag{6.5}$$

The problem above is the well-known Weighted Least Squares problem. In order to arrive at a QP the expression is expanded, utilizing $\|\mathbf{x}\|^2_{\mathbf{Q}} = \mathbf{x}^T\mathbf{Q}\mathbf{x}$. From this, it is seen that the problem easily can be factored into a quadratic and a linear term plus a constant.

$$\phi = \frac{1}{2}\mathbf{U}_k^T\mathbf{\Gamma}_k^T\mathbf{Q}_z\mathbf{\Gamma}_k\mathbf{U}_k - \left(\mathbf{\Gamma}_k^T\mathbf{Q}_z(\mathbf{R}_k - \mathbf{b}_k)\right)^T\mathbf{U}_k + \frac{1}{2}(\mathbf{R}_k - \mathbf{b}_k)^T\mathbf{Q}_z(\mathbf{R}_k - \widetilde{\mathbf{b}}_k)$$

This is a QP, but only weighing the deviation from the reference. Only solving for this part will result in a minimum variance controller, because no penalty is put on the control actions. The penalty of using the manipulated variables is put into the optimization problem in the same way as the penalty for the output deviations. As before it is desirable to write the cost in terms of vectors. The cost is

$$\frac{1}{2}\sum_{j=0}^{N-1} \|\Delta\mathbf{u}_{k+j|k}\|^2_{\mathbf{S}} = \frac{1}{2}\|\mathbf{U}_k - \mathbf{U}_{k-1}\|^2_{\mathbf{S}} \tag{6.6}$$

Since the optimization problem only depends on $\mathbf{U}_k$ and not $\mathbf{U}_{k-1}$ a rewriting is made to eliminate $\mathbf{U}_{k-1}$. The rewriting is based on the fact that $\mathbf{U}_{k-1}$ is just the delayed version of $\mathbf{U}_k$. Putting the above on matrix-vector form gives

$$\overbrace{\begin{bmatrix}\Delta\mathbf{u}_{k|k}\\ \Delta\mathbf{u}_{k+1|k}\\ \vdots\\ \Delta\mathbf{u}_{k+N|k}\end{bmatrix}}^{=\Delta\mathbf{U}_k} = \overbrace{\begin{bmatrix}\mathbf{I} & 0 & 0 & 0\\ -\mathbf{I} & \mathbf{I} & 0 & 0\\ 0 & \ddots & \ddots & 0\\ 0 & 0 & -\mathbf{I} & \mathbf{I}\end{bmatrix}}^{=\mathbf{\Psi}} \overbrace{\begin{bmatrix}\mathbf{u}_{k|k}\\ \mathbf{u}_{k+1|k}\\ \vdots\\ \mathbf{u}_{k+N|k}\end{bmatrix}}^{=\mathbf{U}_k} - \overbrace{\begin{bmatrix}\mathbf{I}\\ 0\\ \vdots\\ 0\end{bmatrix}}^{=\mathbf{I}_0} \mathbf{u}_{k-1}$$

With a further simplification of the notation it becomes

$$\Delta\mathbf{U}_k = \mathbf{\Psi}\mathbf{U}_k - \mathbf{I}_0\mathbf{u}_{k-1} \tag{6.7}$$

where $\mathbf{u}_{k-1}$ is treated as a constant which is updated each sample. The cost associated with the control moves are therefore

$$\frac{1}{2}\sum_{j=0}^{N-1}\|\Delta\mathbf{u}_{k+j|k}\|_{\mathbf{S}}^2 = \frac{1}{2}\|\mathbf{\Psi}\mathbf{U}_k - \mathbf{I}_0\mathbf{u}_{k-1}\|_{\mathbf{S}}^2 \tag{6.8}$$

The expression needs to be written into the standard form of a QP and combined with (6.6). Again the expression has the form of a Weighted Least Squares problem and the problem can be factored into a quadratic and linear term plus a constant

$$\phi = \frac{1}{2}\mathbf{U}_k^T\mathbf{\Psi}^T\mathbf{S}\mathbf{\Psi}\mathbf{U}_k - \left(\mathbf{\Psi}^T\mathbf{S}\mathbf{I}_0\mathbf{u}_{k-1}\right)^T\mathbf{U}_k + \frac{1}{2}(\mathbf{I}_0\mathbf{u}_{k-1})^T(\mathbf{I}_0\mathbf{u}_{k-1})$$

The QP just derived is also constrained by input constraints and it will be handled in the following. The input constraints are also vectorized and the future input signals should satisfy

$$\mathbf{u}_{min} \leq \mathbf{u}_{k+j|k} \leq \mathbf{u}_{max} \quad j = 0, 1, \ldots, N$$

Writing the constraints in vector-matrix form gives

$$\overbrace{\begin{bmatrix}\mathbf{u}_{k,min}\\ \mathbf{u}_{k+1,min}\\ \vdots\\ \mathbf{u}_{k+N,min}\end{bmatrix}}^{=\mathbf{U}_{min}} \leq \overbrace{\begin{bmatrix}\mathbf{u}_{k|k}\\ \mathbf{u}_{k+1|k}\\ \vdots\\ \mathbf{u}_{k+3|k}\end{bmatrix}}^{=\mathbf{U}_k} \leq \overbrace{\begin{bmatrix}\mathbf{u}_{k,max}\\ \mathbf{u}_{k+1,max}\\ \vdots\\ \mathbf{u}_{k+N,max}\end{bmatrix}}^{=\mathbf{U}_{max}}$$

and with notation simplification it gives

$$\mathbf{U}_{min} \leq \mathbf{U}_k \leq \mathbf{U}_{max} \tag{6.9}$$

6.2 Soft Output Constraints

One of the primary reasons for using MPC is that constraints can be enforced on the process. If hard-constraints are implemented on the output there could be feasibility problems since situations will arise where no control sequence can satisfy the constraints. To solve this problem it is utilized that the output constraints are not physical limitations and these constraints can be enforced in a relaxed way so that guaranteed feasibility is maintained.

The time varying hard output constraints are

$$\mathbf{z}_{min,k} \leq \mathbf{z}_{k+j|k} \leq \mathbf{z}_{max,k} \quad j = 1, 2 \ldots, N-1 \tag{6.10}$$

These constraints can be avoided by allowing a violation of the output constraints, by adding a combined quadratic and linear-term to the objective function. This method is described by Scokaert and Rawlings (1999) and Prasath and Jørgensen (2009). The cost function then becomes

$$\phi = \frac{1}{2}\sum_{j=1}^{N} \|\mathbf{z}_{k+j|k} - \mathbf{r}_{k+j|k}\|^2_{\mathbf{Q}_z} + \frac{1}{2}\sum_{j=0}^{N-1} \|\Delta\mathbf{u}_{k+j|k}\|^2_{\bar{\mathbf{S}}} + \sum_{j=1}^{N} \frac{1}{2}\|\boldsymbol{\eta}_{k+j|k}\|^2_{\mathbf{S}_\eta} + \mathbf{S}^T_{\boldsymbol{\eta}_{k+j|k}}\boldsymbol{\eta}_k$$

where $\boldsymbol{\eta}$ is an introduced slack-variable that converts the hard constraints in (6.10), into soft constraints as shown below.

$$\begin{aligned} \mathbf{z}_{k+j|k} &\leq \mathbf{z}_{max,k} + \boldsymbol{\eta}_{k+j|k} \quad j = 1, 2, \ldots, N \\ \mathbf{z}_{k+j|k} &\geq \mathbf{z}_{min,k} - \boldsymbol{\eta}_{k+j|k} \quad j = 1, 2, \ldots, N \\ \boldsymbol{\eta}_{k+j|k} &\geq \mathbf{0} \quad j = 1, 2, \ldots, N \end{aligned}$$

As seen the relaxation i.e. soft constraints are only active when the hard output constraints should have been active. This is important because it does not change the objective function under unconstrained operation. If an output constrain becomes active it forces $\boldsymbol{\eta}$ to some positive value which makes the associated terms in the cost function greater than zero. In this way the constraints are obeyed by using a suitable weight $\mathbf{S}_\eta$.

As before it is desirable to rewrite the cost function into the simple vector-matrix notation. The terms originating from the soft output constraints are then

$$\sum_{j=1}^{N} \frac{1}{2}\|\boldsymbol{\eta}_{k+j|k}\|^2_{\mathbf{S}_\eta} + \mathbf{S}^T_{\boldsymbol{\eta}_k}\boldsymbol{\eta}_{k+j|k} = \frac{1}{2}\boldsymbol{\eta}_k\mathbf{S}_\eta\boldsymbol{\eta}_k + \mathbf{S}^T_{\boldsymbol{\eta}_k}\boldsymbol{\eta}_k \tag{6.11}$$

The constraints are dependent on $\mathbf{z}_{k+j|k}$ which is a function of $\mathbf{u}_{k+j|k}$. The constraints has to be put in vector/matrix notation and thus the expression for $\mathbf{Z}_k$ in (6.2) can be used to express the constraints as a function of $\mathbf{U}_k$. This gives

$$\begin{aligned} &\mathbf{Z}_{min,k} - \boldsymbol{\eta}_k \leq \mathbf{Z}_k \leq \mathbf{Z}_{max,k} + \boldsymbol{\eta}_k \Leftrightarrow \\ &\mathbf{Z}_{min,k} - \mathbf{b}_k - \boldsymbol{\eta}_k \leq \boldsymbol{\Gamma}_k\mathbf{U}_k \leq \mathbf{Z}_{max,k} - \mathbf{b}_k + \boldsymbol{\eta}_k \Leftrightarrow \\ &\overline{\mathbf{Z}}_{min,k} - \boldsymbol{\eta}_k \leq \boldsymbol{\Gamma}_k\mathbf{U}_k \leq \overline{\mathbf{Z}}_{max,k} + \boldsymbol{\eta}_k \\ &\boldsymbol{\eta}_k \geq \mathbf{0} \end{aligned}$$

where

$$\begin{aligned} \overline{\mathbf{Z}}_{min,k} &= \mathbf{Z}_{min,k} - \mathbf{b}_k \\ \overline{\mathbf{Z}}_{max,k} &= \mathbf{Z}_{max,k} - \mathbf{b}_k \end{aligned}$$

The complete Model Predictive Controller is now defined, but it has to be put into one QP.

7 MPC Quadratic Program

The above derivation of the controller is collected into one MI-QP. The problem below is the control problem with soft-constraints.

$$\begin{aligned} \underset{\mathbf{X}_k}{min} \quad & \frac{1}{2}\mathbf{X}_k^T\overline{\mathbf{H}}\mathbf{X}_k + \overline{\mathbf{g}}^T\mathbf{X}_k + \overline{\boldsymbol{\rho}} && (7.1a) \\ s.t. \quad & \mathbf{X}_{min} \leq \mathbf{X}_k \leq \mathbf{X}_{max} && (7.1b) \\ & \mathbf{b}_l \leq \mathbf{A}\mathbf{X}_k \leq \mathbf{b}_u && (7.1c) \\ & \mathbf{X}_{sub} \in [0,1] && (7.1d) \end{aligned}$$

where

$$\mathbf{X} = \begin{bmatrix} \mathbf{U}_k \\ \boldsymbol{\eta}_k \end{bmatrix} \qquad \overline{\mathbf{H}} = \begin{bmatrix} \mathbf{H} & \mathbf{0} \\ \mathbf{0} & \mathbf{S}_{\boldsymbol{\eta}_k} \end{bmatrix} \qquad \overline{\mathbf{g}} = \begin{bmatrix} \mathbf{g} \\ \mathbf{S}_{\boldsymbol{\eta}_k} \end{bmatrix} \tag{7.2a}$$

$$\mathbf{X}_{min} = \begin{bmatrix} \mathbf{U}_{min} \\ \mathbf{0} \end{bmatrix} \qquad \mathbf{X}_{max} = \begin{bmatrix} \mathbf{U}_{max} \\ \infty \end{bmatrix} \tag{7.2b}$$

$$\mathbf{b}_l = \begin{bmatrix} -\infty \\ \overline{\mathbf{Z}}_{min,k} \end{bmatrix} \qquad \mathbf{A} = \begin{bmatrix} \boldsymbol{\Gamma}_k & -\mathbf{I} \\ \boldsymbol{\Gamma}_k & \mathbf{I} \end{bmatrix} \qquad \mathbf{b}_u = \begin{bmatrix} \overline{\mathbf{Z}}_{max,k} \\ \infty \end{bmatrix} \tag{7.2c}$$

$\overline{\boldsymbol{\rho}}$ is omitted because the solution $\mathbf{U}_k^*$ does not depend on it. $\mathbf{X}_{sub}$ is the integer subset of variables from the $\mathbf{U}$ vector that represents the valves. The soft-constraints add variables to the optimization problem, i.e. make the problem larger, but guarantees a solution. The above convex QP is solved every sample and gives the solution, $\mathbf{U}_k^*$, which is a set of control signals for the complete control horizon. At each sample only the first control action is used i.e. $\mathbf{u}_0^*$.

The problem is a MI-QP due to the combination of integer and floating values in $\mathbf{X}$. In order to solve this type of problems one need a (commercial) solver. Just to mention a few there is Cplex (Ilog, Inc.), Xpress-MP (Dash Optimization) and Mosek (Mosek ApS). The Mosek solver is used in this project because its free for academic use and it integrates very well with the Matlab environment. The downside of Mosek is its speed, which showed to be very slow. For later system comparison, a simulation using floating point valve control has also been made. For this optimization problem the standard Matlab solver, quadprog(), was used.

Control weights

The performance (index) is highly dependent on the weighting matrices $\mathbf{Q}_z$, $\mathbf{S}$ and $\mathbf{S}_{\eta_k}$ which are used to achieve the desired performance of the control system. The matrix $\mathbf{Q}_z$ weighs the error of the controlled variables and $\mathbf{S}$ the change-rate of the manipulated variables. An increase in a weight will decrease the variance of the associated controlled or manipulated variable. $\mathbf{S}_{\eta_k}$ weighs how much it should be penalized to violate a constraint. The cost of violating a constraint is much higher than the penalty of error and control moves. For the QP to converge at a minimizer the weights are restricted to be positive semi-definite.

Integer valve positions

The weights on the controlled variables are chosen so, that it penalizes a deviation of the suction pressure from the set-point. The air temperatures should not be kept at a set-point. It should instead be controlled within a band. To achieve this behavior the deviation from the set-point is penalized by zero and soft-constraints are set to keep the temperatures within a defined region. The control actions are penalized by a small weight on the compressor control and a relatively large weight on changing the valve position. This will prevent the valves from opening and closing in a PWM manner.

$$\mathbf{Q}_z = \begin{bmatrix} 50 & 0 & 0 & 0 \\ 0 & 0 & 0 & 0 \\ 0 & 0 & 0 & 0 \\ 0 & 0 & 0 & 0 \end{bmatrix} \qquad \mathbf{S} = \begin{bmatrix} 10^2 & 0 & 0 & 0 \\ 0 & 10^4 & 0 & 0 \\ 0 & 0 & 10^4 & 0 \\ 0 & 0 & 0 & 10^4 \end{bmatrix} \qquad \mathbf{S}_\eta = \begin{bmatrix} 10^3 & 0 & 0 & 0 \\ 0 & 10^5 & 0 & 0 \\ 0 & 0 & 10^5 & 0 \\ 0 & 0 & 0 & 10^5 \end{bmatrix}$$

The block diagonal matrices used in the MPC deviation are then

$$\mathbf{Q}_z = \begin{bmatrix} \mathbf{Q}_z & 0 & 0 \\ 0 & \ddots & 0 \\ 0 & 0 & \mathbf{Q}_z \end{bmatrix} \qquad \mathbf{S} = \begin{bmatrix} \mathbf{S} & 0 & 0 \\ 0 & \ddots & 0 \\ 0 & 0 & \mathbf{S} \end{bmatrix} \qquad \mathbf{S}_\eta = \begin{bmatrix} \mathbf{S}_\eta & 0 & 0 \\ 0 & \ddots & 0 \\ 0 & 0 & \mathbf{S}_\eta \end{bmatrix}$$

The performance of the controller is validated in the later section. Notice that only three cooling sites are operated by this controller, otherwise the computational load exceeds the sample time.

Floating point valve positions

The control structure was originally designed for floating point valve positions and solving this control problem is very easy, by just replacing the Mosek solver with the

quadprog solver. The only modification to the integer setup is the control weights. By trial and error good performance was achieved using the weights below

$$\mathbf{Q}_z = \begin{bmatrix} 4.0 & 0 & 0 & 0 \\ 0 & 11.11 & 0 & 0 \\ 0 & 0 & 11.11 & 0 \\ 0 & 0 & 0 & 11.11 \end{bmatrix} \quad \mathbf{S} = \begin{bmatrix} 0.0816 & 0 & 0 & 0 \\ 0 & 0.1 & 0 & 0 \\ 0 & 0 & 0.1 & 0 \\ 0 & 0 & 0 & 0.1 \end{bmatrix} \quad \mathbf{S}_\eta = \begin{bmatrix} 10^2 & 0 & 0 & 0 \\ 0 & 10^2 & 0 & 0 \\ 0 & 0 & 10^2 & 0 \\ 0 & 0 & 0 & 10^2 \end{bmatrix}$$

The performance of the controller is validated in the later section. Again only three cooling discs are modeled for simplicity.

Constraints

In the following the constraints on the manipulated and controlled variables, **u** and **z**, will be given. In general, these are found from process and actuator knowledge, which in this case are restrictions to the air temperature in the cooling sites and constraints to the compressor bank and valves at the cooling sites.

The soft-constraints on the output are chosen so that safe operation is maintained. Safe operation means that the air temperature is maintained within a band, so that food quality is preserved. It is assumed that the air of all three cooling sites should be bounded within 0 to 5 degrees. The suction pressure is chosen to be within -20 to 0 degrees, which it should never reach in normal operation. The input constraints are naturally chosen so that the valves are operated between 0 and 100%. The same goes for the compressor which is operated from 0 to 100% load.

The constraints are shown in table 1.

Type	Signal	Units	Min.	Max.
Output	P_{suc}	°C	-20	0
	$T_{air,i}$	°C	0	5
Input	$comp$	%	0	100
	OD_i	%	0	100

Table 1: *List of constraints that are used by the MPC.* $i \in [1;2;3]$.

8 Validation

The performance of the controller is investigated by simulations. The performance is highly dependent on the state-estimate and since the linear filter showed superior performance when validated by real data, only the linear Kalman filter will be used. The closed-loop performance with the linear MPC and Kalman filter will be investigated here.

Integer valve positions

The integer valued control setup has been simulated for 200 min. The result is shown in figure 12 and 13. The simulation is made without noise, but still the suction pressure is clearly disturbed. The disturbance is self-inflicted and originates from valves turning on and off in the cooling sites. Inspecting data from Fakta Otterup shows that the effect is also visible in real life and the problem get worse when the compressors are not able to deliver the requested capacity. Using completely variable speed compressors and/or floating point valve control will significantly reduce these problems.

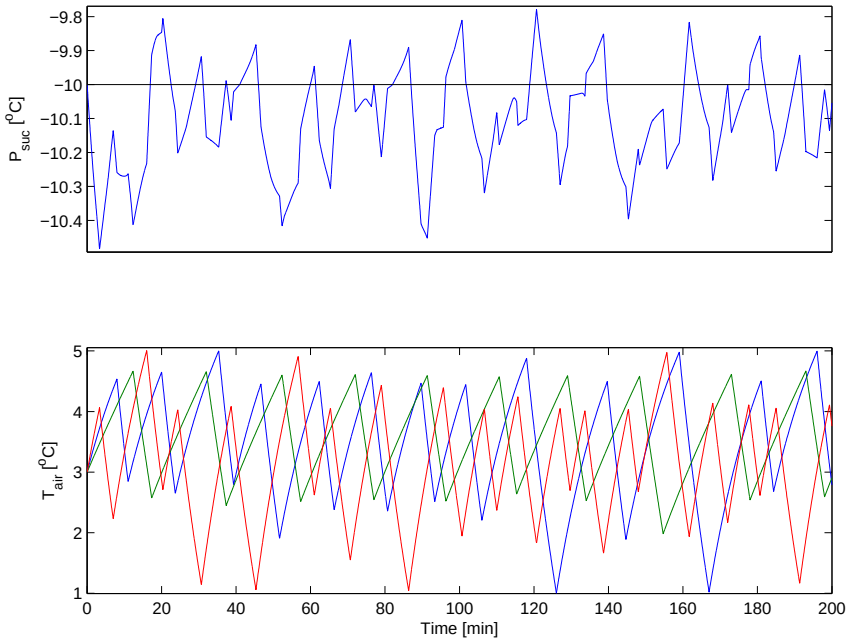

Figure 12: *Plot of outputs using integer controlled valves. No disturbances present.*

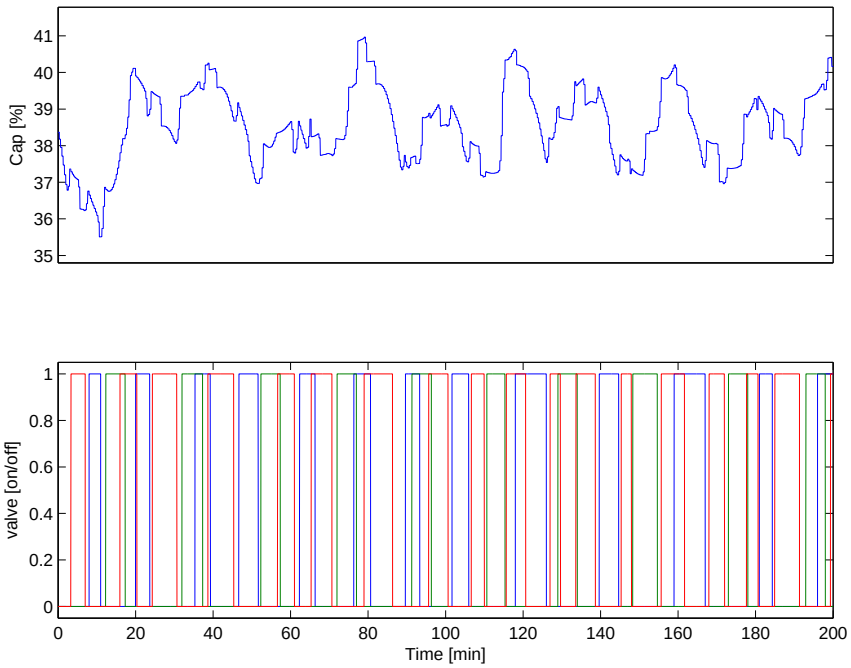

Figure 13: *Plot of inputs using integer controlled valves. No disturbances present.*

The simulation also shows that despite the bad nature of the system, the cooling sites are desynchronized within a short period of time to reduce the fluctuation of the suction pressure. This means that the control system works for this state of operation. The controller is also able to handle the significant change in load due to opening and closing of the supermarket. Figure 14 and 15 shows the simulation where the load on the display cases and bypassed refrigerant is decreased to 50% at time 40 min into the simulation.

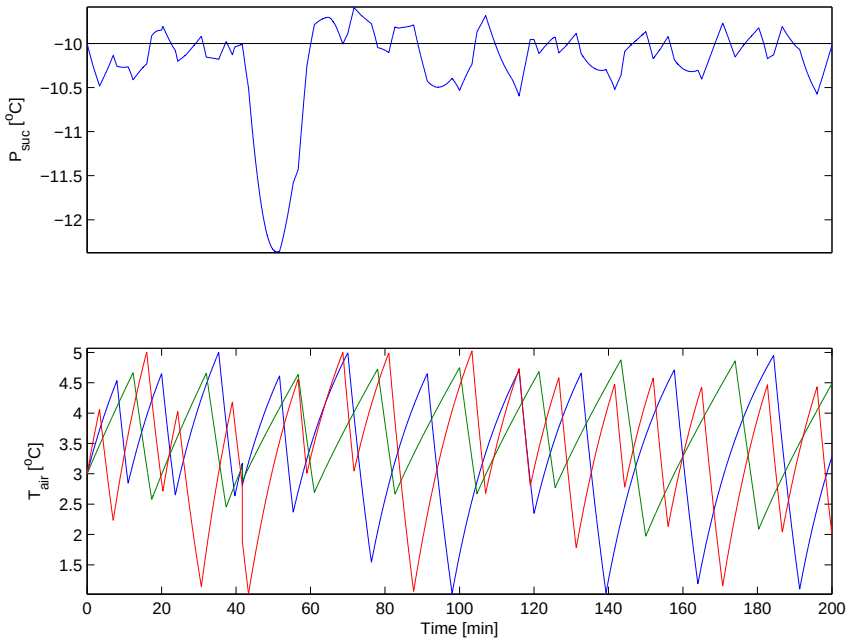

Figure 14: *Plot of outputs using integer controlled valves while hit by a 50% reduction in load and bypass ref. at t=40 min.*

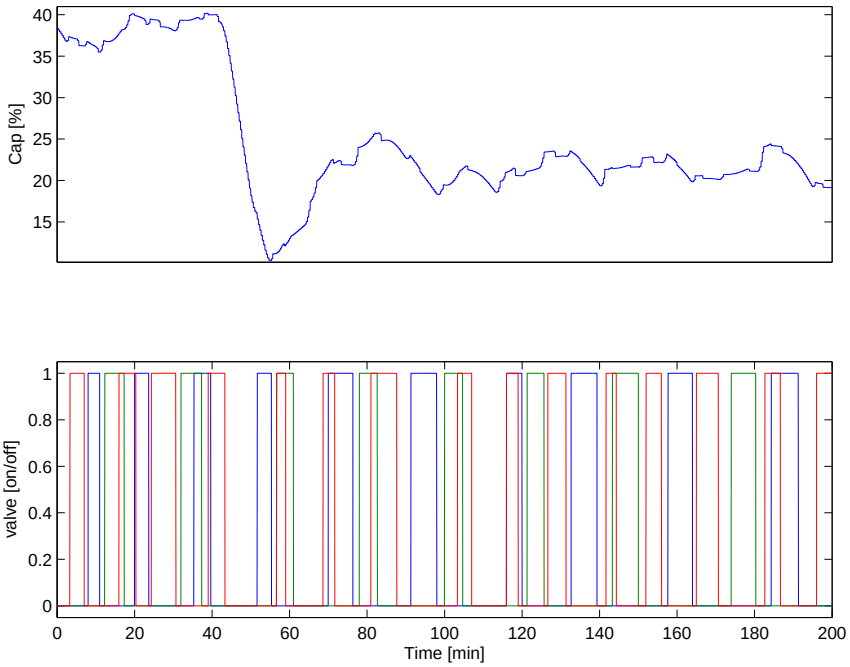

Figure 15: *Plot of inputs using integer controlled valves while hit by a 50% reduction in load and bypass ref. at t=40 min.*

Floating point valve positions

The floating point control setup has been simulated for 100 min. The result is shown in figure 16 and 17. The simulation consists of 3 events. First the temperature reference is changed from 3 to 4 degrees, then the load is decreased by 50% to simulate when the supermarket closes and last the bypassed flow of mass is set to zero. The first event, from 8 to 25 min where the temperature reference is changed, clearly makes the temperature in the cooling sites change. It takes approximately 15 min to reach a new steady-state and in the meantime the valves rapidly closes to increase the temperature. This has the side effect that the requested cooling drops and the compressor compensates to keep the suction pressure constant. Notice that the requested cooling capacity is lower after the temperature has been increased. The second event occurs 40 min into the simulation, where the load is decreased by 50%. This leads to a smaller load on the cooling site which must be compensated by the valves to keep the desired air temperature. Until the load has been rejected the air experiences a large decrease in temperature for about 20 min. The decrease is not serious due to the short period and seldom occurrence. Notice the fact that the load is not the dominant source of heat, but $\dot{Q}_{fan}$ is. This is clear from the small change in opening degree after the load has changed. $\dot{Q}_{fan}$ do not only originates from the fans, but also from air infiltration and freezing of moisture in the air. Last the bypassed refrigerant is set to zero at time 75 min, which reduce the load on the compressors. The disturbance clearly shows up in the suction pressure until the compressor has stabilized at the new steady-state. This is due to the penalization of the change of compressor capacity. As seen the required compressor capacity has dropped after it has settled, as expected.

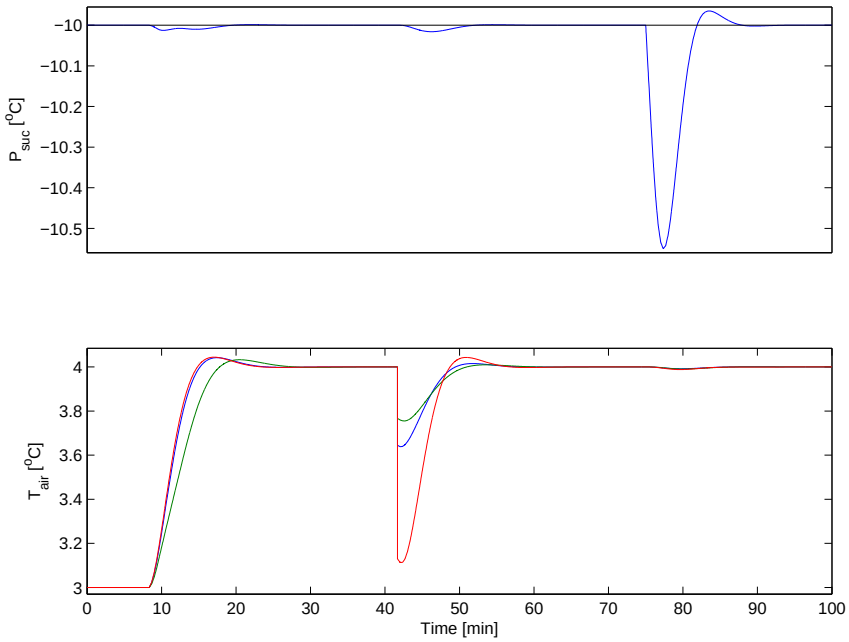

Figure 16: *Plot of outputs for floating point controlled valves.*

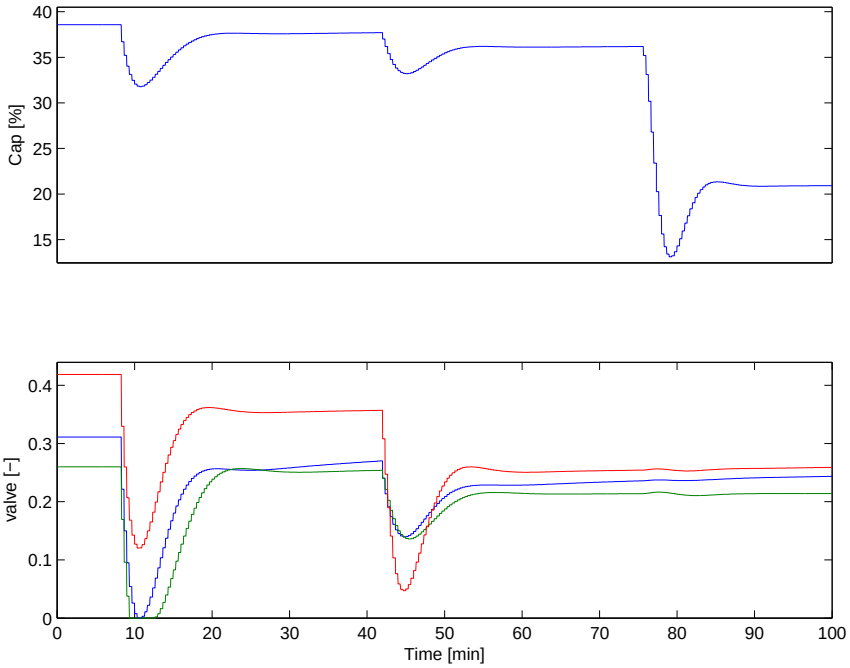

Figure 17: *Plot of inputs for floating point controlled valves.*

The two simulations clearly shows that it is a huge advantage to use floating point valve control, since it reduce the self-inflicted disturbance of the suction pressure. The

advantage is then that the compressor control will get more stable and the suction pressure could get increased when allowed by the ADAP KOOL controller. Thus reducing energy consumption. The disadvantage is that the evaporators will more often be half full of refrigerant or so and ice will build up. Danfoss has developed an expansion valve that distribute the refrigerant and therefore eliminate the problem. It is highly recommended to use this type of AKV.

The faster computation time of solving a QP compared to a MIQP results in the possibility to increase the prediction horizon. Increasing it from the previous 5 minutes to 10 minutes gives better damped responses and shorter settling time. The computational time increases from 0.0048 to 0.018 seconds when increasing the prediction horizon to 10 minutes.

Part II

Compressor Control

The idea that motivates this part of the project is to design a compressor control that stabilizes the suction pressure by utilizing both feedback and feedforward. The suction pressure, the controlled variable, is used as feedback and the opening and closing of valves in the cooling sites are used as feedforward. Feedforward of disturbances have shown very effective in many applications (such as district heating) and is deemed to improve performance. As in part 1 of the report, the proposed controller will be based on Model Predictive Control (MPC). The advantage of this controller is its ability to handle the system dynamics, constraints and disturbances.

9 Modeling

The dynamics of the suction pressure is very fast and thus has to be controlled by a fast sampling control system. The present data is sampled every 1 min and is not fast enough to capture all the fast (and important) dynamics of the system. Still it has been tried to estimate a simple PEM model which gave the fit as shown in figure 18 and 19. The first figure shows how well the model fits the training data and the second figure shows how well the model fits the test data. The two data series are slit so that the test dataset continues the training dataset. The output of the dataset is the suction pressure and the inputs are the running compressor capacity and the seven opening degrees of the valves of the cooling sites.

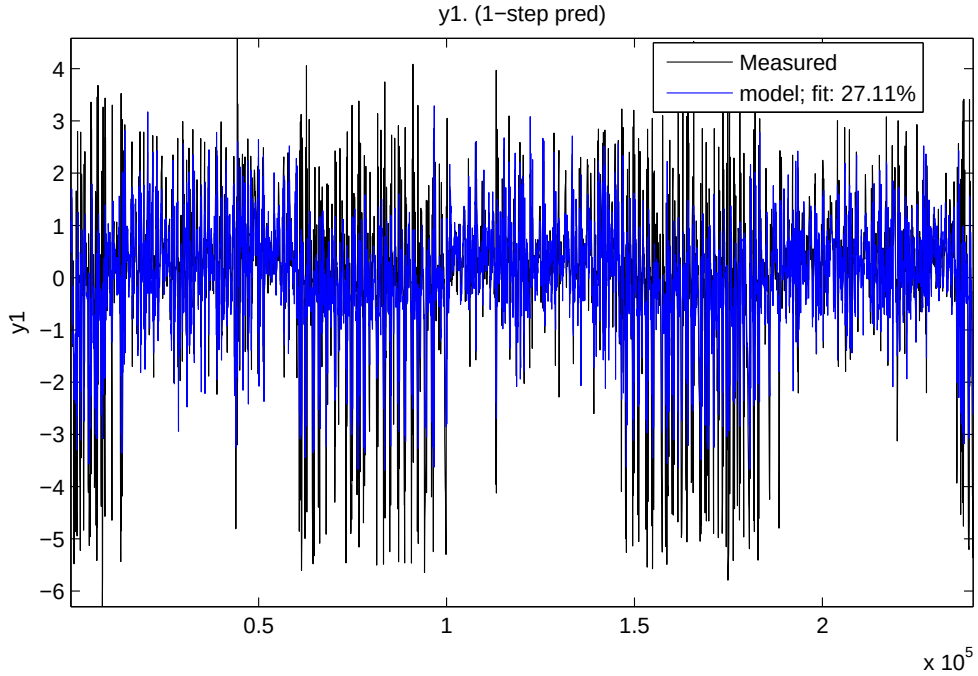

Figure 18: *Suction pressure; Training data and model response for the 1-step predictor. X-axis is no. of samples. $T_s = 60$ sec*

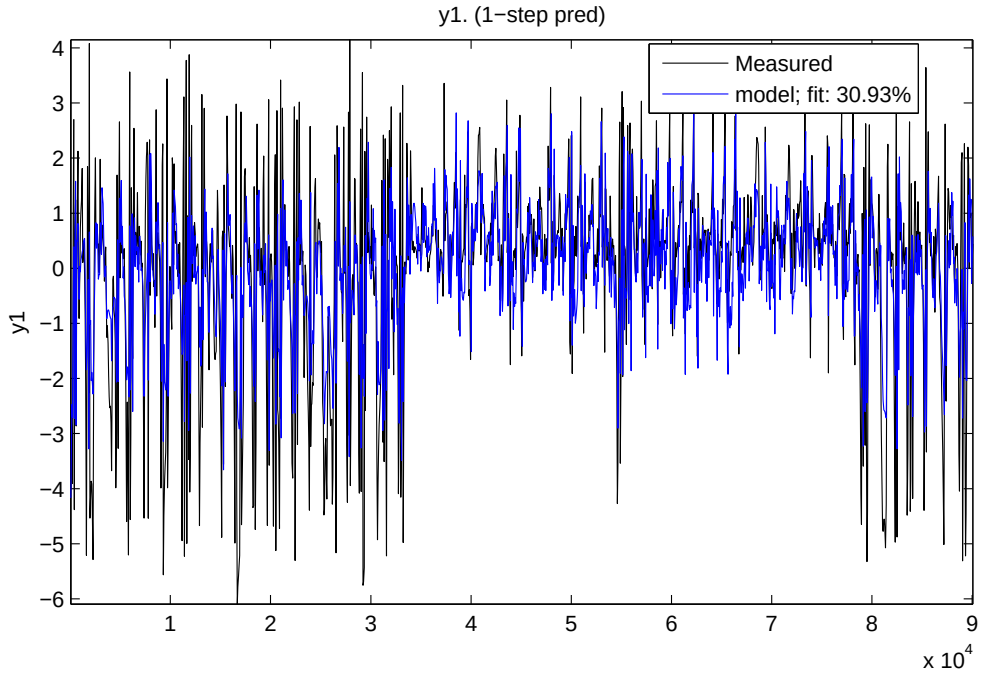

Figure 19: *Suction pressure; Test data and model response for the 1-step predictor. X-axis is no. of samples. $T_s = 60$ sec*

Figure 18 and 19 shows that the model, stated in equation 9.1, has captured all the slow dynamics but cannot explain the high frequency noise. The noise might arise from start/stop of compressors and the fact that the valves actually are PMW controlled can also have an impact. Examining the residuals, in figure 20, show that the model have captured much of the information in the data, since the residuals are almost white noise.

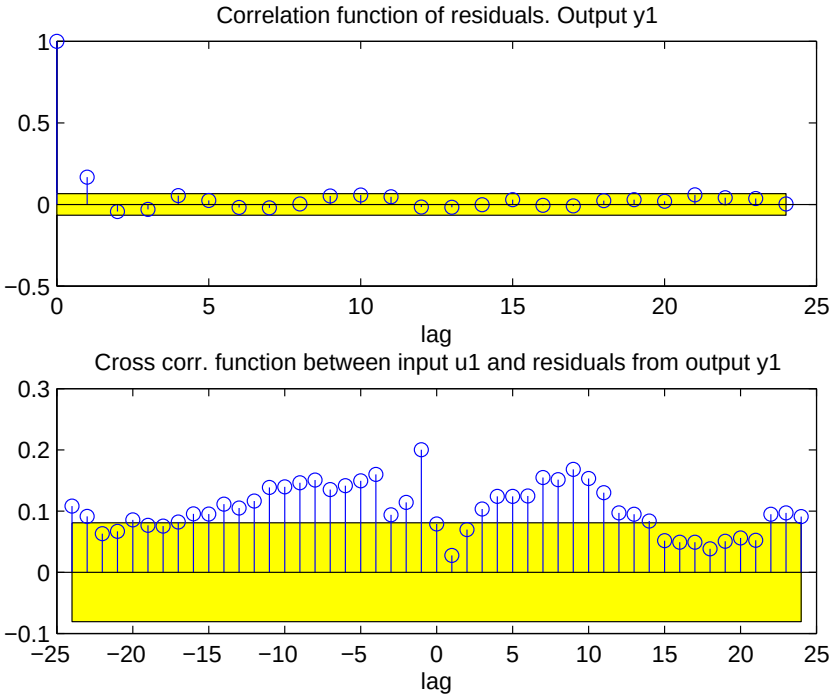

Figure 20: *Residual evaluation using test data from compressor to suction pressure.*

The plotted residuals are based on the test data. The estimated state-space model was estimated using the PEM black-box estimator in Matlab. The model was estimated with focus on prediction and gave the result

$$\mathbf{x}_{k+1} = \mathbf{A}\mathbf{x}_k + \mathbf{B}\mathbf{u}_k + \mathbf{E}\mathbf{d}_k + \mathbf{K}\mathbf{e}_k \tag{9.1a}$$

$$\mathbf{y}_k = \mathbf{C}\mathbf{x}_k + \mathbf{e}_k \tag{9.1b}$$

with

$$\mathbf{A} = \begin{bmatrix} 0 & 1 & 0 \\ 0 & 0 & 1 \\ 0.029258 & -0.60552 & 1.424 \end{bmatrix} \quad \mathbf{B} = \begin{bmatrix} -0.10943 \\ 0.00866 \\ 0.0068899 \end{bmatrix} \quad \mathbf{C}^T = \begin{bmatrix} 1 \\ 0 \\ 0 \end{bmatrix} \quad \mathbf{K} = \begin{bmatrix} 0.34529 \\ 0.1221 \\ 0.10108 \end{bmatrix}$$

$$\mathbf{E} = \begin{bmatrix} 0.016301 & 0.78675 & 1.0763 & 0.94925 & 0.45373 & 1.5324 & 0.98432 & 0.93104 \\ 0.0036179 & 0.20164 & 0.1983 & 0.31112 & 0.12109 & 0.17796 & 0.35645 & -0.26475 \\ 0.0023047 & 0.22852 & 0.30776 & 0.32694 & 0.089884 & 0.22146 & 0.34994 & -0.14564 \end{bmatrix}$$

The input, $\mathbf{u}$, is the running compressor capacity and the output, $\mathbf{y}$, is the suction pressure. The disturbances are running fridge compressor capacity and the seven akv opening degrees. A step response analysis show that the suction pressure will drop approx. 0.1 degree by increasing the running compressor capacity by 1%. Notice that the model and system is sampled every minute, $T_s = 60$ sec, where else the earlier model is based on 20 sec sampling.

The bad fitting quality / percent, shown in figure 18 and 19, indicate that it has not been possible to estimate the system model. Therefore it has been decided not to develop a new controller.

10 Control

The present strategy is to stabilize the suction pressure by a PI-controller, without feed-forward, which determine a requested compressor capacity. To meet the requested capacity a scheduler is used to determine which compressors should be running at present time. Often one of the compressors are fitted with a frequency converter making it easier to meet the requested capacity. Decoupling the controller and scheduler is advantageous since it simplifies the controller. A future MPC setup should also utilize this structure, since an MPC including scheduler will have to solve a computational difficult mixed integer optimization problem.

It was not possible to identify a system model with sufficient accuracy, and the controller has not been designed. As mentioned earlier, this is due to the sample time of 60 sec, which is too slow for identification of a model for compressor control.

Part III

System Performance

A supermarket is one of the most electricity-intensive types of retail stores. This is due to the need for refrigeration of the foodstuff, which uses a large amount of electricity. Some states that energy expenses represent the most significant portion of the annual operating budget after labor costs for the grocery retail sector. At the same time the profit margins of supermarkets are thin, and reducing the cost of operation i.e. energy consumption is an increasing concern to the supermarket owners.

The supermarket owners do not have the deep insight and most of all tools to optimize operation of the refrigeration system. Therefore they often face difficulties in identifying potential savings and how to achieve these savings. In order to assist these in their effort this part of the project has concentrated on estimating the load of each cooling site, as well as the total load and give a measure of how well the total refrigeration system is performing. The performance measure of the total refrigeration system will offer an opportunity to identify the worst performing supermarkets and therefore identify the most cost-effective and rewarding opportunities for energy savings. Knowledge of the energy consumption of each cooling site makes it possible to identify which are performing badly and therefore reveal the potential of replacing/upgrading to a more energy efficient cooling site. All in all the information can be used to improve system efficiency.

The refrigeration system is sketched in figure 21, to give a brief overview of the position of sensors and naming convention.

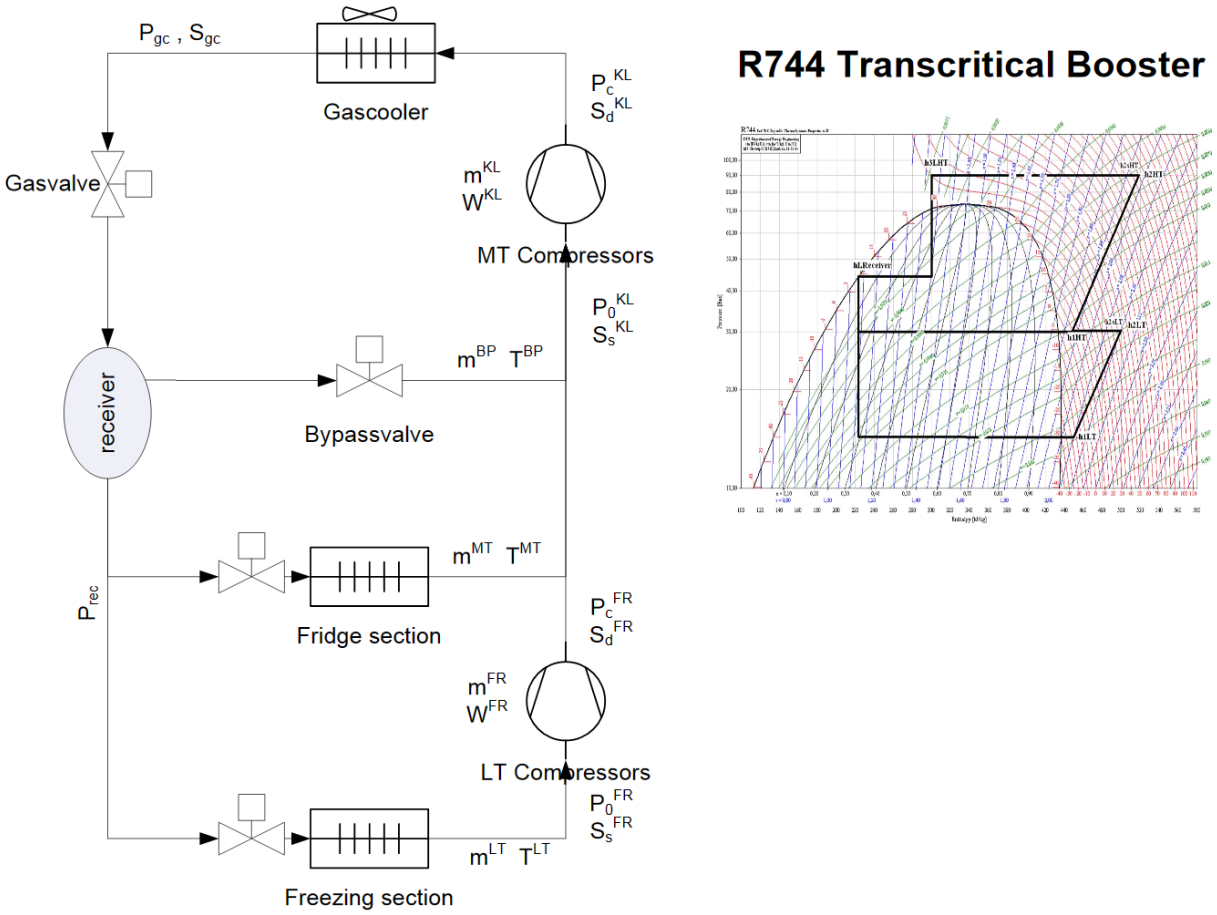

Figure 21: *Description of the system and naming convention.*

11 Cooling Site Energy Consumption

Normally it is not possible to determine the energy consumption of each cooling site, since mass flow meters are very expensive. Fakta Otterup has been fitted with mass flow sensors measuring, among others, the total flow of refrigerant used by all seven fridges and all four freezers in the store respectively. Using these sensors makes it possible to estimate the refrigeration load from each cooling site. For this purpose valve size knowledge, opening degree, pressure difference and other factors are also used in order to determine how much each of the cooling sites contributes to the total flow of refrigerant.

11.1 Theoretical Load from OD

Initially engineers consult the specifications delivered by the expansion valve manufacturer, in order to estimate the theoretical capacity or load of a cooling site. The valves are known and so is their theoretical capacity. A part of the data-sheet belonging to the Danfoss valves used in Fakta Otterup is shown in figure 22. The relation below is used to determine the delivered capacity given the size, opening degree of the valve and pressure difference across the valve. The relation is

$$\dot{Q}_{akv} = f\left(\text{AKV}, P_{rec} - P_0\right) \cdot \text{OD} \tag{11.1}$$

where f is a function of the pressure difference and valve type/size. OD is the opening degree. P_{rec} is the reciever pressure and P_0 is the suction pressure. The characteristic of the valve is nonlinearly dependent on the pressure difference, and f is therefore described by the previously mentioned valve specific table.

R 744

Valve type	Capacity in kW at pressure drop across valve Δp bar								
	2	4	6	8	10	12	14	16	18
AKV 10 - 1	0.8	1.1	1.3	1.5	1.7	1.8	2.0	2.1	2.2
AKV 10 - 2	1.2	1.7	2.1	2.4	2.7	2.9	3.2	3.4	3.6
AKV 10 - 3	2.0	2.8	3.4	3.9	4.3	4.8	5.1	5.5	5.8
AKV 10 - 4	3.1	4.3	5.3	6.2	6.8	7.5	8.1	8.7	9.1
AKV 10 - 5	4.8	6.8	8.3	9.6	10.7	11.7	12.7	13.5	14.3
AKV 10 - 6	7.7	10.8	13.2	15.3	17.0	18.7	20.2	21.5	22.7
AKV 10 - 7	12.2	17.3	21.0	24.5	27.2	29.8	32.3	34.4	36.3
AKV 15 - 1	19.1	27.0	32.9	38.3	42.6	46.7	50.5	53.8	56.9
AKV 15 - 2	30.6	43.2	52.6	61.2	68.1	74.7	80.8	86.1	91.0
AKV 15 - 3	48.2	68.2	82.9	96.5	107	118	127	136	143
AKV 15 - 4	76.5	108	132	153	170	187	202	215	227
AKV 20 - 1	76.5	108	132	153	170	187	202	215	227
AKV 20 - 2	122	173	210	245	272	298	323	344	363
AKV 20 - 3	191	270	329	383	426	467	505	538	569
AKV 20 - 4	306	432	526	612	681	747	808	861	910
AKV 20 - 5	482	682	829	965	1074	1177	1273	1357	1434

Figure 22: *List of delivered capacity as a function of pressure across the valve and type.*

Table 22 is based on ideal conditions where the refrigerant only consists of liquid at a certain temperature, no sub-cooling and no energy loss in the pipes. Further the table is not corrected for the evaporation temperature. These conditions will reduce the accuracy of the relation since the conditions can be far from satisfied in real life conditions.

The seven fridges and four freezers have all been fitted with a Danfoss valve as follows;

Fridges	POS 40A	POS 40B	POS 40C	POS 30	POS 30B	POS 45	POS 50
Valve type	AKV 10-5	AKV 10-5	AKV 10-4	AKV 10-5	AKV 10-3	AKV 10-5	AKV 10-2

Freezers	POS 25A	POS 25B	POS 25C	POS 20
Valve type	AKV 10-2	AKV 10-2	AKV 10-2	AKV 10-3

The resulting refrigeration load, calculated by (11.1), of each fridge and freezer cooling sites are plotted in figure 23 and 24 respectively. The noise in the data originates from the fact that the cooling sites are actually controlled by a hysteresis controller giving a time varying load. Notice that the data is heavily low-pass filtered to remove dynamic effects from the hysteresis controller. Low-pass filtering is performed by using `smooth(.)` in Matlab.

POS 40 A, B and C have almost the exact same behavior. This is due to the similarities in construction and usage of the three sites. The sites is not covered in day time and constructed like a shelf. This gives large variations between night and day and an overall high energy consumption. POS 30(B) cools a fridge room, giving variations in the load due to employee activity. POS 45 chills vegetables and is therefore very similar to POS 40 in usage and construction. POS 50 is a covered display case containing meet, which has to the chilled at a very certain temperature. The AKV of the site is therefore continuously controlled which gives very stable and low refrigeration load. The spikes in load is due to defrosting. All the freezers have a continuously controlled AKV and is covered to reduce energy usage. As the figure indicate this gives a very stable load which does not show day and night variations. The large spikes in load is due to defrosting.

Estimating the load from the AKV's have shown to be rather good. The AKV load is investigated by summing the individual AKV contributions and compare it to the total cooling load measured by a sensor. The result is shown in figure 25 and 26 (Blue line is the AKV estimate and Green line is the measured load).

The combined AKV load is calculated by the relation below.

$$\dot{Q}_{akv}^{MT} = \sum_{i=1}^{7} \dot{Q}_{akv,i}^{MT} \qquad \dot{Q}_{akv}^{LT} = \sum_{i=1}^{4} \dot{Q}_{akv,i}^{LT} \tag{11.2}$$

The summed AKV load is only slightly low-pass filtered to make comparison easier (assuming that the mass-flow meter receives a low-pass filtered flow of energy).

The load is measured by a coriolis mass flow meter. Knowing the enthalpy of the refrigerant and the flow of mass, makes it possible to calculate the load. The energy

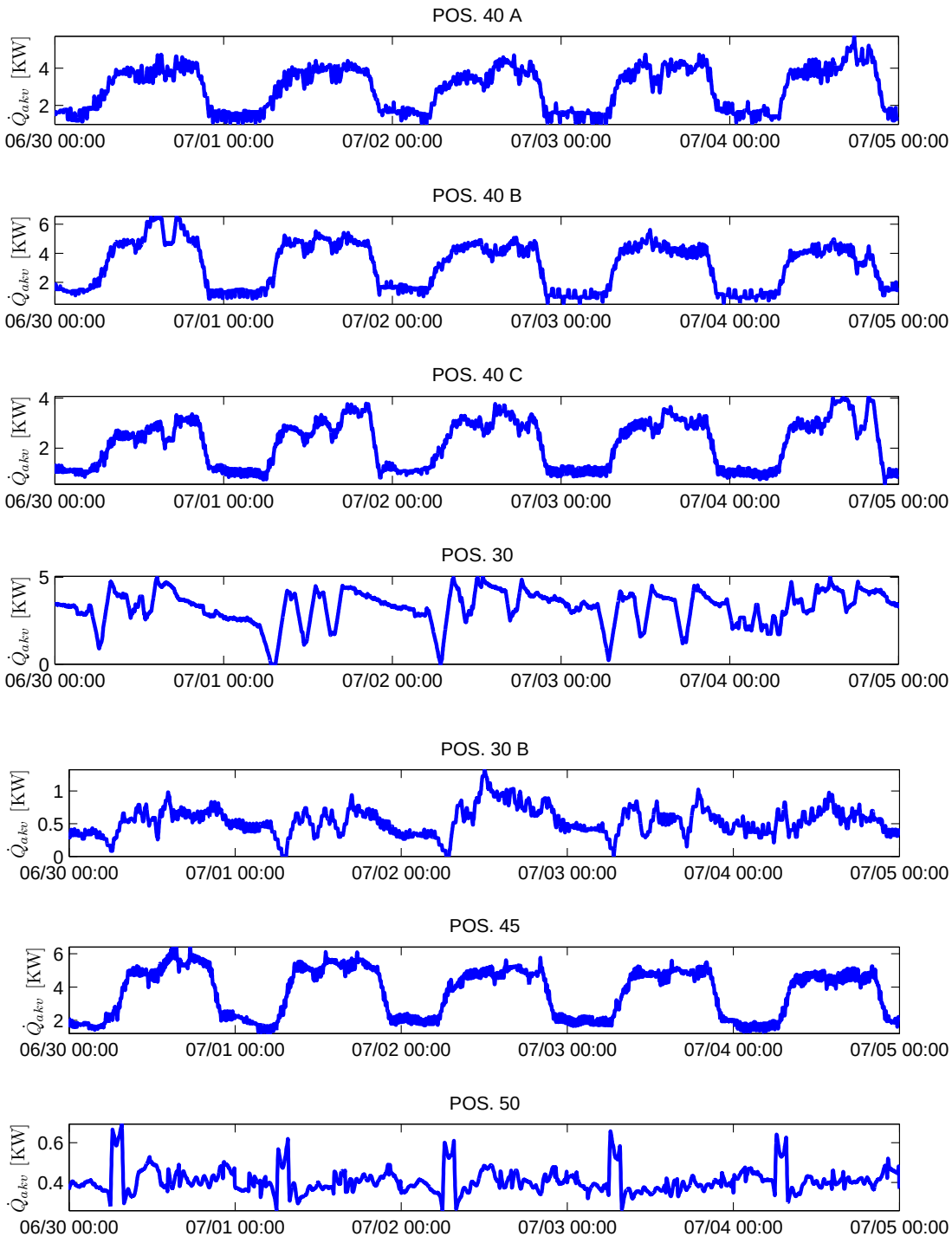

Figure 23: *Individual load for each cooling site. The data is sub-sampled to remove dynamic behavior and only 5 days are shown.*

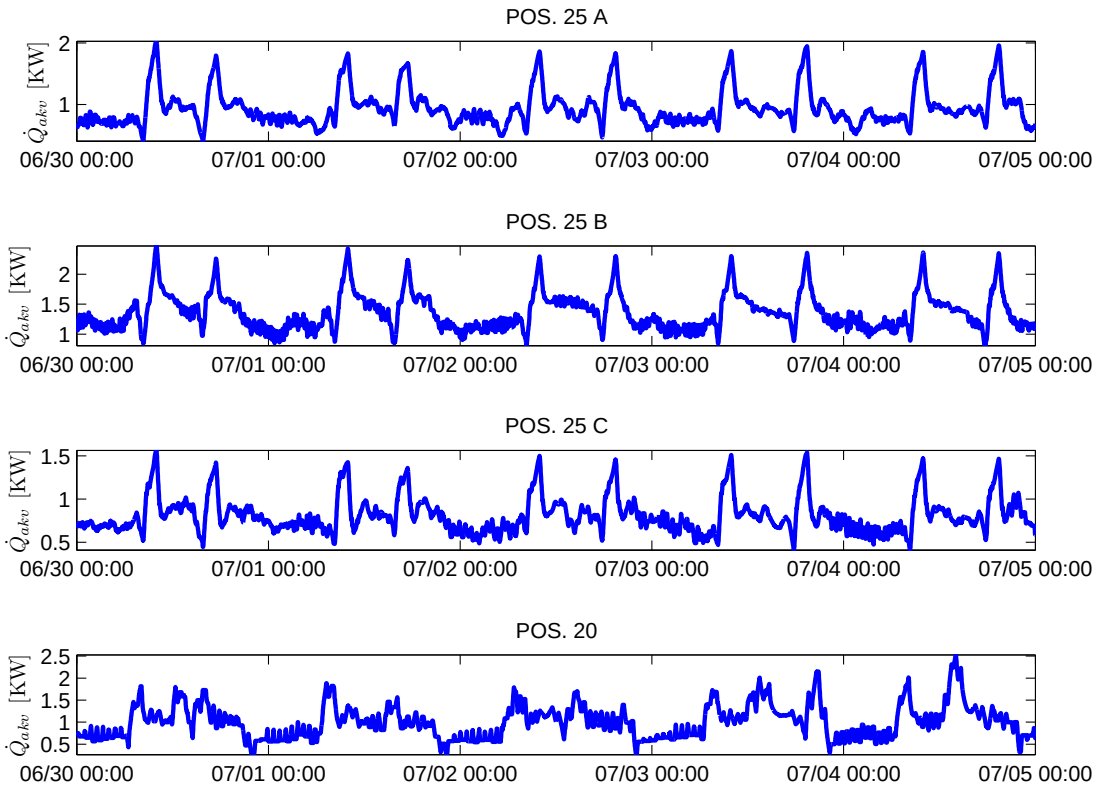

Figure 24: *Individual load for each cooling site. The data is sub-sampled to remove dynamic behavior and only 5 days are shown.*

load is calculated as follows

$$\dot{Q}^{MT} = m^{MT}\left(HTP\left(T^{MT}, P_0^{KL}\right) - HTP\left(TBubP\left(P_{rec}\right), P_{rec}, \text{'liquid'}\right)\right) \tag{11.3}$$

$$\dot{Q}^{LT} = m^{LT}\left(HTP\left(T^{LT}, P_0^{FR}\right) - HTP\left(TBubP\left(P_{rec}\right), P_{rec}, \text{'liquid'}\right)\right) \tag{11.4}$$

As seen the enthalpy is given by the difference of enthalpy at the mass flow meters and the receiver. The receiver contains refrigerant at the boiling point and thus the functions has to be supplied with the the initial guess of liquid or vapor.

It is easy to identify, in figure 25, that there is a small difference between the total AKV and total measured load (for both the fridges and freezers). There are several reasons to his, but in all the the estimate is very good. Each of the AKV loads, $\dot{Q}^{MT}_{akv,i}$, describing the load are tryed corrected using a linear polynomial fit. The function that we want to fit is as follows

$$\dot{Q}^{MT}_{akv,fit} = \sum_{i=1}^{7} c_i \dot{Q}^{MT}_{akv,i} \qquad \dot{Q}^{LT}_{akv,fit} = \sum_{i=1}^{4} c_i \dot{Q}^{LT}_{akv,i} \tag{11.5}$$

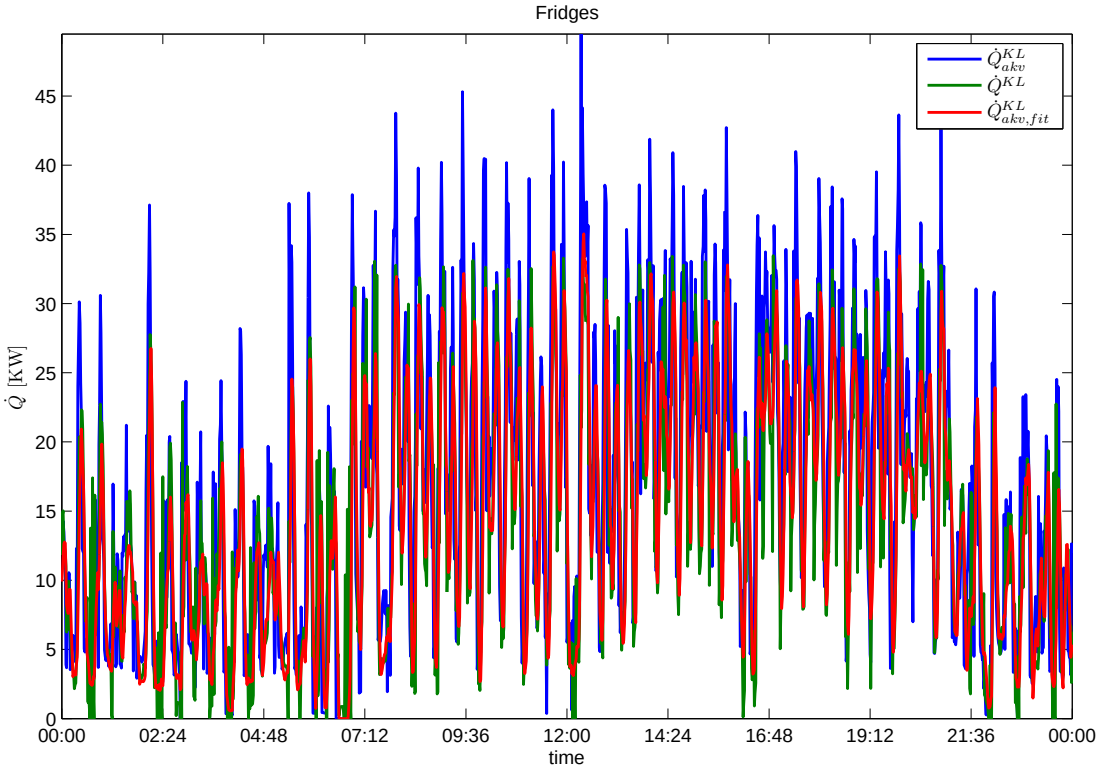

Figure 25: *30-06-2012, Shows the fridge refrigeration load estimated, measured by the mass flow meter and last the corrected estimated refrigeration load.*

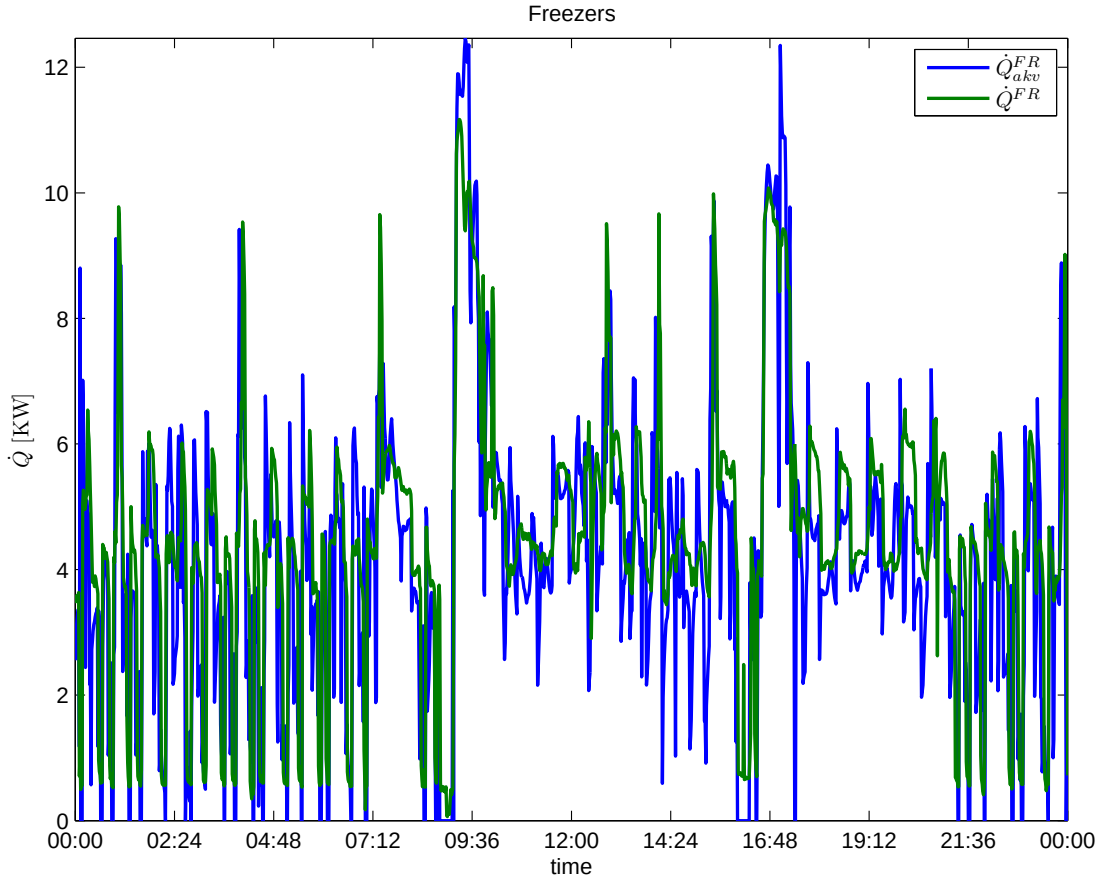

Figure 26: *30-06-2012, Shows the freezer refrigeration load estimated and measured by the mass flow meter.*

The least squares fit determines the coefficients c such that they minimize the sum of squared residuals. These are given by

$$\rho = \sum_{all} \left(\dot{Q}^{MT/LT} - \dot{Q}^{MT/LT}_{akv,fit} \right)^2 = \sum_{all} \left(\dot{Q}^{MT/LT} - \sum_{i=1}^{7} c_i \dot{Q}^{MT/LT}_{akv,i} \right)^2 \tag{11.6}$$

This is a linear system of equations in the coefficient vector. The system can be put to the matrix-vector form

$$\mathbf{r} = \mathbf{y} - \mathbf{Fc} \tag{11.7}$$

where boldface indicate vetors and matrices. $\mathbf{y}$ is equal to $\dot{Q}^{MT/LT}$, $\mathbf{c}$ is a vector of unknown constants and $\mathbf{F}$ is a matrix of $[\dot{Q}^{MT/LT}_{akv,1}\ \dot{Q}^{MT/LT}_{akv,2}\ ...\ \dot{Q}^{MT/LT}_{akv,7}]$. Hence the partial derivative of the sum of errors with respect to the unknown constants is

$$\nabla\rho = -2\mathbf{F}^T\mathbf{r} = -2\mathbf{F}^T(\mathbf{y} - \mathbf{Fc}) = -2(\mathbf{F}^T\mathbf{y} - \mathbf{F}^T\mathbf{Fc}) \tag{11.8}$$

For this vector to be the zero vector, $\nabla\rho = 0$, we must solve the linear system of equations with respect to the coefficient vector $\mathbf{c}$, which gives

$$\mathbf{c} = \left(\mathbf{F}^T\mathbf{F}\right)^{-1}\mathbf{F}^T\mathbf{y} \tag{11.9}$$

For the sake of numerical precision the QR factorization is used, which in Matlab is done simply by the command $\mathbf{c} = \mathbf{F}\backslash\mathbf{y}$.
The list of constants, $\mathbf{c}$, are then

Cooling site	POS 40A	POS 40B	POS 40C	POS 30	POS 30B	POS 45	POS 50
c, factor	0.583	0.725	1.333	0.502	1.989	0.977	1.910
c, conf. int.	±0.03556	±0.03663	±0.05758	±0.05073	±0.1634	±0.0287	±0.3054

Freezing site	POS 25A	POS 25B	POS 25C	POS 20
c, factor	1.221	0.836	0.978	1.048
c, conf. int.	±0.06858	±0.03645	±0.07424	±0.02903

The table show that the correction is very large and vary from cooling site to cooling site. Notice the 95% confidence interval, which indicate that the parameters are very certain. The parameters were estimated using data from the 30-June-2012. The data shown in figure 25 is also from 30-June-2012, and the same data is therefore used to validate the fit. The resulting estimated total energy flow, $\dot{Q}^{MT/LT}_{akv,fit}$, is shown in figure 25 (Red line). The corrected cooling load is very close to the measured one. Sadly this calculation only holds if the time-delay of each cooling site are negligible. This is not the case and some error is expected. A more plausible way of determining the individual load is to use the "AKV-method" mentioned earlier or simply install a mass-flow sensor on each cooling section (even though this solution is very expensive).

11.2 Cooling Load Dependence

The cooling load depends on several factors. Most significant is the indoor temperature, the indoor humidity and the opening and closing of the supermarket. For the cooling sites which are defrosted using heaters, the defrosting also make a significant contribution to the subsequent cooling load. It is deemed impossible to predict the dependency of the individual cooling sites, because the individual cooling is hardly possible to estimate correctly. The dependency of factors are therefore estimated for the total load on the fridges and freezers. Assuming that the total (measured) load changes instantly when the factors change, make it possible to estimate the dependence by s linear polynomial fit. This is done by letting **y** equal to the measured cooling load and **F** equal to the temperature, humidity and opening indicator in (11.7) as seen below

$$\mathbf{r} = \dot{Q}^{MT} - \begin{bmatrix} T_{indoor} & SH_{indoor} & I_{open} \end{bmatrix} \mathbf{c}_{MT} \tag{11.10}$$

$$\mathbf{r} = \dot{Q}^{LT} - \begin{bmatrix} T_{indoor} & SH_{indoor} & I_{open} & I_{defrost,1} & I_{defrost,2} \end{bmatrix} \mathbf{c}_{LT} \tag{11.11}$$

This type of fit is based on a static relation between the inputs and outputs. It is evident that $\dot{Q}^{MT}$ and $\dot{Q}^{LT}$ changes as the cooling sites request cooling. These dynamics has to be removed and is done by heavy low-pass filtering of both inputs and outputs to the linear model.
The regressors, **F**, are formed by the indoor temperature, humidity and opening/closing of the supermarket. If defrost is performed by electrical heaters, these are also incorporated. The indoor temperature is measured together with the relative humidity. The indicator variable for the opening and closing is constructed using the official opening and closing times of the specific supermarket. The fridges are not using heaters in order to defrost properly, but the freezers are. The freezers are therefore fitted with two defrost indicators. In order to remove the temperature dependence of the relative humidity the specific humidity, SH, is used instead. The conversion is based on calculating the saturated water pressure from which the actual water pressure is determined as the fraction given by the relative humidity. The specific humidity is given as; assuming the total pressure of air equal to $1025 \cdot 10^5$ Pa

$$P_{h_2o} = \frac{RH_{indoor}}{100} \cdot (1.0007 + 3.46 \cdot 10^{-6} \cdot 1015) \cdot 6.1121 e^{\frac{17.502 \cdot T_{indoor}}{240.97 + T_{indoor}}} \tag{11.12}$$

$$SH_{indoor} = 0.622 \cdot \frac{P_{h_2o}}{1015 - P_{h_2o}} \cdot 1000 \quad [\mathrm{g/m^3}] \tag{11.13}$$

The system of linear equations are solved for both systems to determine the coefficient vectors $\mathbf{c}_{MT}$ and $\mathbf{c}_{FR}$. The parameters are fitted using data from the 30-June-2012 to 05-July-2012. The equation in (11.9) is solved and the result is shown in table 2.

	c_1	c_2	c_3	c_4	c_5
Fridges	398.45±14.63	-82.95±44.361	8608.9±112.46		
Freezers	167.54±2.403	-74.28±7.22	939.6±20.52	3188.3 ±103.9	2786.3±146.8

Table 2: *Parameters describing the dependency for the cooling site loads.*

In order to determine whether the parameters are significant the variance of the parameters were calculated. The variance of these are given by (Madsen, 2007, p. 37) and states

$$Var(\mathbf{c}) = \sigma^2(\mathbf{F}^T\mathbf{F})^{-1} \tag{11.14}$$

The estimated variance of the innovations, σ^2, are estimated by

$$\sigma^2 = \frac{(\mathbf{y} - \mathbf{Fc})^T(\mathbf{y} - \mathbf{Fc})}{N - p} \tag{11.15}$$

N is the number of observations and p is the number of parameters. The 95% confidence interval is found by multiplying the standard deviation of each parameter by 2.5758. The result is also shown in table 2. As seen the confidence interval is quite narrow. It indicates that the parameter are significant and that the output does depend on the input variables.

Calculating the estimated load is performed by

$$\hat{\dot{Q}}^{MT} = \begin{bmatrix} T_{indoor} & SH_{indoor} & I_{open} \end{bmatrix} \mathbf{c}_{MT} \tag{11.16}$$

$$\hat{\dot{Q}}^{LT} = \begin{bmatrix} T_{indoor} & SH_{indoor} & I_{open} & I_{defrost,1} & I_{defrost,2} \end{bmatrix} \mathbf{c}_{LT} \tag{11.17}$$

Plotting the measured against the estimated load makes it possible to validate the fit quality by visual inspection. The data for validation is from 30-June-2012 to 05-July-2012 and is therefore the same as the parameters were estimated from. The plots are shown in figure 27 and 28.

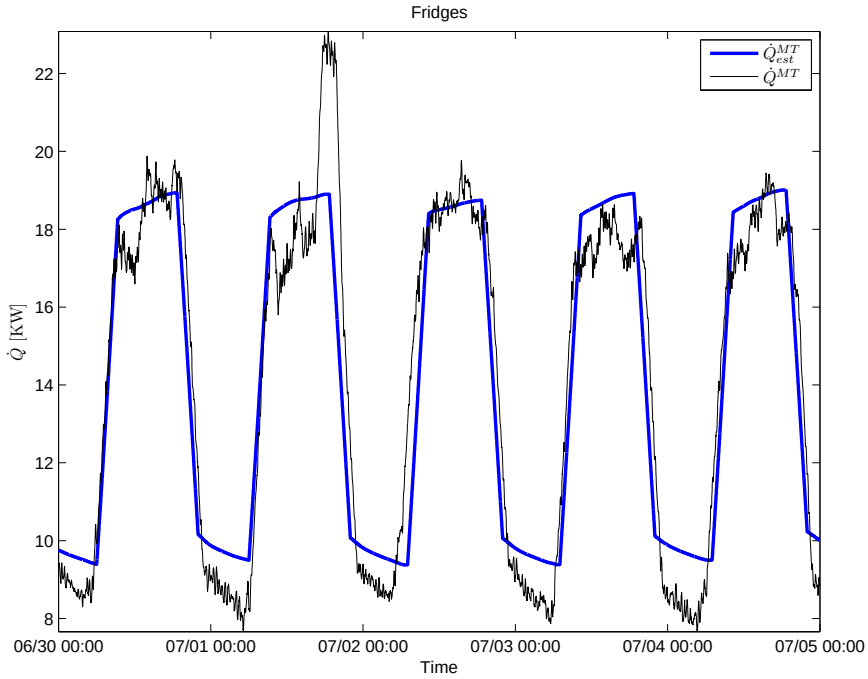

Figure 27: *Total measured and estimated load through a period of 4 days. Date: 30-June-2012 to 05-July-2012*

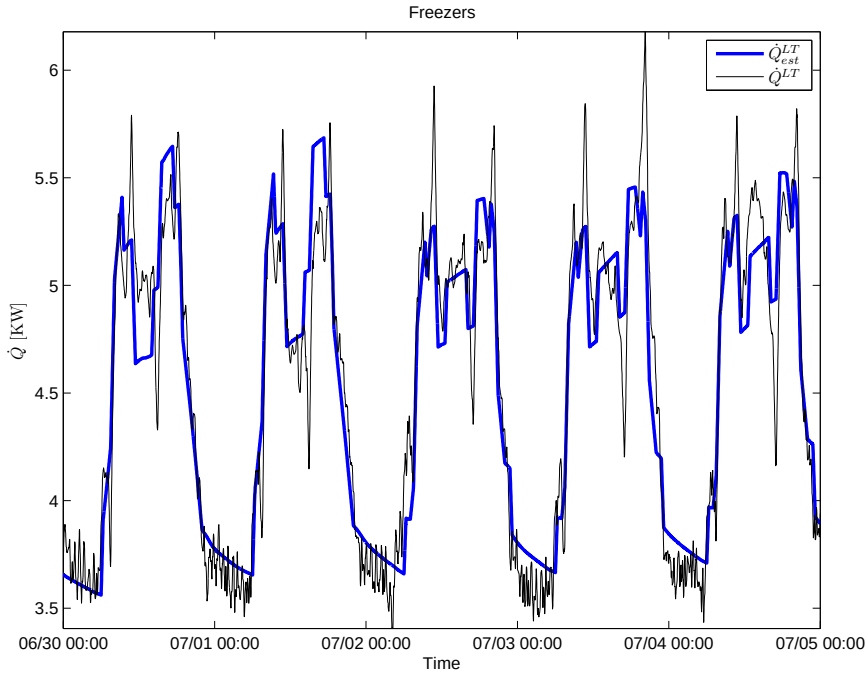

Figure 28: *Total measured and estimated load through a period of 4 days. Date: 30-June-2012 to 05-July-2012*

The estimated total load actually follows the complete data-set well. There are some temporary large deviations, which may be caused by synchronous defrosting or other phenomenas which are not covered by this model. The model is assumed accurate to determine the load given this supermarket.

The uncertainty of the estimate has to be considered. Calculating the estimation error variance by equation (11.15) gives the following 95% confidence interval.

$$conf = 2.5758\sqrt{\sigma^2_{MT}} = \pm 3668 \text{ W} \tag{11.18}$$

$$conf = 2.5758\sqrt{\sigma^2_{LT}} = \pm 592.97 \text{ W} \tag{11.19}$$

The confidence interval of the freezers are relatively larger compared to the size of the load. The uncertainties are also evident from figure 28.

11.3 Vortex mass-measurement

The supermarket, Fakta Otterup, has been equipped with three very expensive coriolis mass-flow sensors. These are very accurate and has proven able to measure the mass-flow of refrigerant. Though, there exists cheaper methods for flow measurements which could be used. In the future it would be nice to have cheaper ways of measuring the mass-flow and thus the vortex method has been investigated. The sensor has been installed in the liquid stream of the receiver.
A vortex sensor provides a measure of the volume-flow, $\dot{V}_{flow}$, and the temperature, T_{flow}. From these it is possible to estimate the mass-flow by

$$\dot{m}_{vortex} = \dot{V}_{flow} / VTP(T_{flow}, P_{rec}, 0) \tag{11.20}$$

It turns out that the massflow estimated from the vortex sensor is very accurate compared to the massflow of the trusted coriolis sensors. For comparison the flows from the two sensors is shown in figure 29 .

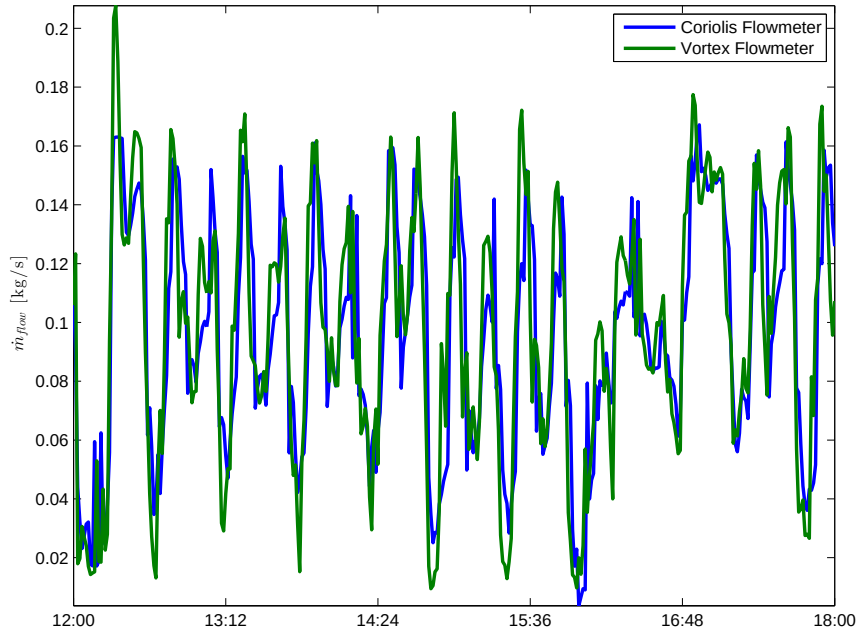

Figure 29: *30-June-2012, Total flow of refrigerant measured by the Coriolis mass-flow sensor and Vortex volumen-flow sensor.*

In the plotted period, the total massflow was 34.978 kg and 34.587 kg for the vortex and coriolis sensor respectively.

11.4 Coefficient Of Performance

11.4.1 True COP

The Coefficient Of Performance (COP) is of special interest to the supermarket owner, because it is a measure of how optimal the refrigeration system is performing. Looking directly at the cooling load only give a picture of how much energy which are needed to keep the food refrigerated, not how efficiently the compressor and rest of the refrigeration cycle delivers the cooling. For that purpose the COP is developed. The relation is as follows

$$COP = \frac{\dot{Q}}{\dot{W}} \tag{11.21}$$

Where $\dot{Q}$ is the cooling load and $\dot{W}$ is the power used to deliver that amount of cooling. The refrigeration system is divided into a fridge and freezer part, and as such it would be interesting to study the COP of the fridge, freezer and total refrigeration system

individually. The refrigeration load from the fridges and freezers are given, using the measured mass-flow and the enthalpy of the stream, as follows

$$\dot{Q}^{MT} = m^{MT}\left(HTP\left(T^{MT}, P_0^{KL}\right) - HTP\left(TBubP\left(P_{rec}\right), P_{rec}, \text{'liquid'}\right)\right) \tag{11.22}$$

$$\dot{Q}^{LT} = m^{LT}\left(HTP\left(T^{LT}, P_0^{FR}\right) - HTP\left(TBubP\left(P_{rec}\right), P_{rec}, \text{'liquid'}\right)\right) \tag{11.23}$$

MT and LT is an acronym for fridges and freezers.

The construction of the refrigeration system is so, that the freezer compressors are attached to the fridge cooling system as a load similar to the cooling sites. This eases the load on the freezer compressors, but of course also increase the load on the fridge compressors. This means that the total load on the fridge compressors is a sum of the freezer load and the fridge load. In the same way a fraction of the fridge power usage originates from the freezers and has to be taken into account.
The COP for the fridge and freezers are then

$$COP_{MT} = \frac{\dot{Q}^{MT}}{\frac{\dot{Q}^{MT}}{\dot{Q}^{MT}+\dot{Q}^{LT}}\dot{W}^{KL}} \tag{11.24}$$

$$COP_{LT} = \frac{\dot{Q}^{LT}}{\dot{W}^{FR} + \frac{\dot{Q}^{LT}}{\dot{Q}^{MT}+\dot{Q}^{LT}}\dot{W}^{KL}} \tag{11.25}$$

$$COP_{total} = \frac{\dot{Q}^{MT} + \dot{Q}^{LT}}{\dot{W}^{KL} + \dot{W}^{FR}} \tag{11.26}$$

Figure 30 shows the calculated COP by the above equations.

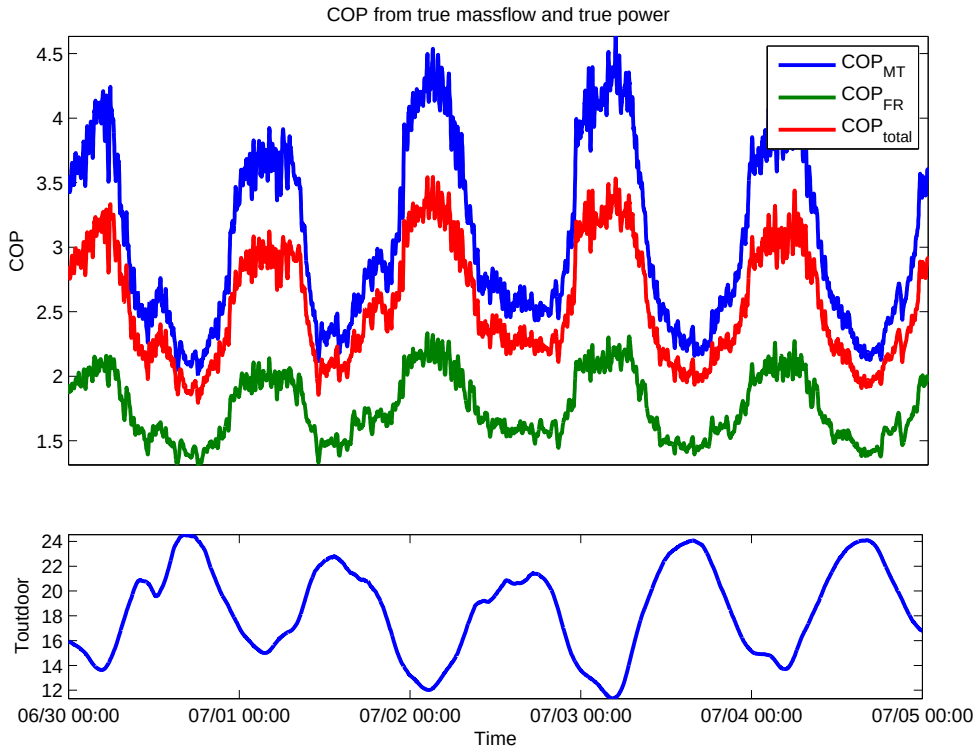

Figure 30: *Plot of COP (Coefficient Of Performance) for the fridge, freezer and total system.*

As seen the fridge COP is significantly higher than the freezer COP. This makes sense, since it is more efficient to have a low difference between the cold and hot side of the refrigeration system. Further it is noticed that the efficiency is higher at night time than at day time, again due to the lower difference between the hot and cold sides in the refrigeration system. Generally the total COP lies between 1.8 to 3.3 at day and night respectively.

11.4.2 Estimated COP

Generally it is not possible to calculate the true COP due to the expensive Coriolis mass-flow sensors. Another approach has been presented by Danfoss, where no mass-flow sensors are used and the COP is estimated from already present sensors in common supermarkets. The approach is based on the fact that the mass-flows can be estimated by the displacement and speed of the compressors and enthalpies from temperature and pressure sensors. The idea has been introduced in a commercial product by ”ClimaCheck Sweden AB”, and has ever since been subject for criticism

due to unrealistic COP estimates. In order to validate the method presented here the estimated COP and the true one is compared.

First the mass-flows and power consumption of the two compressor racks are estimated by the relations below

$$\dot{m}^{KL} = \eta_{vol}^{KL}\rho^{KL}\frac{run_{comp}^{KL}}{100}\frac{V_{sl}^{KL}}{3600} \qquad \dot{m}^{FR} = \eta_{vol}^{FR}\rho^{FR}\frac{run_{comp}^{FR}}{100}\frac{V_{sl}^{FR}}{3600} \tag{11.27}$$

$$\rho^{KL} = \frac{1}{VTP(S_s^{KL}, P_0^{KL}, 1)} \qquad \rho^{FR} = \frac{1}{VTP(S_s^{FR}, P_0^{FR}, 1)} \tag{11.28}$$

And the compressor power is estimated by

$$\dot{W}^{KL} = \frac{1}{\eta_{is}^{KL}}\dot{m}^{KL}\left(HTP(S_{ds}^{KL}, P_c^{KL}) - HTP(S_s^{KL}, P_0^{KL})\right) \tag{11.29}$$

$$\dot{W}^{FR} = \frac{1}{\eta_{is}^{FR}}\dot{m}^{FR}\left(HTP(S_{ds}^{FR}, P_c^{FR}) - HTP(S_s^{FR}, P_0^{FR})\right) \tag{11.30}$$

with

$$S_{ds}^{KL} = TVSP(STP(S_s^{KL}, P_0^{KL}), P_c^{KL}) \tag{11.31}$$

$$S_{ds}^{FR} = TVSP(STP(S_s^{FR}, P_0^{FR}), P_c^{FR}) \tag{11.32}$$

The displacement volume is easily found by inspecting the metal plate on the compressors to; $V_{sl}^{KL} = 6.5 \cdot 70/50 + 12.0$ and $V_{sl}^{FR} = 2.71 + 3.48$. Further, the Volumetric and Isentropic efficiencies of the compressors has to be known to the equations. These are seldom known, but is estimated by a relation given for a Bitzer compressor by

$$\eta_{vol} = b_1 + b_2\frac{P_c}{P_0} + b_3\left(\frac{P_c}{P_0}\right)^2 \tag{11.33}$$

$$\eta_{is} = a_1 + a_2\frac{P_c}{P_0} + a_3\left(\frac{P_c}{P_0}\right)^{1.5} + a_4\left(\frac{P_c}{P_0}\right)^3 + a_5\left(\frac{P_c}{P_0}\right)^{-1.5} \tag{11.34}$$

with

$$a_1 = 4.39004614408 \quad a_2 = -3.5085777881 \quad a_3 = 1.5130806248; \tag{11.35}$$

$$a_4 = -0.0236297366209 \quad a_5 = -2.31968952362 \tag{11.36}$$

$$b_1 = 0.967 \quad b_2 = -0.037 \quad b_3 = 0 \tag{11.37}$$

The earlier mass-flows, $\dot{m}^{KL}$ and $\dot{m}^{FR}$, has to be transformed into the flows through the bypass-valve, the medium pressure cooling sections and the low pressure cooling sections. The amount of bypassed refrigerant can be estimated by a fraction of the

total mass-flow through the gas cooler. First this fraction is determined by dividing the enthalpy at the gas cooler into a fraction of the dew and bubble enthalpy .

$$HTP_{gc} = (1-x) \cdot HBubP(P_{rec}) + x \cdot HDewP(P_{rec}) <=> \tag{11.38}$$

$$x = \frac{HTP_{gc} - HBubP(P_{rec})}{HDewP(P_{rec}) - HBubP(P_{rec})} \tag{11.39}$$

Where the gas cooler enthalpy has to be determined by the relation

$$HTP_{gc} = \begin{cases} HTP(S_{gc}, P_{gc}, 0) & \text{if } P_{gc} > P_{krit} \\ HBubP(P_{gc}) & \text{else} \end{cases} \tag{11.40}$$

The critical pressure, P_{krit}, is defined as the pressure where the refrigerant goes from subcritical to transcritical operation. The bypass mass-flow, as well as the flows through the fridges and freezers, are then simply determined by

$$\dot{m}^{BP} = x \cdot \dot{m}^{KL} \tag{11.41}$$

$$\dot{m}^{LT} = \dot{m}^{FR} \tag{11.42}$$

$$\dot{m}^{MT} = \dot{m}^{KL} - (\dot{m}^{BP} + \dot{m}^{LT}) \tag{11.43}$$

The bypassed mass-flow will be split into two parts, such that the load of having a bypass is divided into a proportion originating from cooling in the fridges and freezers. The fraction is simply found by taking the ratio between the fridge and freezer load of the bypassed mass-flow

$$\dot{m}^{BP}_{MT} = \dot{m}^{BP} \frac{\dot{m}^{MT}}{\dot{m}^{LT} + \dot{m}^{MT}} \tag{11.44}$$

$$\dot{m}^{BP}_{LT} = \dot{m}^{BP} \frac{\dot{m}^{LT}}{\dot{m}^{LT} + \dot{m}^{MT}} \tag{11.45}$$

The refrigeration load has to be expressed in power, not mass-flow. The enthalpies of the flows is multiplied by the mass-flow and the energy is determined as shown

$$\dot{Q}^{MT} = \dot{m}^{MT}(HTP(S_2^{KL}, P_0^{KL}) - HTP(TBubP(P_{rec}), P_{rec}, 0)) \tag{11.46}$$

$$\dot{Q}^{LT} = \dot{m}^{LT}(HTP(S_2^{FR}, P_0^{FR}) - HTP(TBubP(P_{rec}), P_{rec}, 0)) \tag{11.47}$$

The temperatures, S_2^{KL} and S_2^{FR} is the temperature of the refrigerant just after it leaves the evaporators. These are approx. $S_2^{KL} \approx -3\ ^oC$ and $S_2^{FR} \approx -21\ ^oC$. The refrigeration load is now determined and the power used by the compressors has to be determined as well, to construct the COP of the fridge and freezers respectively. The power of the compressors was determined earlier, but due to the design of the system, the power of the fridge and freezers has to be found. This is because of the booster setup where the

load of the freezers are attached at the fridge system as an additional load. The power used is therefore

$$\dot{W}^{MT} = \dot{W}^{KL} \frac{\dot{m}^{MT} + \dot{m}^{BP}_{MT}}{\dot{m}^{LT} + \dot{m}^{MT} + \dot{m}^{BP}} \tag{11.48}$$

$$\dot{W}^{LT} = \dot{W}^{FR} + \dot{W}^{KL} \frac{\dot{m}^{LT} + \dot{m}^{BP}_{LT}}{\dot{m}^{LT} + \dot{m}^{MT} + \dot{m}^{BP}} \tag{11.49}$$

The COP of the system is calculated by the relation below

$$COP_{MT} = \frac{\dot{Q}^{MT}}{\dot{W}^{MT}} \tag{11.50}$$

$$COP_{LT} = \frac{\dot{Q}^{LT}}{\dot{W}^{LT}} \tag{11.51}$$

$$COP_{total} = \frac{\dot{Q}^{MT} + \dot{Q}^{LT}}{\dot{W}^{MT} + \dot{W}^{LT}} \tag{11.52}$$

The three COP's have been plotted in figure 31 together with the true COP. As seen the total estimated COP (COP Total) is closely relted to the true COP (COP true total) and have a similar trend. The accuracy of the result can get even better by filling in the true volumetric and isentropic efficiencies.

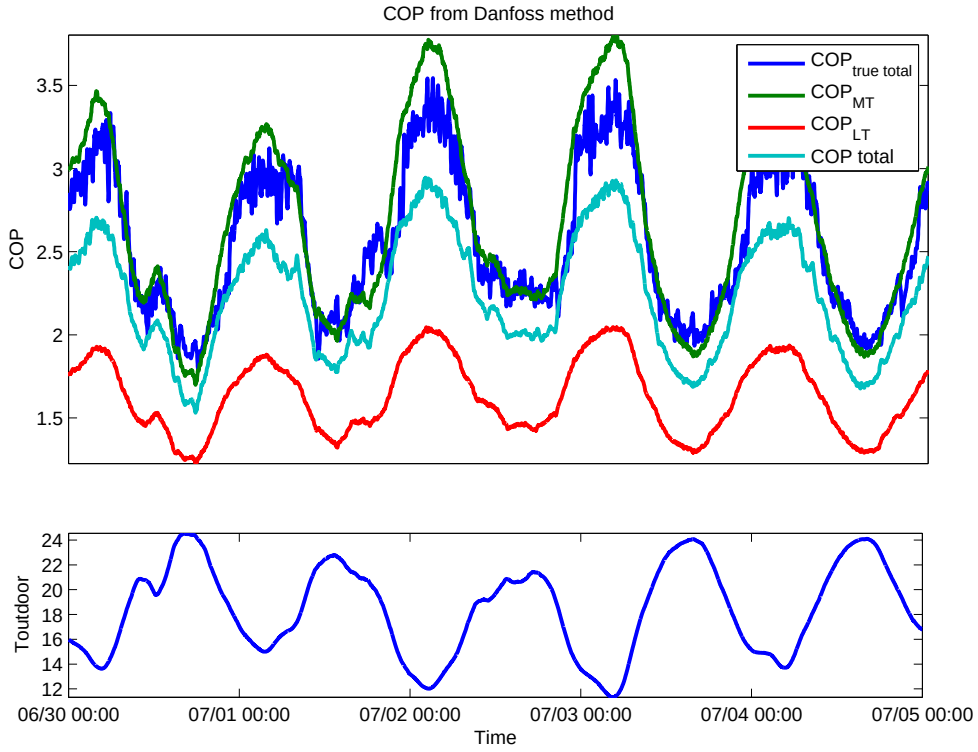

Figure 31: *Plot of COP (Coefficient Of Performance) for the fridge, freezer and total system estimated by the methods of Danfoss.*

11.4.3 Optimal COP

The second law of thermodynamics puts a fundamental limit on the thermal efficiency of all cooling systems. Even an ideal cooling system has an upper limit on the efficiency. From Carnot's theorem, for any engine working between two temperatures, the maximal efficiency is given by

$$COP_{MT}^{car} = \frac{T_{1,L}}{T_H - T_{1,L}} \tag{11.53}$$

$$COP_{LT}^{car} = \frac{T_{2,L}}{T_H - T_{2,L}} \tag{11.54}$$

$$COP_{total}^{car} = \frac{\dot{Q}_{MT} COP_{KL}^{car} + \dot{Q}_{LT} COP_{FR}^{car}}{\dot{Q}_{MT} + \dot{Q}_{LT}} \tag{11.55}$$

The low temperature, T_L, is equal to the cold side of the cooling process i.e. approx $T_{1,L} = 2°\text{C}$ and $T_{2,L} = -20°\text{C}$. The hot side of the process is given by the outdoor temperature i.e. $T_H = T_{outdoor}$. The Carnot efficiency of the total system is approximated by weighting the two Carnot efficiencies by their energy-flow.

In order to compare the actual efficiency of the process relative to the limit of efficiency, the ratio between these are used. The clever thing is that one gets a number between 0 and 1, indicating zero efficiency and maximum efficiency decoupled from seasonal temperature variations. The ratio is simply given by

$$\eta_{car} = \frac{COP}{COP^{car}} \tag{11.56}$$

The result is shown in figure 32. The figure show the efficiency of the total system using the load estimated using the mass-flow sensors and power sensors.

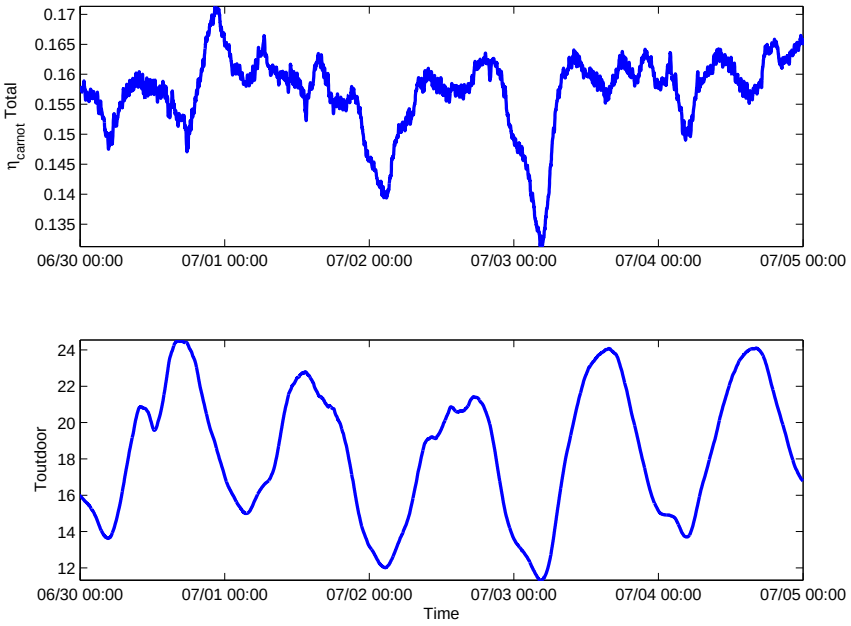

Figure 32: *Ratio between the true COP and the reference Carnot COP. Calculated for the total system.*

From figure 32 it is clear that there is a potential for improvement as the refrigeration system have generally a low efficiency. This is notable when considering that the system is known to use less energy than the preceding HFC based generation of refrigeration systems. One should however bear in mind that maximum achievable η_{car} in praxis is limited to around 0,5. It can be seen that for the days chosen the efficiency vary with time. The difference between the highest and the lowest value corresponds to a 20% decrease in efficiency. It would be expected that a decrease would correspond to an increase in the outdoor temperature where the trans critical CO2 process is known to have a poor performance, but on the contrary it corresponds to low temperatures in the night. The reason for this is probably that the load in the night is very low and the resulting frequent on/ off cycling of the compressors reduce the efficiency.

The ratio between COP's, η_{car}, can be used to identify supermarkets where the refrigeration systems are running uneconomically and start initiatives to reduce the energy usage. If mass-flow sensors are not available, the estimated load using the AKV's could be used.

11.5 Estimation of Volumetric and Isentropic efficiencies

The isentropic efficiency is estimated by isolation in equation (11.29). The mass-flow and power consumption is measured, and thus the unknown efficiency is known.

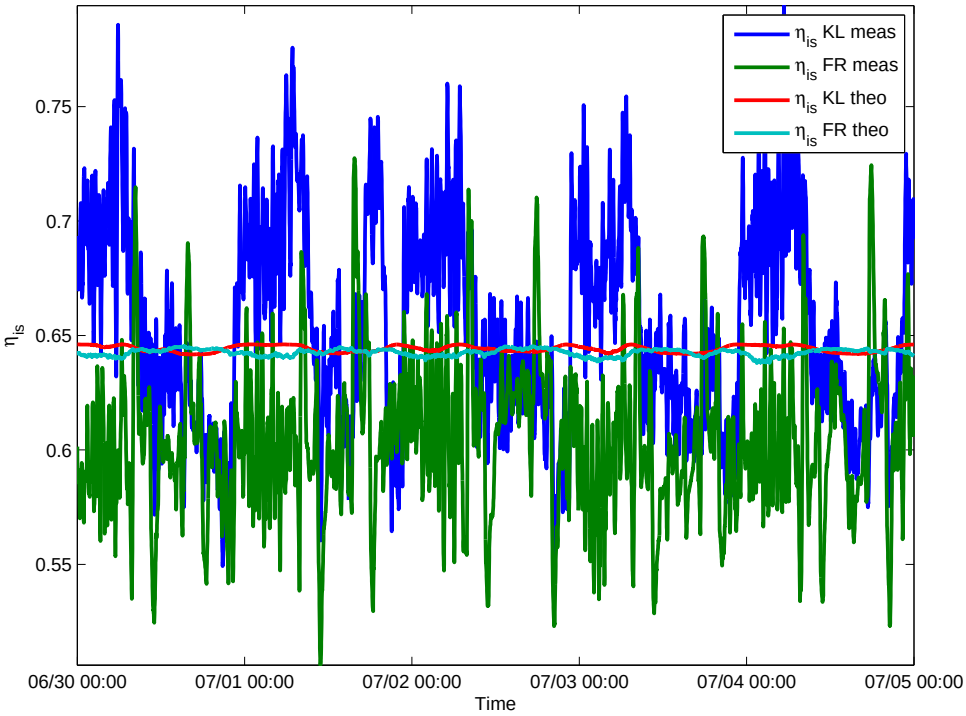

Figure 33: *Estimation of isentropic efficiency.*

The volumetric efficiency is estimated by isolation in equation (11.27). The mass-flow and running capacity is measured/known, and thus the unknown efficiency is known.

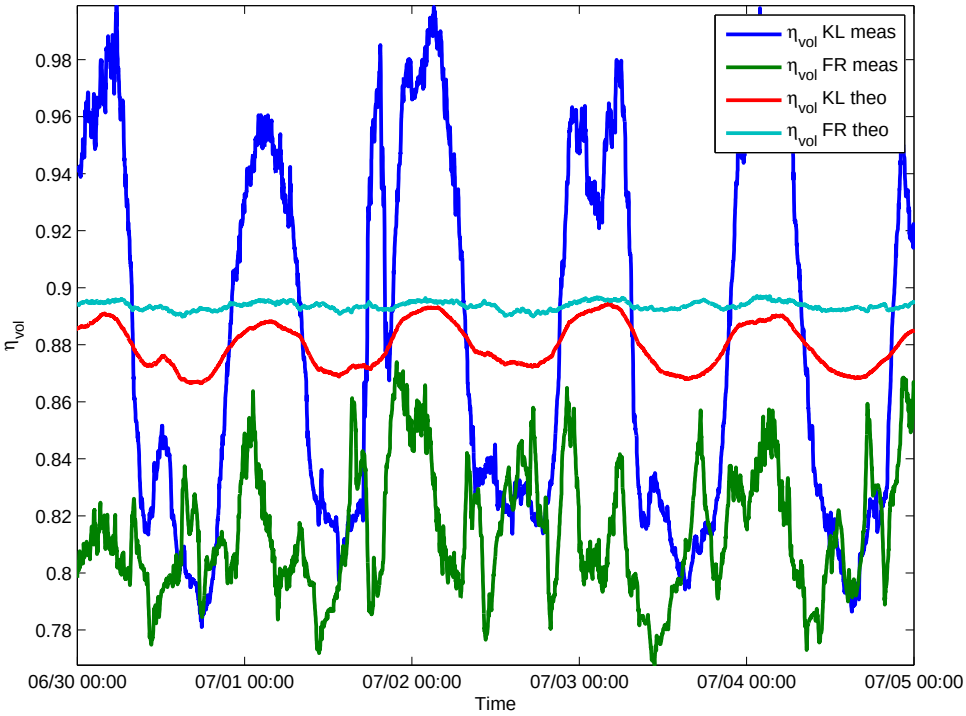

Figure 34: *Estimation of volumetric efficiency.*

12 Conclusion

The report has presented an approach to control and monitor the performance of supermarket refrigeration systems. Simulations showed that the proposed Model Predictive Controller can reduce synchronization by coordinating the cooling sites with the compressor capacity. The computational load of running the controller is though significant and refrigeration systems of more than three cooling sites are not computational feasible to solve in real-time. A feed-forward control solution was also proposed for the compressor-rack controller, but due to the low sample frequency, it turned out to be impossible to identify a model and do control. The refrigeration performance has been investigated using both Coriolis mass-flow sensors and general methods applicable to standard supermarkets. This made it possible to correct and verify that the load can be estimated using the characteristics of the valves or the compressor rack. Both methods only make use of already installed sensors in standard supermarkets, thus making the methods commercial applicable. The estimated COP can be used to continuously optimize the performance of the system.

13 Plots of Operation

Data has been logged with 1 min sample interval since 25/08-2011 and until now (04-10-2011). Generally the data has often been corrupted by data-dropouts for shorter and longer periods, a system malfunction at the refrigeration system and the power sensors did not work through the entire period. The data sequences which has been used for this project was therefore carefully selected. The data at used as training data is from the period 25-08-2011 09:29:00 to 25-08-2011 14:59:00. Test data is from the period 26-08-2011 09:29:00 to 26-08-2011 14:59:00. Below is a list of figures showing data (the entire day at 25-08-2011) from the cooling sites, compressors and the gas cooler.

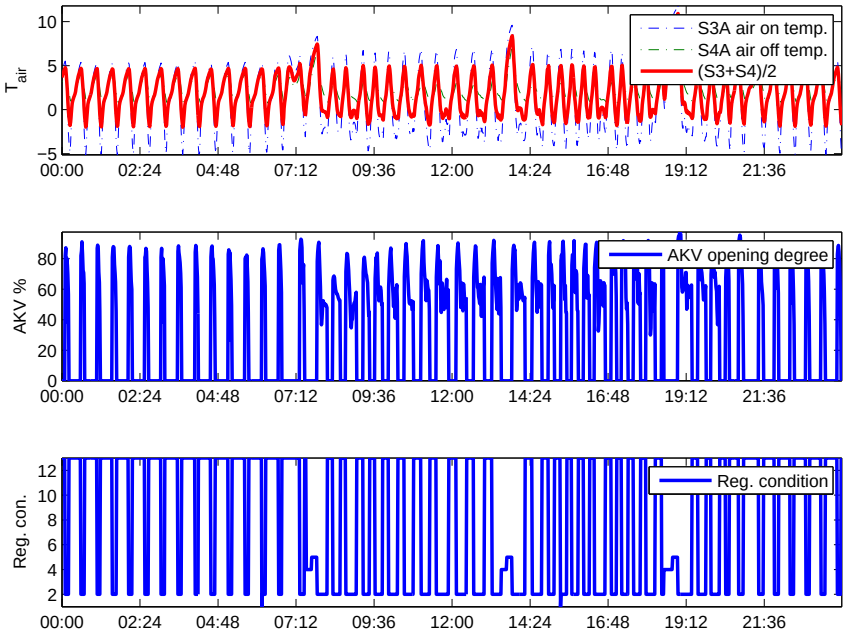

Figure 35: *25-08-2011, POS 40A*

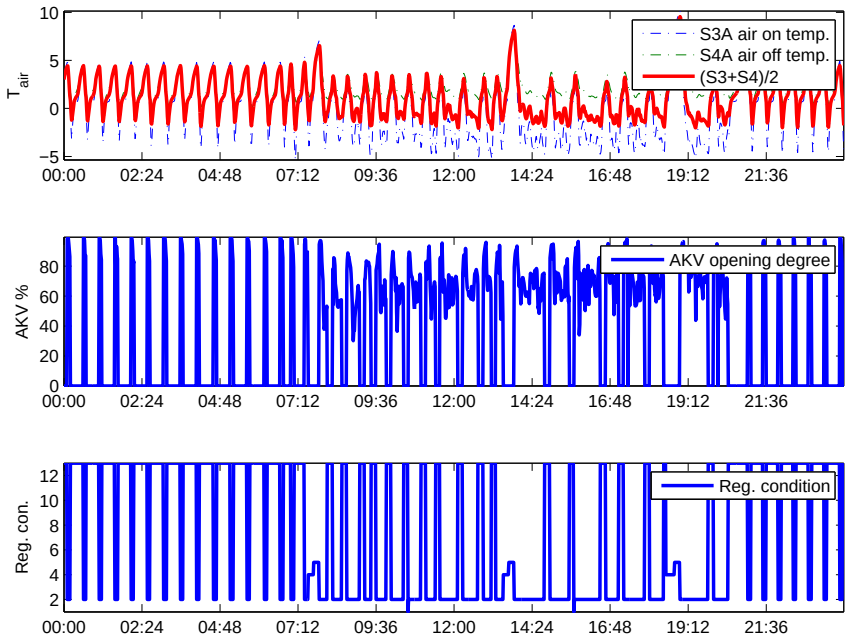

Figure 36: *25-08-2011, POS 40B*

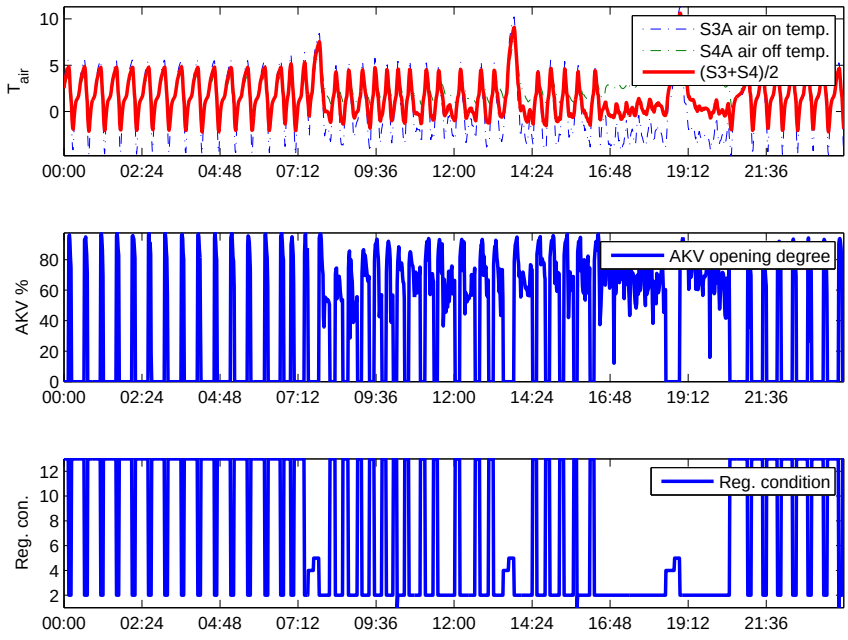

Figure 37: *25-08-2011, POS 40C*

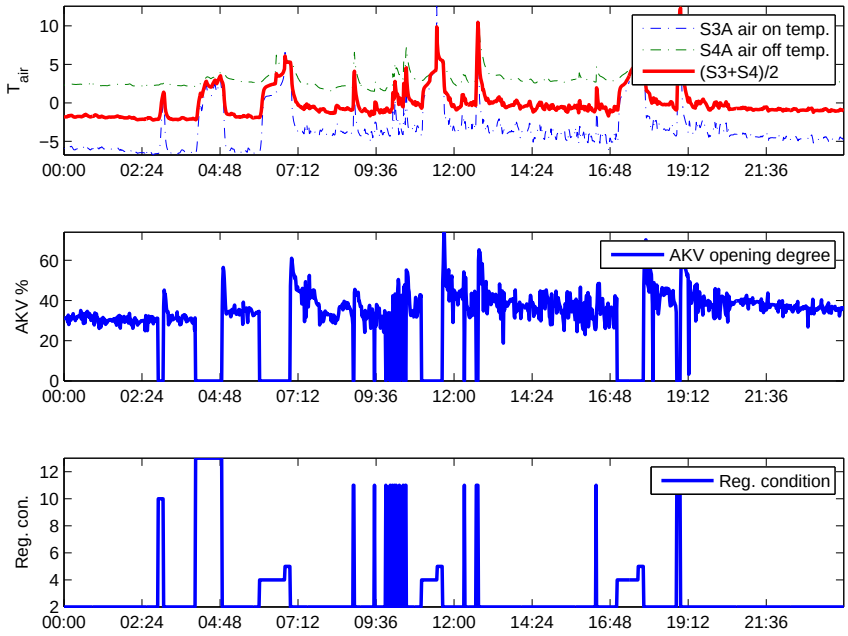

Figure 38: *25-08-2011, POS 30*

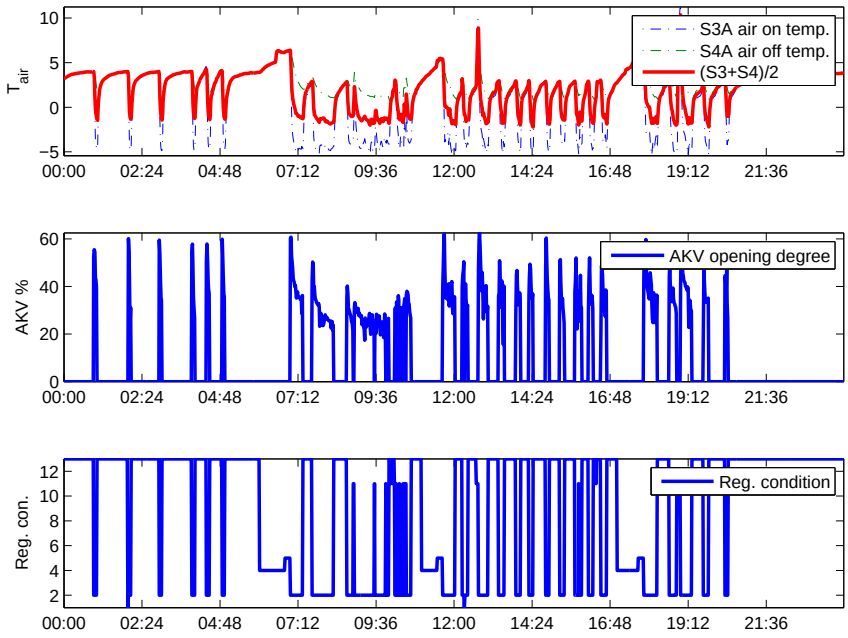

Figure 39: *25-08-2011, POS 30B*

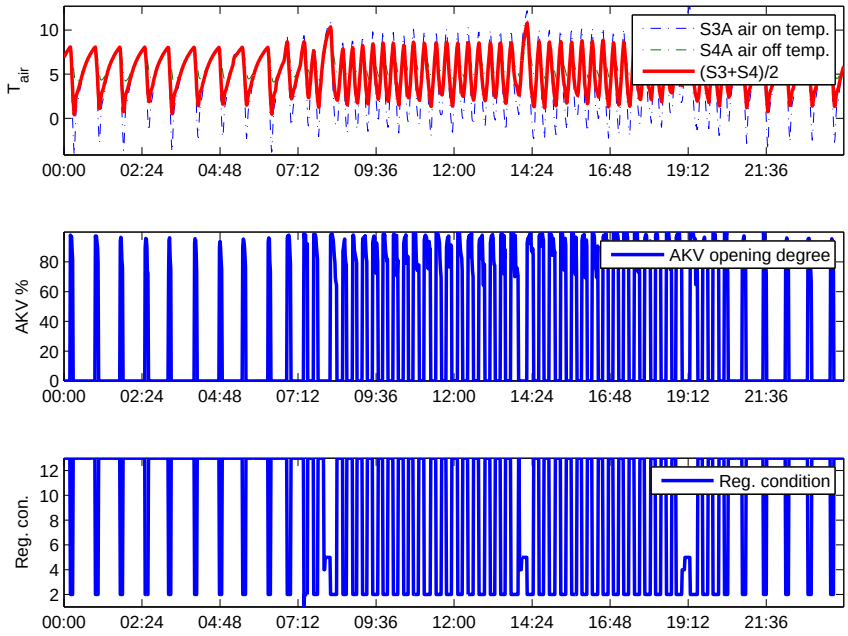

Figure 40: *25-08-2011, POS 45*

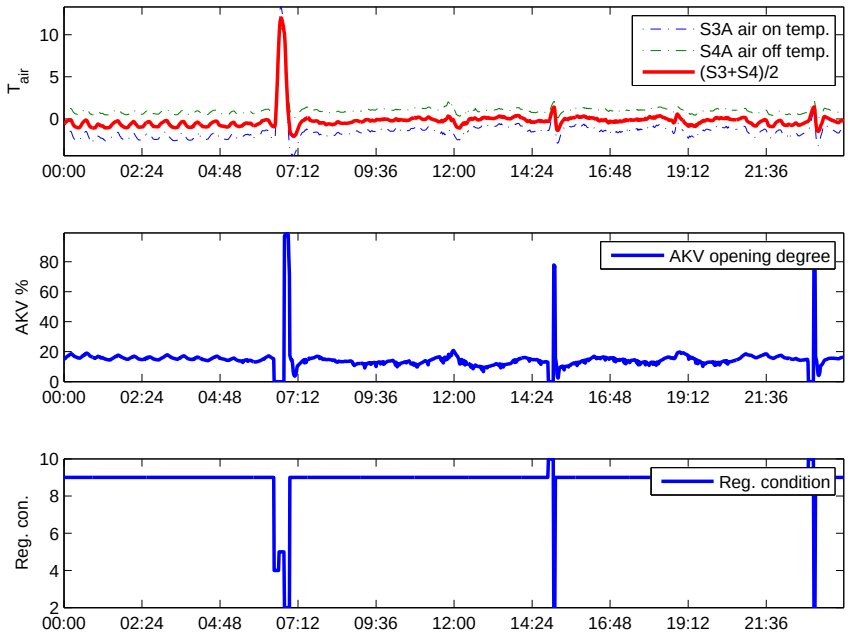

Figure 41: *25-08-2011, POS 50*

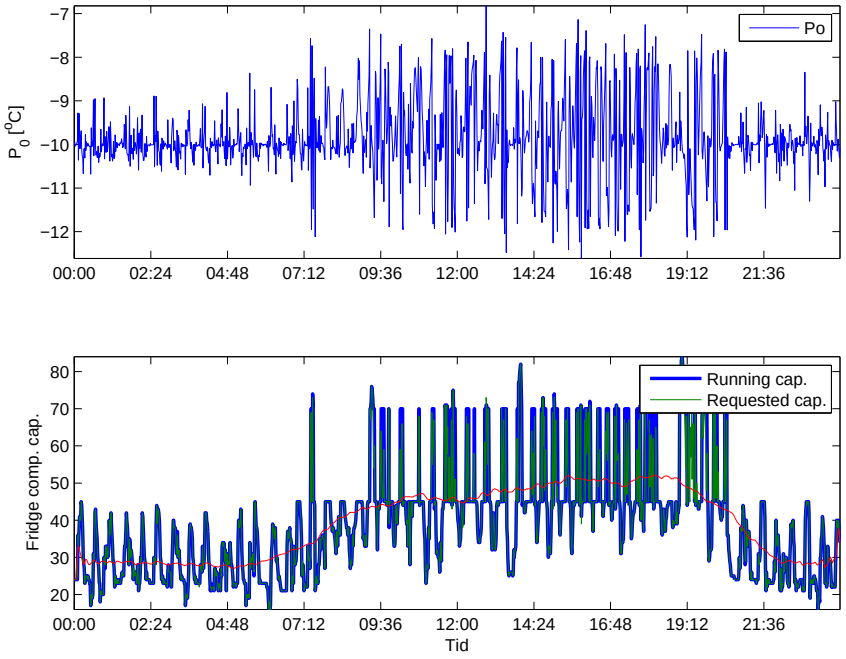

Figure 42: *25-08-2011, Fridge compressor and fridge suction pressure.*

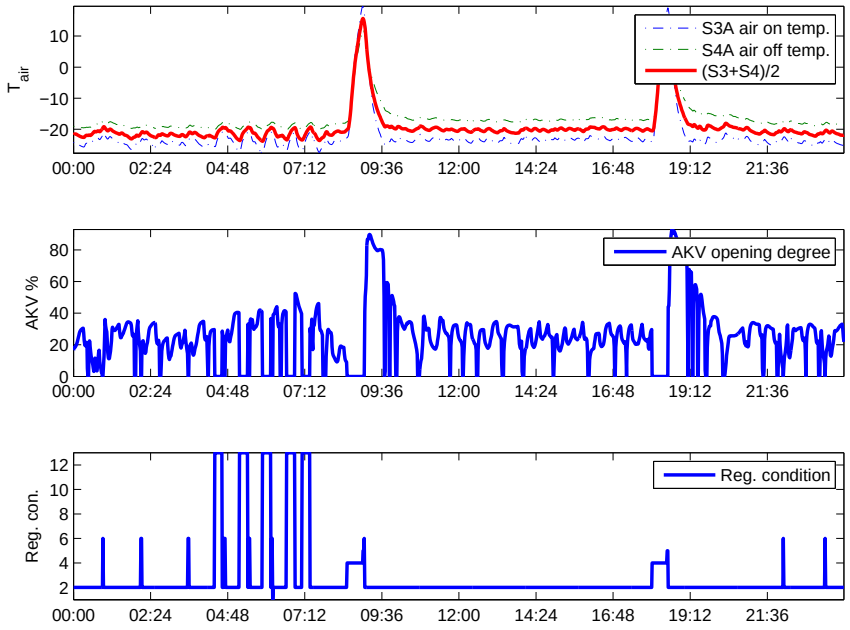

Figure 43: *25-08-2011, POS 25A*

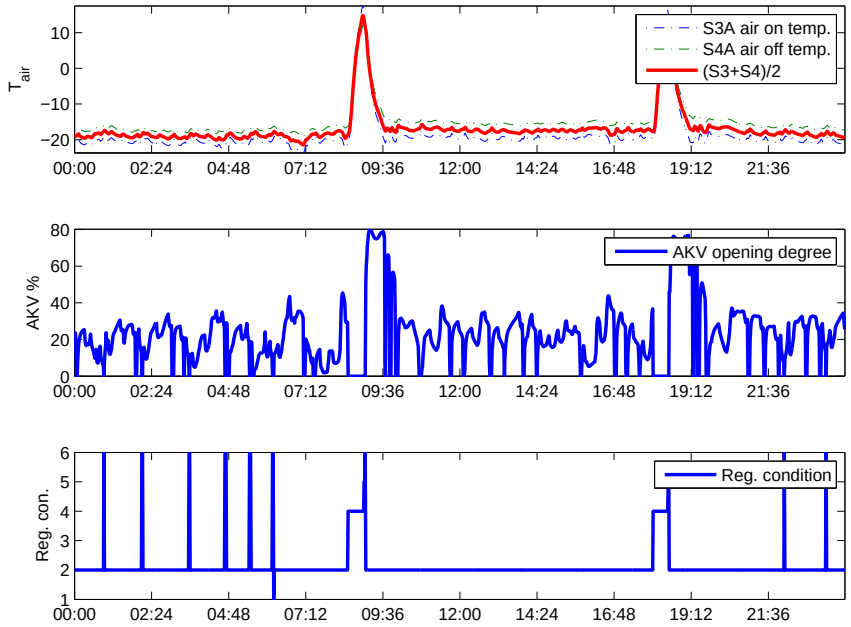

Figure 44: *25-08-2011, POS 25B*

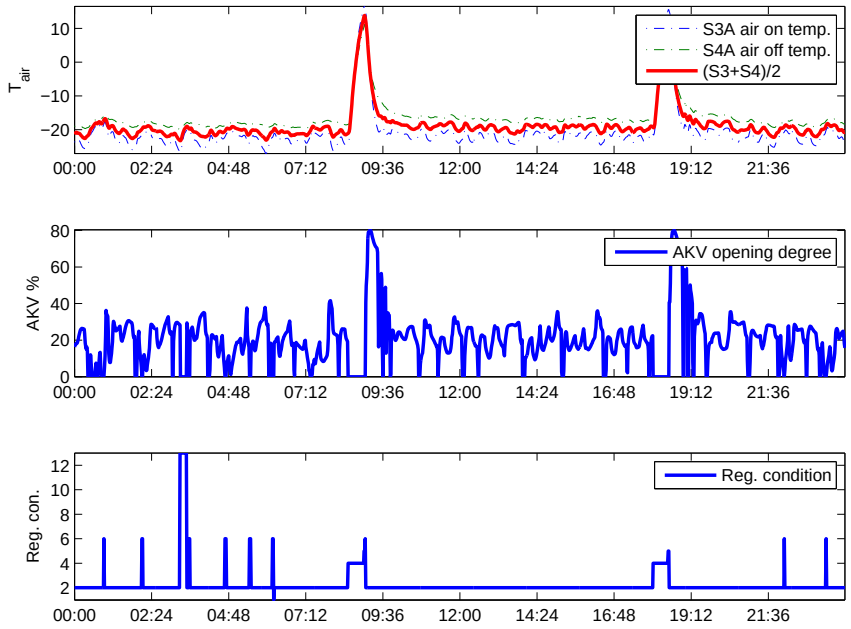

Figure 45: *25-08-2011, POS 25C*

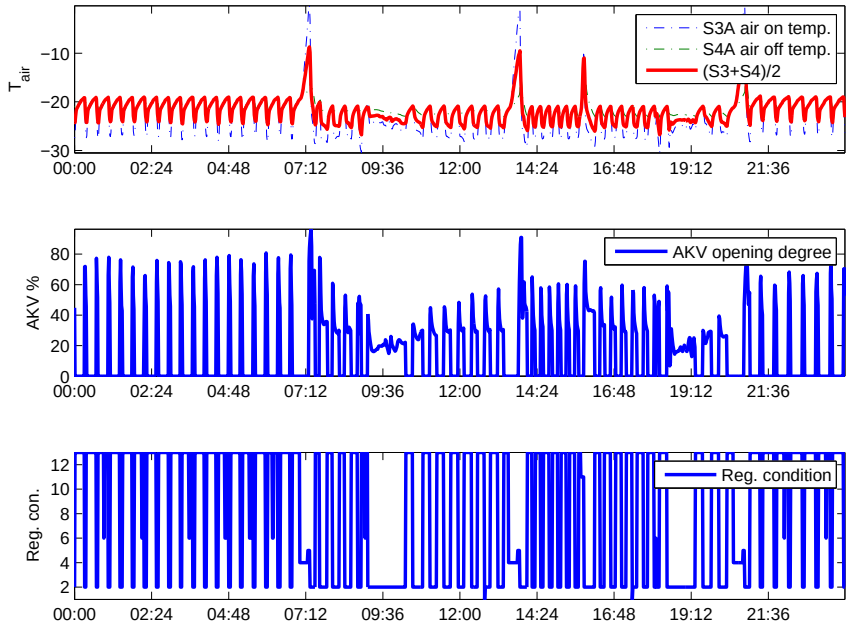

Figure 46: *25-08-2011, POS 20*

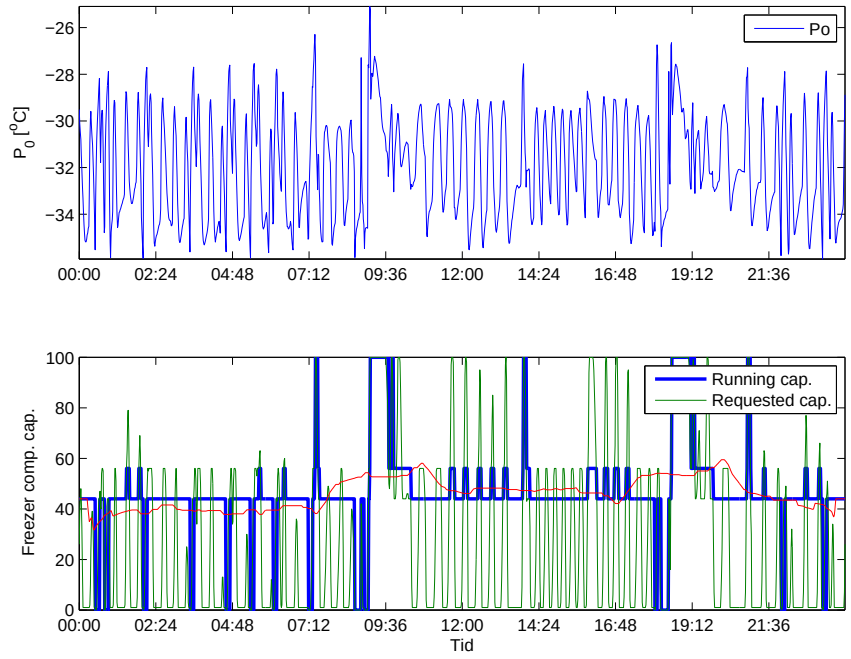

Figure 47: *25-08-2011, Freezer compressor and freezer suction pressure.*

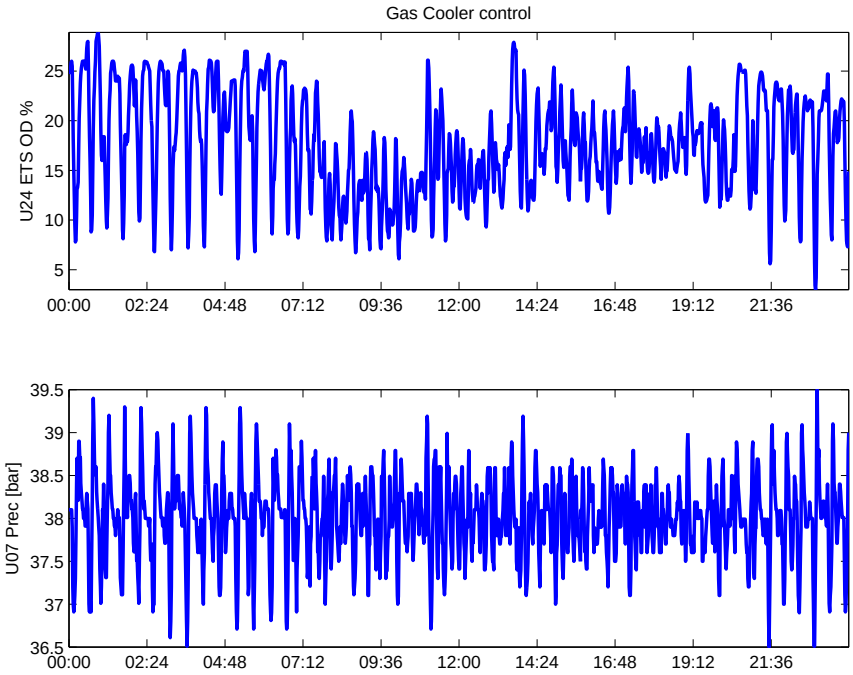

Figure 48: *25-08-2011, Gas cooler showing gas bypass valve and controlled high pressure at the cooling site.*

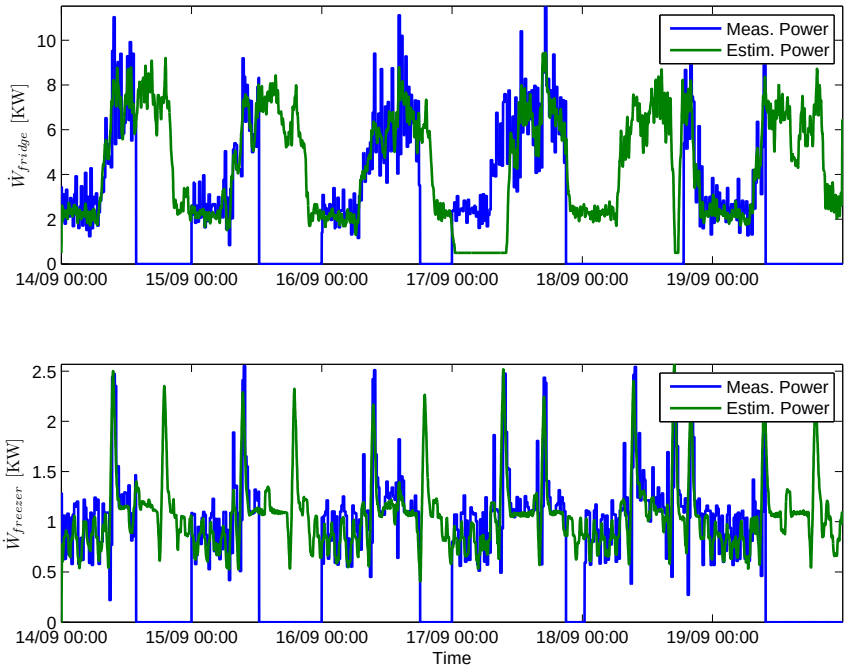

Figure 49: *Plot of estimated power consumption against measured.*

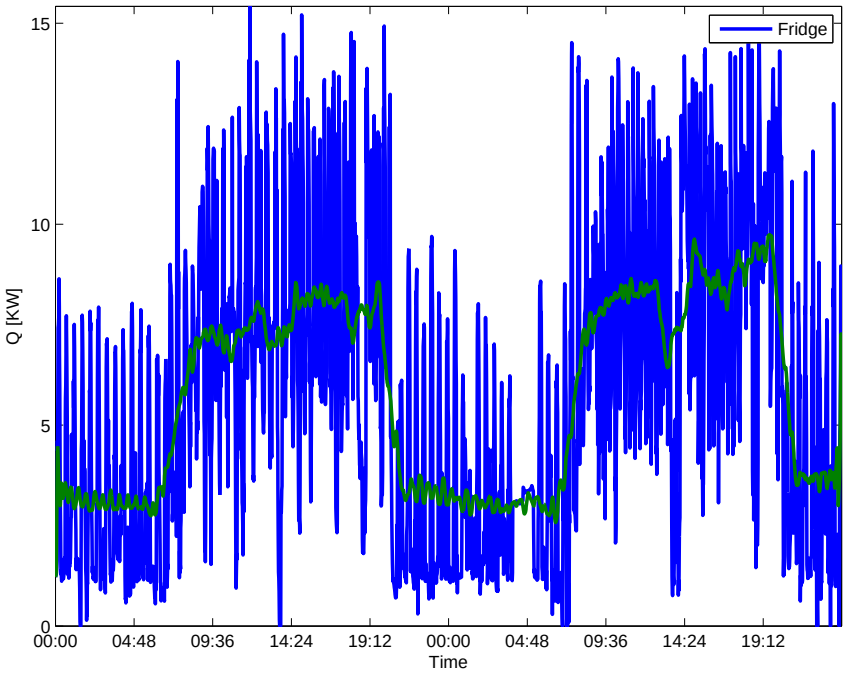

Figure 50: *25-08-2011, Plot of measured mass-flow at the fridges.*

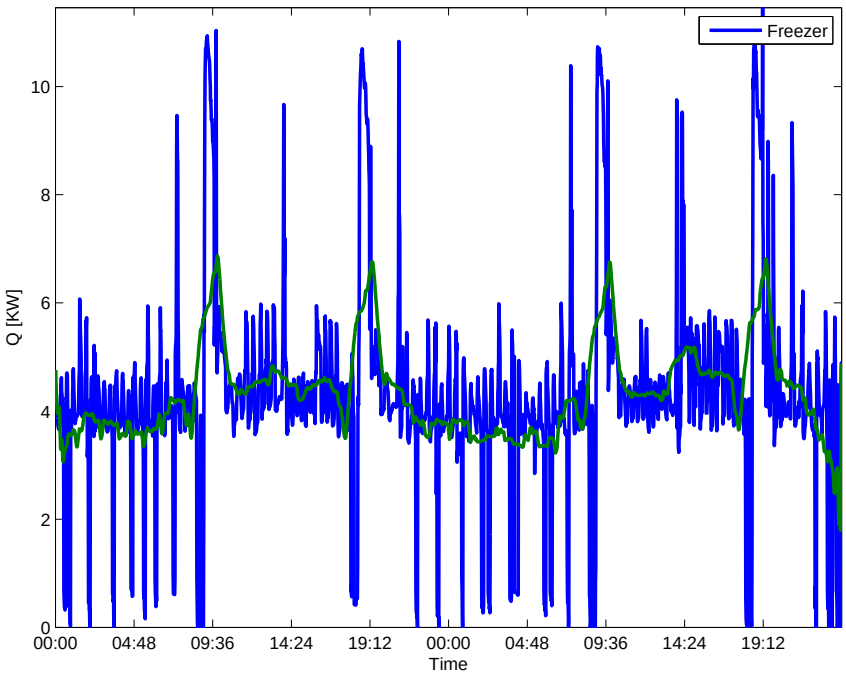

Figure 51: *25-08-2011, Plot of measured mass-flow at the freezers.*

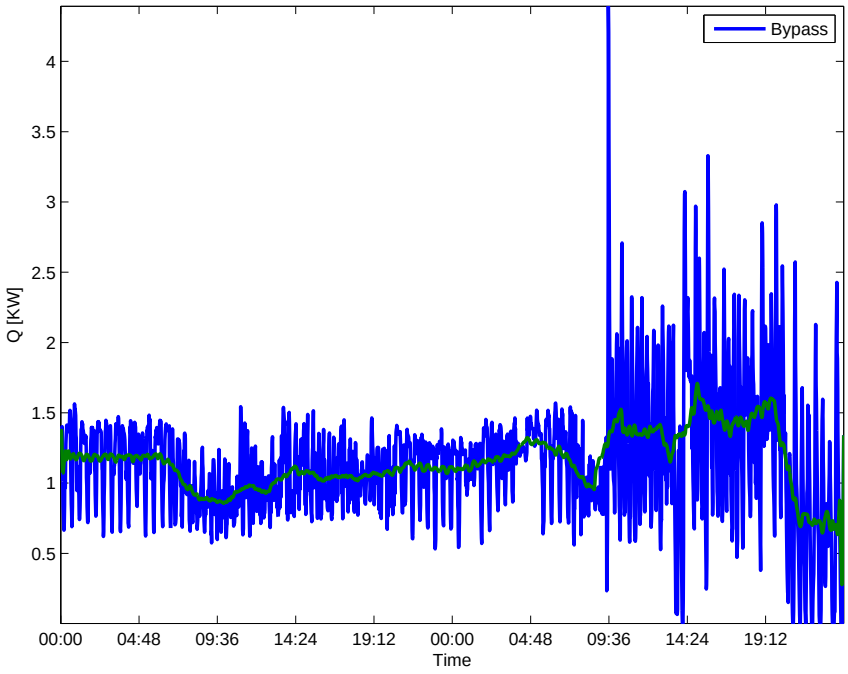

Figure 52: *25-08-2011, Plot of measured mass-flow at the by pass.*

References

Elbert Hendricks, Ole Jannerup, and Paul Haase Sørensen. *Linear Systems Control*. Springer, 2008. ISBN 978-3-540-78485-2.

John Bagterp Jørgensen. *Linear Model Predictive Control Toolbox*. 2-control ApS, 2004.

John Bagterp Jørgensen, Jakob K. Huusom, and James B. Rawlings. Finite horizon mpc for systems in innovation form. -, 2011.

Lars Finn Sloth Larsen. *Model based Control of Refrigeration Systems*. Budolfi tryk Aps, 2005. ISBN 87-90664-29-9.

Lennart Ljung. *System Identification - Theory for the user*. Prentice Hall, 2nd edition, 1999.

Jan Marian Maciejowski. *Predictive Control with Constraints*. Pearson Prentice Hall, 2002. ISBN 978-0-2031-9823-6.

Henrik Madsen. *Time Series Analysis*. Chapman & Hall, 2007. ISBN 1-4200-5967-X.

Kenneth R. Muske and Thomas A. Badgwell. Disturbance modeling for offset-free linear model predictive control. *Journal of Process Control*, Vol. 12:617–632, 2002.

Gabriele Pannocchia and James B. Rawlings. Disturbance models for offset-free model-predictive control. *AIChE*, Vol. 49, 2003.

Niels Kjølstad Poulsen. *Stokastisk Adaptiv Regulering*. IMM Danmarks Tekniske Universitet, 2007.

Guru Prasath and John Bagterp Jørgensen. Soft constraints for robust mpc of uncertain systems. *ADCHEM*, 2009.

Pierre O. M. Scokaert and James B. Rawlings. Feasibility issues in linear model predictive control. *AIChE Journal*, Vol. 45, No. 8, 1999.

Dan Simon. *Optimal State Estimation*. Wiley-Interscience, 1nd edition, 2006.

Morten Juel Skovrup. Energy engineering - windali, August 2003. URL `http://www.et.web.mek.dtu.dk/WinDali/Index.html`.